PET pharmacokinetic course

Kobe, Japan, May 17 - 19, 2007

Course Manual

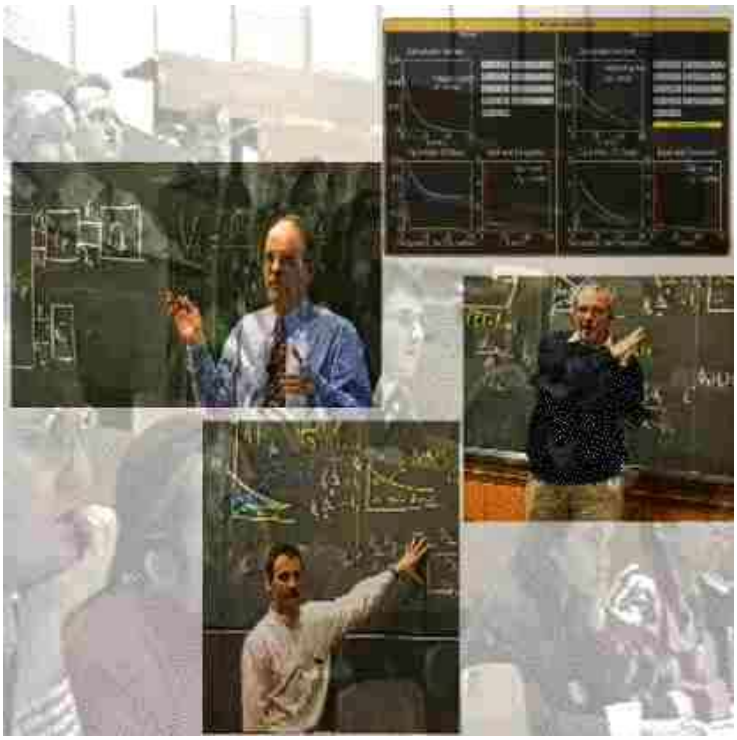

International Society of Cerebral Blood Flow and Metabolism Summerschool 2007

International Society for Cerebral Blood Flow and Metabolism

PET Pharmacokinetic Course

Manual

Editors:

R. P. Maguire, PhD

Prof. K. L. Leenders, MD, PhD

Osaka, Japan, 2007

Course tutors:

Richard E. Carson, PhD *Yale University, USA.*

Vincent Cunningham, PhD *GlaxoSmithKline, UK*

Roger N. Gunn, PhD *GlaxoSmithKline and Oxford University, UK*

Hidehiro Iida, PhD, DSc *Osaka, Japan.*

Gitte Moos Knudsen, MD, PhD *University Hospital Rigshospitalet, Copenhagen, Denmark.*

Robert A. Koeppe, MD, PhD *PET physics section, Division of Nuclear Medicine, University of Michigan Medical School, Ann Arbor, USA*

Kazuhiro Koshino, *Osaka, Japan.*

Adriaan A. Lammertsma, PhD *PET centre, University Hospital Vrije Universiteit, Amsterdam, The Netherlands*

Klaus L. Leenders, MD *Neurology Dept., University Medical Centre Groningen, The Netherlands*

Paul Maguire, PhD *Pfizer, USA.*

Wolfgang Müller-Schauenburg, MD, PhD *Department of Nuclear Medicine, University Hospital, Tübingen, Germany*

Antti Sohlberg, Osaka, Japan.

Claus Svarer, PhD *University Hospital Rigshospitalet, Copenhagen, Denmark.*

Hiroshi Watabe, PhD Osaka, Japan.

Cover image:
Photo montage from this course in Villigen, Switzerland, 1997

Copyright statement

Example citation for this work:

Chapter Authors Name; in "PET Pharmacokinetic course manual"; 2007; Eds. Maguire, R.P., and Leenders, K.L.; Chapter No., Kobe, Japan.

Foreword

This text forms the basis for a three day seminar course on PET - pharmacokinetics. The course has grown from an original idea of W. Müller-Schauenburg to compose an interactive introduction to the concepts and models used for PET data analysis. Through contributions from: Paul Scherrer Institute, Switzerland, MHH Hannover, Copenhagen University Hospital, University Medical Centre Groningen, A. Lammertsma AZVU PET Centre, J. van den Hoff PET Center Rossendorf, R. Koeppe, University of Michigan Medical School, R. Blasberg Memorial Sloan Kettering Cancer Centre, Richard Carson NIH and Bob Innis NIMH, this manual has developed into an accompanying text which aims to serve as an introduction to the field, in the areas of cerebral blood flow, glucose metabolism measurement and neuroreceptor kinetic quantification. The current revision brings the text up to date and, it is hoped provides a text, which can be read equally well before or after the course.

The main aim of the PET Pharmacokinetic Course is to explain pharmacokinetics in the context of PET measurements. Pharmacokinetics can in general, be defined as the quantification of the time course of a drug and its metabolites in the body and the development of appropriate models to describe the observations [Rowland, M., T. N. Tozer (1989). Clinical Pharmcokinetics. Pennsylvania, Lea and Febiger.] Taking the brain as a model, various examples of quantifying the time course of radiolabelled substances e. g. water or glucose, with the PET camera are developed. Three measurement fields are addressed: regional cerebral blood flow, glucose utilisation and neuroreceptor binding. For each topic, theoretical models for analysing the PET signal obtained will be explained. The mathematical techniques and pharmacological concepts required are introduced separately.

During the course, the basics for understanding pharmacokinetic modelling are outlined within the first day. As the course evolves, the model configurations become increasingly complex. The various computer exercises, designed to complement the theoretical parts, and encourage the interaction between participants and tutors, together with the computer simulations shown in some talks are expected to help merge theory with practice. The participants are invited to ask questions and make comments as much as possible.

Table of Contents

Overview

The **Introduction** starts with some very basic remarks concerning PET compartment analysis.

In the section **Mathematical Basis of Modelling,** exponential functions are shown to be inherent to the solution of the differential equations, which describe biological signal change in PET. Convolution plays a role when the tracer is administered over an extended time and the measured uptake is considered as a sum of time shifted exponential functions. Parameter estimation methods that are used for curve fitting procedures are also introduced.

Basic Pharmacokinetic Concepts are explained in the next chapter in order to introduce important pharmacokinetic quantities, their relationships, units and special role in model set-ups for analysing PET data. The idea of simplifying complex biochemical phenomena in tissue using compartments is illustrated by the Renkin Crone model for quantifying perfusion in brain.

Cerebral blood flow - one tissue compartment model describes the Kety-Schmidt model, a single-tissue-compartment model, as a standard method for analysing regional cerebral blood flow based on the Fick-principle. Partition coefficient, already mentioned within Basic Pharmacokinetic Concepts is revisited and explained in relation to the measurement of perfusion. Practical aspects of data measurement tracer showing fast kinetics, such as decay, delay and dispersion are also addressed.

Energy metabolism (FDG) - two tissue-compartment model. Using the example of FDG to measure regional glucose usage, the two tissue-compartment model is introduced. Compartments for free and bound FDG are illustrated. These can more generally be used to represent free and bound ligand for a number of other PET-tracers. Simplification methods are also addressed.

Linearisations introduces model adaptations to simplify data analysis and computation. In contrast to the non-linear parameter estimation procedures discussed in section 2.4, the desired parameter is deduced using the general linear model. For different models, methods exist which differ in their assumptions and realisation. The Logan plot, van den Hoff linearisation and Gjedde Patlak analysis are explained.

The chapter on **in-vivo and in-vitro** methods is intended to help understanding of in-vivo PET kinetics from the point of view of in-vitro experiments, which may be more familiar to some. This chapter introduces a closed two-compartment model and uses it to explain the in-vitro model. This model is then used as a foundation to discuss the in-vivo binding processes seen in PET. The concepts of (B_{max}), binding potential, and dissociation constant (K_d) are introduced.

The chapter **Receptor kinetics - modelling and practical applications** introduces the full pharmacokinetic model used for in-vivo ligand binding studies in PET. A step by step protocol for setting up a receptor density investigation is given, together with hints and practical information for analysing receptor data and performing PET scans in general.

The chapter **Steady State Analysis** discusses the influence of competitive binding on the expected tracer signal. It also describes experimentation in the presence of varying

amounts of unlabelled ligand as a means to determining B_{max} and K_d separately. The optimum model configuration is adapted to take the equilibration time and the particular radiotracer under investigation. Advantages and disadvantages when simplifying mathematical models in order to estimate the parameter of interest are illustrated.

Equilibrium measurements describe the bolus and infusion technique to achieve equilibrium conditions in-vivo. This method is a sensitive technique, which allows changes in occupancy during the measurement to be detected. This allows measurements of changes that occur over short time intervals e.g. because of a pharmacological challenge, to be measured. Issues surrounding the achievement of equilibrium and possible misinterpretation if this is not properly established are discussed.

Receptor kinetics - simplifications and limitations explains in detail the application of the concept of volume of distribution to simplify interpretation of the PET signal. Limitations of modelling with reversible and irreversible ligands are also discussed.

Data driven methods are explained and derived in terms of general compartment systems, which use either plasma or a reference tissue input. These methods characterise the system's impulse response function and do not require the a-priori selection of a particular model. The three methods are: Graphical analysis (Patlak and Logan), Spectral analysis and Basis pursuit.

Nomenclature and units

Nomenclature and units in the literature on PET have not been standardised. Efforts were made during the European Union task group meeting on modelling to decide on common terms, however the adoption of this recommendation is slow. There is no extra standardisation for medical measurement units defined by the Systeme International d'unites (ISO 31 TC 12). In this text, we have used the S.I. system as far as possible, however to achieve correspondence with the literature compromises have been made. Exceptions to the SI system are: the use of min (1 min = 60 s) and min^{-1} instead of s and s^{-1} (or Hz), and ml (1 ml = 1 cm^3) for physiological rate constants. Where possible units in this text follow the United States National Institute of Standards and Technology recommendations on units and orthography, however the units may also be those most commonly found in the literature and have been adopted as shown by the example of perfusion:

$$F = \frac{\Phi}{V} \qquad [\mathrm{ml \cdot min^{-1} \cdot 100g^{-1}}]$$

which would be given the conventional unit min^{-1}.

For the sake of simplicity, functions of time will not be written using the explicit dependence notation at each occurrence e.g. notation c_p is used in preference to $c_p(t)$ where possible. [Goodman A W, Ratti, J S; Finite mathematics with applications; pp 477-488; Macmillan ; New York;1979].

Noting that the compartment models developed here normally assume that the blood concentration time course is measured, models are named using the recommendations of the European task group. In this standard, the model is named based on the number of compartments in tissue. Using this scheme, the model for regional cerebral blood flow is a single tissue-compartment model, that for FDG is a two tissue-compartment model and the standard receptor model, when left unsimplified, is a three tissue-compartment model. See also the notes on the usage of K_1 and $k_{n=2..4}$ in section 2.6.

Throughout the course, reference is made to volumes of distribution V_d, V_f etc. As will be explained in section 3.4, these are numerically identical to the alternative "partition coefficient". However they represent two different concepts. The partition coefficient is conceptually a unitless ratio of concentrations. The concept of volume of distribution is a unitless ratio of relative volumes. At the appropriate point in the text it will be easier to employ one or other of these (numerically identical) variables to explain a given phenomenon, therefore both have been retained.

Table 1. Abbreviations

Symbol	Quantity	Units
λ	Radioactive decay const.	min^{-1}
Φ	Physical flow	$ml \cdot min^{-1}$
ρ	Apparent partition coefficient	unitless
τ_d	Dispersion constant	min
B_{max}	Available receptor site concentration	$mol \cdot l^{-1}$
BP_F, BP_P, or BP_{ND},	Binding potential	Unitless or $ml.cm^{-3}$
c_a	Radioactivity concentration in arterial blood (or molecular conc.)	$Bq \cdot ml^{-1}$ ($mol \cdot l^{-1}$)
c_b	Bound radioactivity concentration in tissue (or molecular conc.)	$Bq \cdot ml^{-1}$ ($mol \cdot l^{-1}$)
c_f	Free radioactivity in tissue concentration (or molecular conc.)	$Bq \cdot ml^{-1}$ or ($mol \cdot l^{-1}$)
c_p	Tracer plasma radioactivity concentration (or molecular conc.)	$Bq \cdot ml^{-1}$ ($mol \cdot l^{-1}$)
c_p^{glu}	Concentration of glucose in plasma	($mol \cdot l^{-1}$)
c_t	Radioactivity concentration in tissue - the PET tomographic measurement (or the molecular conc.)	$Bq \cdot ml^{-1}$ ($mol \cdot l^{-1}$)
c_t^L	Concentration of ligand or substance "L", in tissue.	
c_w	Radioactivity concentration in whole blood (or molecular conc.)	$Bq \cdot ml^{-1}$ ($mol \cdot l^{-1}$)
c_r	Radioactivity concentration in a reference tissue.	$Bq \cdot ml^{-1}$ ($mol \cdot l^{-1}$)
E	Extraction fraction	unitless

F	Perfusion	$ml \cdot min^{-1} \cdot 100ml^{-1}$ or min^{-1}
f_P	free fraction of ligand in plasma	unitless
f_{ND}	free fraction of ligand in tissue	unitless
K_1	Rate constant from blood to tissue (calibration constant)	min^{-1} or $ml \cdot g^{-1} \cdot min^{-1}$
K_d	Equilibrium dissociation constant	$mol \cdot l^{-1}$
K_d^L	Equilibrium dissociation constant of ligand or substance "L"	$mol \cdot l^{-1}$
K_i	Influx rate constant for an irreversible model	min^{-1}
$k_{n\, n \in 2,3,\ldots}$	Rate constant "n"	min^{-1}
k_{off}	Dissociation rate constant	min^{-1}
k_{on}	Bimolecular association rate constant	$min^{-1} \cdot mol^{-1} \cdot l$
N	Number of molecules	unitless
o^L	Occupancy of receptor sites by ligand 'L'.	unitless
P	Permeability	$cm \cdot min^{-1}$
Q	Mass of substance	g
S	Capillary surface area	$cm^2 \cdot g^{-1}$
SA	Specific activity	$TBq \cdot mmol^{-1}$
T	Characteristic time	min
$t_{1/2}$	Half-life	min
t	Time	min

V_d	General volume of distribution (Identical to tissue/blood partition coefficient)	$ml.cm^{-3}$
V_i $i \in f,ns,nd,s$	Distribution volume of a particular compartment, e.g. f=free, ns=non-specifically bound, nd=non-displaceable, s=specific.	$ml.cm^{-3}$
V_b	Intra-vesical blood volume in V_d (proportion of tissue volume occupied by intravascular blood)	unitless

1. Introduction

K.L. Leenders, University Medical Centre Groningen

1.1 PET data and models

The starting point for analysing data is not the model but the measured data. This is in general, the tissue activity time course, measured by the PET camera and the blood data (whole blood or plasma) calculated from blood samples drawn during the PET scan see Fig. 1-1.

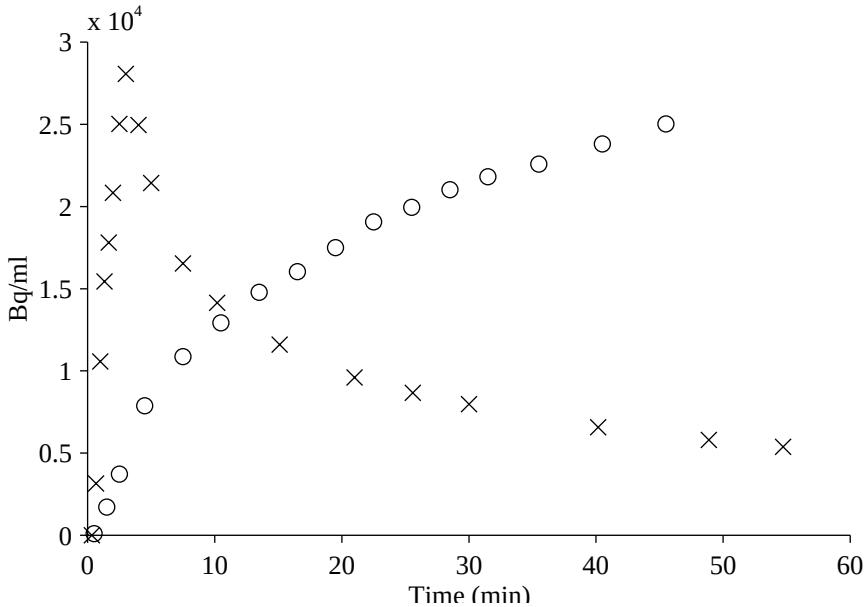

Figure 1-1. Plot of the plasma concentration time course 'x' and the time course in a small frontal region of interest measured by PET 'o' after injection of 200 MBq of FDG into a healthy human subject.

This, and the knowledge of the biochemical and physiological behaviour of the applied radiotracer in brain tissue, is the basis for developing a mathematical model in order to describe the observed data. It is common use in the field of pharmacokinetics to define physiologically separate pools of tracer substance whether in space or time as “compartments”. Fig. 1-2.

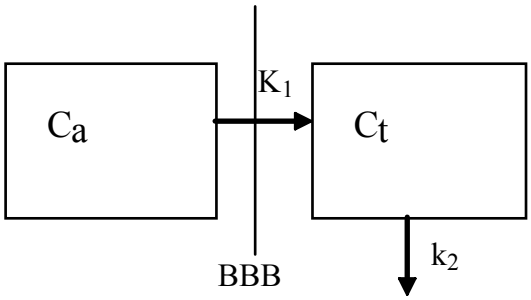

Figure 1-2. A general compartment model where c_a defines the concentration of substance in arterial blood, K_1 the rate of change of substance over the blood brain barrier BBB to the tissue-compartment defined by c_t, the concentration of substance in tissue. k_2 is the efflux rate from tissue back into blood.

In Fig 1-2, the tissue concentration is affected by a rate of movement of substance from blood into tissue and by a rate of loss of substance from the tissue. Changes in the tracer tissue concentration c_t can be described in terms of the tracer blood concentration c_a and the two unidirectional rate constants K_1 and k_2. By expressing the values of these parameters mathematically, the values of these parameters can be computed form the measured data.

For a very good introduction to the basic principles of tracer methods, please also read "Tracer Kinetic Methods in Medical Physiology" (Lassen, N. A. and Perl, W.; 1979;).

1.2 General assumptions of the PET tracer method

General assumptions of the methods that need only be true during the experiment.

1.3 Tracer assumption

This assumption states that the physiological processes and molecular interactions are not influenced by the PET measurement. In the large majority of PET studies (but not all), this assumption is easily met. For example, consider the injection of 400 MBq of a tracer with a (rather low) specific activity of 4 TBq·mmol^{-1}. This is equivalent to the injection of only 0.1 μmol of tracer. Note that some models, in particular some of the receptor models, this assumption may be violated

1.4 Constant state (Steady state) assumption.

This assumption states that the physiological processes and molecular interactions are in a constant state during the PET measurement. This is an extension of the previous assumption that dealt with the influence of the PET measurement on the system. Thus, during a perfusion measurement the perfusion should be constant and during a metabolism scan the metabolism should be constant. The "Steady state" here does not refer to the tracer itself.

1.5 Instantaneous mixing assumption.

The models presented during this course are based on distinct compartments (see chapter 2). This assumption states that the concentration in these compartments is homogeneous. This is an essential assumption for the use of compartment model as used during this course. Alternative, distributed models, can be developed, but these will not be discussed here.

1.6 References

Lassen, N. A. and Perl, W.; Tracer kinetic methods in medical physiology; 1979; Raven; New York;

2. Mathematical basis of modelling

R.P. Maguire, GNIP Project, Groningen, The Netherlands.
W. Müller-Schauenburg, University of Tübingen, Germany.

2.1 Introduction - compartments and mathematics

In this short course, there will be a focus on pharmacokinetic modelling of PET data, obtained after the injection of a radiolabelled tracer into the blood stream. After the tracer has been introduced, both the blood concentration and perhaps more importantly, the tissue tracer concentration are measured over time. From physical and physiological considerations, it is expected that transport and binding rates of the tracer will be determined by local concentration differences. For many processes the rate of accumulation or washout of a substance or its tracer analogue will be linearly related to the concentration difference across a boundary - which can be physical (a membrane) - or notionally between e.g. bound and unbound receptor. These boundaries partition the measured tracer activity concentration in tissue into a number of distinct compartments, which are the basis of the mathematical models that will be developed here. In figure 2-1 a example of a single compartment is illustrated.

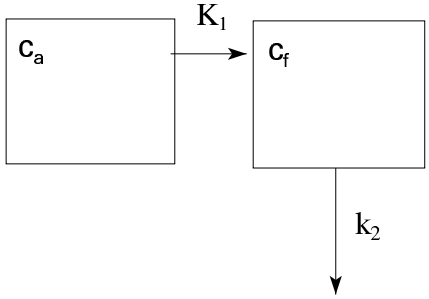

Figure 2-1 Diagram of a compartment model. The concentration in the central compartment c_t receives input from the compartment c_a at a rate determined by K_1. k_2, on the other hand, is the rate of loss of concentration from the compartment. The downward arrow associated with k_2 signifies that the return is to the venous compartment, and thus k_2 makes no contribution to c_a.

Equation (2.1) describes the rate of change of the concentration in the compartment, due to gains from an input concentration rate that is known (K_1c_a) and losses driven by the concentration in the compartment itself (k_2c_t).

$$\frac{dc_t}{dt} = K_1c_a - k_2c_t \qquad (2.1)$$

Differential equation (2.1) describes the dependence of the change of concentration in one compartment on the concentration of another compartment. This equation has been derived from considerations of conservation of mass which, by assuming a particular dilution volume, lead to equations in concentrations. By knowing, or hypothesising, a given configuration of compartments a set of differential equations to describe the exchange processes between them can easily be derived. Since PET data consists of local

measurements of the radioactivity time course of a tracer in tissue (rather than the rate of change), it is necessary to solve these equations, before a direct comparison can be made. This is not a trivial problem and this chapter describes in detail two elements of the required solution: the function e^{kt} and convolution.

2.2 The function $f(t)=e^t$ ("e function or exponential")

In mathematics the function $f(t)=e^t$ has a very important property, namely:

$$\frac{de^t}{dt} = e^t \tag{2.2}$$

from this we can also derive the following

$$\frac{de^{-kt}}{dt} = -ke^{-kt} \tag{2.3}$$

This equation states that the differential of the exponential function is the exponential function. So the rate of change of this function in time is equal to the value of the function at any time. Consider equation (2.1) again. In this equation, the differential of concentration appears on one side of the equation and the concentration itself on the other side, in an analogous way to the differential of the function and the function itself in equation (2.2). Since the property expressed in equation (2.2) is unique to this function, it plays a very important role in solving the differential equations that arise in compartmental modelling. It is not the aim of this course to dwell on techniques for solving differential equations, so at the outset we state the solution to equation (2.1):

$$c_t = K_1 e^{-k_2 t} \otimes c_a \tag{2.4}$$

Using (2.3) we can verify that $c_t=K_1e^{-kt}$ is a solution of (2.1) with a sharp input (an impulse, generating a start value K_1 at t=0) with no further input (i.e. c_a=0 at times greater than t=0). This solution of (2.1) is called "impulse response function" (IRF).

The rest of this chapter will concentrate on explaining this type of equation, the function e^{-kt}, the meaning of the convolution operator "$\otimes$", and their physical interpretation. For a more rigorous explanation, the reader might consult a textbook on linear differential equations e.g. (Bittinger 1981).

2.2.1 Constant fraction - Radioactive decay

All of the examples of PET measurement (activity time courses etc.) in the later chapters of this manual will have been corrected for the radioactive decay of the PET tracer. This means that the time activity curves which will be shown are directly proportional to the tracer's physical concentration at all times, rather than to the tracer's observed radioactivity concentration. In this subsection, radioactive decay will nevertheless be considered since it provides a simple and interesting illustration of the function e^{-kt}.

Consider a space, filled with the radioactive gas [C-11]CO_2. For each molecule there is a constant probability P that it will decay, emitting a detectable particle, in a given time period Δt. The number of radioactive molecules left in the container as time progresses is shown schematically in figure 2-2 .

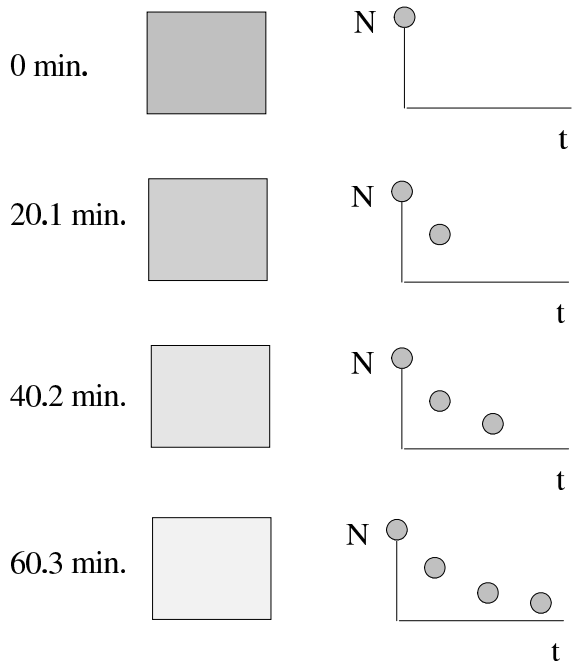

Figure 2-2 Schematic representation of radioactive decay. On the left hand side of the diagram, the number of radioactively labelled molecules in a compartment is shown, darker indicates higher concentration. On the right hand side, the actual number of molecules left, at each time point, has been plotted.

Since the probability of a radiolabelled molecule decaying is constant in a fixed time interval, the number of molecules which decay in a given time interval depends on the number of molecules that are present (that are left). The number of radioactive molecules is decreasing continuously and so will the *rate* of change. However, from the constant probability of decay, it can also be deduced, that a *constant fraction* of the radioactive molecules left will decay at any instant. This can be rewritten in equation form:

$$\frac{dN}{dt} = -kN \tag{2.5}$$

Where N is the number of molecules (a pure number) and k (units:min^{-1}; decay constant; the logarithmic decrement) is the fraction which are lost per time interval, at any instant. Using the properties of equation (2.2) this equation can be solved:

$$N(t) = N_0 \, e^{-kt} \tag{2.6}$$

Where N_0 is the initial number of radioactive molecules and $N(t)$ is the number of molecules at any time t (units: min).

2.2.2 Compartmental representation and properties of the function e^{-kt}

Although no molecules physically leave the container, there is a loss of radioactive molecules. Conceptually a 'system' with this behaviour can be represented using a compartment diagram such as that in figure 2-3

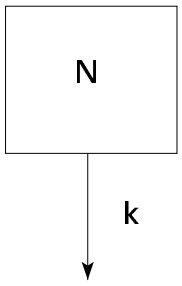

Figure 2-3 Compartment diagram representation of radioactive decay

The rate constant (k) determines the shape of the 'exponential curve', the graph of the function in time. Increasing k will cause a faster decay, and decreasing it will have the opposite effect. In this sense, it describes part of the characteristics of a compartmental system. The rate constant k can also be expressed in different units. Firstly, if k is inverted, then a new variable with the units of time can be found:

$$T = \frac{1}{k} \tag{2.7}$$

This variable T ("characteristic time", units: min) also characterises (numerically speaking: parameterises) the function e^{-kt}. If T is larger (longer), then the curve will decay more slowly. If T is smaller (shorter) then decay is faster. Considering equation (2.6) again, it can be seen that at time $t=T$, then:

$$\frac{N}{N_0} = e^{-1} = \frac{1}{e} \approx 0.37 \tag{2.8}$$

So in time T, 37 % of the initial molecules are left, thus 63% have decayed. The fraction of molecules which have decayed at successive multiples of this characteristic time T are; T (63%), $2T$ (86%), $3T$ (95%), $4T$ (98%), $5T$ (99%)…$7T$ (99.91%), illustrating the asymptotic behaviour of the e^{-kt} function.

Another expression of the rate k is the half-life $t_{1/2}$ (min.). It is calculated by considering the time at which exactly half of the radioactive molecules have decayed, and can be calculated thus:

$$0.5 = e^{-kt_{1/2}} \tag{2.9}$$

$$2 = e^{kt_{1/2}} \tag{2.10}$$

$$t_{1/2} = \frac{\ln(2)}{k} = \frac{0.693}{k} \tag{2.11}$$

The reader may find it useful, as an exercise, to set $N(t)/N_0$ to 0.5, and $t=t_{1/2}$ in equation (2.6) to verify this result. As with the characteristic time T, a series of successive fractions can be calculated for $t_{1/2}$; calculated from $(1/2)^n$, where n is the multiple of $t_{1/2}$.

Using equation (2.5) it can also be seen that the tangent to the graph of e^{-kt}, at t=0, has a gradient of $(-kN_0)$, and will intercept the t axis at time $1/k$ i.e. T (the "y-axis" intercept is N_0).

2.3 Convolution

As shown above, the function e^{-kt} can be used to characterise the time course of radioactivity, or indeed of concentration, in compartments under specific circumstances. An assumption in the discussion above has been that the compartment has an initial radioactivity, or an initial concentration, and that there is no further input during the time under study. In PET-pharmacokinetics, this is rarely the case. In general, the aim is to derive compartment time courses, based on an input concentration that is known, but varies in time. The input concentration to the tissue-compartments is generally the blood supply and in order to calculate the time course in these compartments it is necessary to combine the e^{-kt} function with the convolution.

2.3.1 Linearity - system input and output

Consider the system in Figure 2-3 . It has been stated that it will always decay with a shape of function characterised by e^{-kt}, and that the time activity course will be proportional to the number of radioactive molecules at the start. This is true, so long that the molecules are delivered into the system instantaneously (as an impulse) and is illustrated in Figure 2-4. using three different starting numbers of radioactive molecules, and a half-life of 21 min. From the graph, it is possible to confirm that the proportions of 1:0.5:0.1 are maintained at every time point in the curves. (Note that these curves are idealised, radioactive decay is a stochastic (probabilistic) process. With as few as even 10000 molecules, and the given time resolution, the curves would be associated with a lot of statistical fluctuation.)

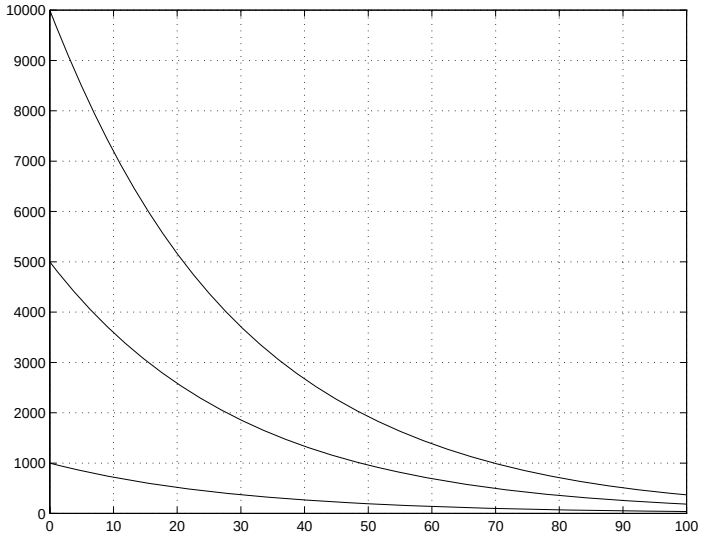

Figure 2-4. Graphs of the decay of 10000, 5000, and 1000 molecules, according to equation (2.6).

2.4 Delta function - unit impulse

The discussion here has considered the "system response" (model) as the number of molecules left in the system as a function of time. The system response to an ideal instantaneous delivery of molecules at t=0 characterises the system in some way. One step farther in mathematical abstraction is to idealise the start function (delivery of molecules) as an infinitesimally short impulse. The mathematical function that expresses the ideal is the *Dirac delta δ(t) function*, which is an infinitely short pulse with an integral of 1 unit at time t=0 - the perfect unit impulse. The output of the system for a δ(t) input is equal to the system response, also called the *convolution kernel.* The system response to a delta input (unit impulse) characterises the system in a standardised way. Note, in employing this concept, the concept of discrete molecules is ignored and the system is described by a smooth continuous function.

2.5 Linearity and shifting in time

Now consider entering three amounts of molecules into the system at slightly different times, say at 10000 at 1 min., 5000 at 5 min. and 1000 at 13 min, then the responses can be summed in a linear way to arrive at the overall expected response, as shown in Figure 2-5 .

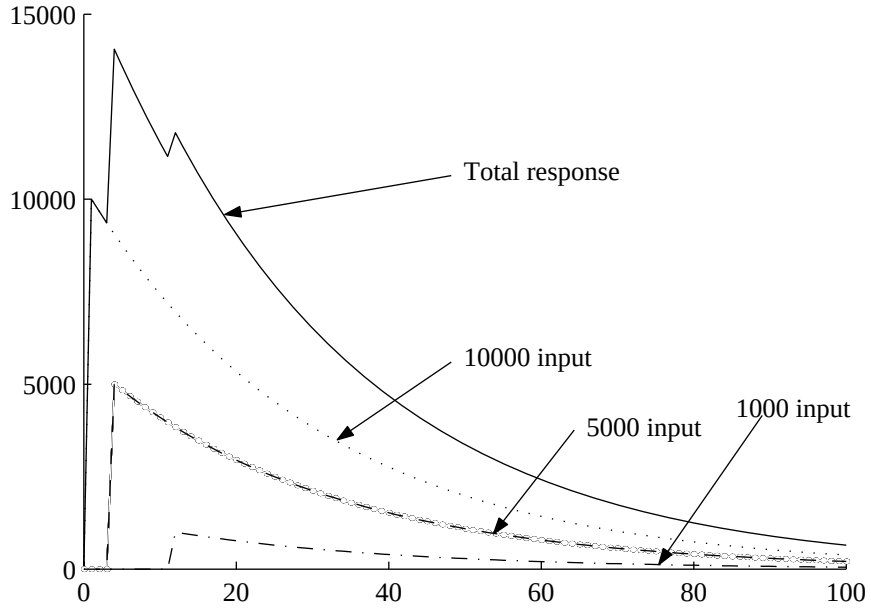

Figure 2-5 The effect of injecting three boli at 1, 5 and 13 min. The total response can be calculated by summing the response from the separate time shifted responses.

This simple linear addition of the separate responses is the key to understanding the convolution principle. By considering the input to a compartment as a series of separate impulses, which can be summed (superposed) to form a continuous response, the convolution can be broken down into its constituent components.

2.5.1 Convolution as a sum of system responses.

By knowing the response of the system to a unit impulse, it follows from the principle of linearity that the response to a bolus input of arbitrary magnitude can be estimated. By knowing the response of the system to a unit impulse, it is then possible to calculate the system response to an impulse of any magnitude. The unit impulse response is a basic description of the systems dynamic (kinetic) behaviour. Calculating the systems response to any input (not only a bolus) can be achieved by convolving the response to a unit impulse (convolution kernel) with the input (arbitrary input function.). By dividing an arbitrary input into a series of unit impulses of varying magnitude, shifted in time, and superposing the system responses, the total system response - output - can be calculated.

2.6 Bolus injection and constant infusion

Using the tools of the unit response function and the convolution, the special conditions of bolus injection and constant infusion can be examined. A bolus injection, if it is delivered instantaneously, is equivalent to the conditions of the unit impulse that have previously been discussed. Therefore, the observed behaviour of the system (the response) is the unit impulse response, scaled to the input magnitude. Knowing the input magnitude, the unit impulse can be determined by division. (Note that the units will depend on the measurement e.g. mol, $mol \cdot l^{-1}$, $Bq \cdot ml^{-1}$). An example of an arbitrary compartmental system response is given in figure 2-6 , using the injection of a known amount (25 mg) of substance into an arm vein, and subsequent measurement of the substance concentration in blood.

It should again be stressed that in this experiment, and in the rest of this text, the data have been corrected for radioactive decay. The loss of substance concentration from plasma in this case is due to physiological clearance from plasma.

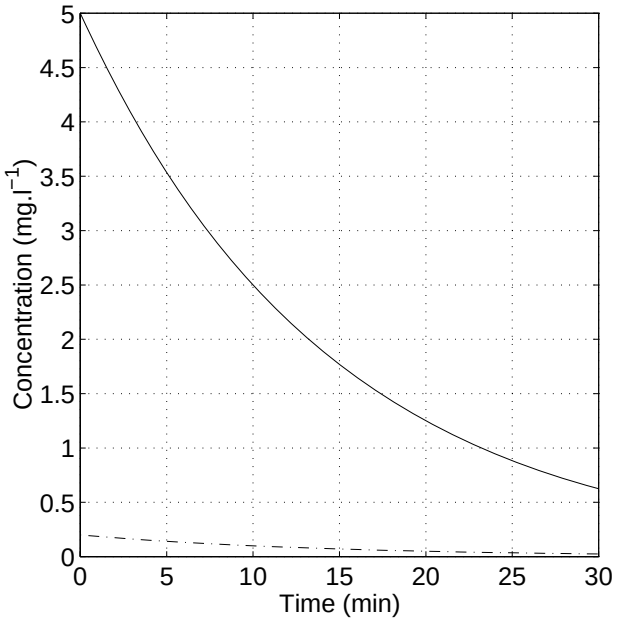

Figure 2-6 The measured concentration of a substance in plasma after injection of 25 mg (solid line). The concentration is measured in mg·l^{-1}. The inferred unit impulse response is also given (dot-dash line).

From this data the response to a unit input can be estimated by division by 25 mg and is shown as a dotted line in figure 2-6 . Using this impulse response - the measured concentration time course after bolus injection - the response to an arbitrary input can be estimated graphically. Note the impulse response function here is the expected concentration time course in plasma for a given injected mass of substance. This implies that the impulse response function has units (l^{-1}). In PET the input is normally the measured activity concentration in blood and the response is the activity concentration time course in tissue (as measured using the PET camera). Although the input and response have the same units, the literature often attributes units of (ml blood/mg tissue/ min) to the constant K_1, which is capitalised to denote a change in measurement variable hidden in the response function. It could be argued that K_1 should be considered as part of the input (a scaling factor), rather than a rate constant of the model. Although K_1 will be used as a parameter of the models in this test, the reader may wish to consider conceptually K_1 as scaling the "input". Since K_1 has a linear relationship with the output, it can be considered mathematically as either part of the input or part of the system response (model). In the convolution, equation K_1 can be associated with either input or the system response (model).

Consider calculating the response to a constant infusion of the same substance used above (say 5 mg·min^{-1}). Arbitrarily each 5 min section of infusion could be thought of as a single bolus, given around the midpoint of that section, and containing the same amount of substance as would be delivered in the 5 min, i.e. 25 mg. Next, the response to each of those input impulses could be calculated by multiplying the unit response by 25, yielding

the curve in figure 2-6 . The individual responses are then positioned (shifted) at the appropriate position on the time axis. Finally, these are summed to yield an approximation to the response.

The result of these operations is given graphically in Figures 2-7 and 2-8 . The first figure shows the infusion and its approximation, and the second figure, the individual system responses to the separate boli, and the sum total. Note how the system response to the infusion reaches a saturation plateau at later time points. The time taken to reach this plateau, the initial gradient of the plasma concentration and the plateau are determined by the input and unit impulse response.

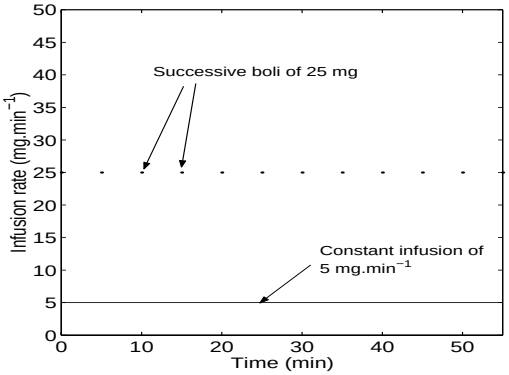

Figure 2-7 A constant infusion (solid line) considered as a series of boli (points), each equivalent to 5 min. of the infusion.

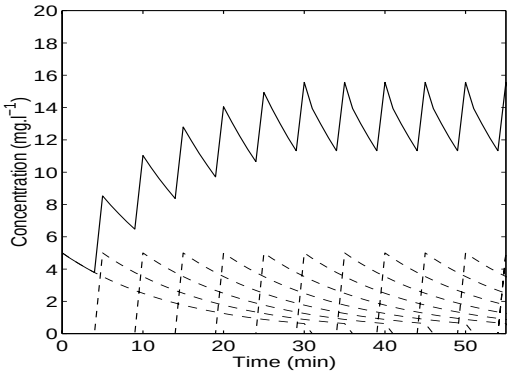

Figure 2-8 Response to each of the boli (dashed lines) in the previous figure, and the total response (solid line).

Referring back to the single compartment model in equation (2.4) , the convolution of the system unit impulse response (e^{-k2t}) and the input function c_a, (i.e. the process of shifting and adding of bolus responses which has been shown above) yields the expected tissue activity concentration c_t, which is equivalent to the integral:

$$c_t(t) = K_1 \int_0^t e^{-k_2(t-\tau)} c_a(\tau) d\tau \qquad (2.12)$$

Where t is the time for which the convolution is required. It is interesting to see that in this notation, the system impulse response is mirrored in time since the term '-τ' appears. Careful thought can confirm that this is indeed reasonable, since 'older' contributions have already decayed, in a manner governed by e^{-k2t}. Note, as has been mentioned before, the output for a delta function input is identical to the 'system response':

$$e^{-k_2 t} = \int_0^t e^{-k_2 (t-\tau)} \delta(\tau) d\tau \tag{2.13}$$

2.7 Parameter estimation (curve fitting)

2.7.1 Explaining data using models

The pharmacokinetic models developed in this course are used to interpret PET measurements. They are necessarily much simpler than complete physiological models, because they are adapted to the spatial and temporal resolution of the PET instrument. Indeed, the appropriateness of the model can be determined from the measured data (Landaw & DiStefano III 1984) (see comments on the application of F-test in chapter 7.7). The variables (parameters) in the mathematical descriptions of the models are typically rate constants (the constants vary between regions and subject, but are fixed for one homogeneous region during the measurement), distribution volumes and other physiological measurement quantities. Using the measured input signal - the blood activity time course - the mathematical model can be used to calculate the expected tomographically measured tissue time activity course for a chosen set of model variables. This can then be compared with the measured data. The aim of parameter estimation (fitting) is to find estimates variables which best explain the measured data.

2.7.2 Linear and non-linear regression

If a mathematical model is linear, that is, if there is direct proportionality between the model variables and the predicted response, then an optimal set of estimates can be computed directly in one iteration using linear regression. However pharmacokinetic models are typically non-linear - sums of a number of exponential functions, where each decay constant in the equation represents a compartment.

Whether using non-linear or linear estimation, the optimum estimate of the model variables for a given data set is determined by minimising the sum of the squared differences between the model prediction and the measured data. This can be shown rigorously (Beck & Arnold 1977) to be a reasonable definition in terms of a maximum likelihood estimation. If the expected variance for each of the data points is known, then the normalised statistic χ^2, which is the variance weighted sum of squares, can be minimised. χ^2 values give a direct indication of the level of confidence with which we can trust the estimated values. The χ^2, sum of squared difference or other functions, used to determine goodness of fit are termed cost functions. Generally, algorithms for solving the least squares problem start

with a best guess of the solution and by determining the change in the cost function for a given change in the model variables a new best estimate is determined. This procedure continues iteratively until no further improvement can be made.

Even for non-linear equations it may be possible to transform the data such that there is a linear relationship between the dependent and independent variables allowing linear regression to be used (Blomquist 1990;Patlak et al. 1983). In that case, a solution can be computed in one iteration. Further examples of these linearisations will be given in chapter 6.

2.7.3 Non-linear search algorithm

There are two main methods to determine the modification to the parameters at each iteration in a non-linear fit. Firstly, the method of steepest descent, in which an increment is added to the variables depending on the local gradient of the cost function with respect to each of the variables independently. Secondly, Taylor series methods which model the local variation of the cost function as a linear function and solve for a local solution using linear regression. The latter of these two methods is also called Gauss-Newton minimisation. Although there are a number of other algorithms available e.g. Simplex algorithm (James & Roos 1976) and others (Nelder & Mead 1965;Ralston & Jennrich, I 1978), for many applications the Marquardt-Levenberg algorithm (Levenberg 1944;Marquardt 1963), which represents a compromise between steepest descent and Taylor-Series methods has been shown to perform well.

2.7.4 Local minima

In contrast to linear fitting, no non-linear algorithm is guaranteed to reach the optimal solution. Algorithms may find a local solution to the least squares problem. An example is the case where the current estimation predicts a solution that is lower than the data in the early part of the curve and greater for later points. If in this case small positive and negative variations in the parameters cause the curve to shift up or down, the sum of squares cost function will increase for both these changes. This gives the appearance that the solution between these two yields a minimum sum of squares. A better solution is possible, where the data points are randomly scattered about the model curve, however the search algorithm may be satisfied with the local solution.

2.7.5 Accuracy of the solution

The final values calculated are estimates of the values of the variables in the underlying system at the time of measurement. If the measurement data is not associated with any measurement error, it should be possible to determine the parameters of the underlying system exactly, except in very specific circumstances. If there is noise in the system, that is, if the measurement data are associated with some measurement uncertainty then there will be inaccuracy in the estimates. If two parameters are highly correlated - small changes in the parameters cause similar changes in the predicted response - then as the measurement error increases the precision with which either of the two parameters can be determined by non-linear parameter estimation techniques will diminish very rapidly.

Measurement strategy, patient movement, instrument dead time, measurement background and pharmacological effects will all affect the blood and tissue data and hence the outcome. It is important to remain critical about these and other measurement error sources when applying parameter estimation methods.

2.8 General Linear Model

2.8.1 Linear equations

The compartment models that have been introduced in this course yield operational equations containing exponential functions. It has been stated that, generally, the number of separate exponential functions in the operational equation is equal to the number of compartments in the pharmacokinetic model. Consider a simple equation with two exponential functions *where the decay constants a_1 and a_2 are known a-priori*:

$$c(t) = (\beta_1 e^{-a_1 t} + \beta_2 e^{-a_2 t}) \tag{2.14}$$

The total concentration c(t) is a mixture of the two known exponential functions $e^{-a_1 t}$ and $e^{-a_2 t}$, with linear coefficients β_1+β_2. Since the two constants *a* are fixed for every time point a set of equations expressing the relationship between the measured concentration at each time point and the two known exponential functions can be written:

$$\begin{pmatrix} c(t_1) \\ c(t_2) \\ \vdots \\ c(t_{n1}) \end{pmatrix} = \begin{pmatrix} e^{-a_1 t_1} & e^{-a_2 t_1} \\ e^{-a_1 t_2} & e^{-a_2 t_2} \\ \vdots & \vdots \\ e^{-a_1 t_n} & e^{-a_2 t_n} \end{pmatrix} \begin{pmatrix} \beta_1 \\ \beta_2 \end{pmatrix}$$

In this form, the separate measurements of c(t=t_1..t_n) form a vector. On the right hand side of the equation is a matrix, with the two exponential functions in two columns. Each column is a *basis function* and the two basis functions add together in a linear way, with the scaling coefficients β, to make the total function that is equal to c(t). Considering each element of the vector on the left hand side and the corresponding rows of the matrix individually, along with the coefficients, it should be possible to see that the matrix expresses a set of equations, analogous to equation (2.14), in each of the t=t_1..t_n. The matrix vector representation above can be written using vector and matrix variables:

$$\mathbf{c} = \mathbf{X}\boldsymbol{\beta} \tag{2.15}$$

Where the **bold** type indicates a matrix or vector. This equation expresses the general linear model (GLM).

Although in this simple example the input function is implicitly a delta function, it is also possible to add a function to describe a varying input function, which is convolved with the system response to form the output. In the simplest case, this simply involves modifying the basis functions.

2.8.2 GLM and compartment models

The general linear model is a powerful framework for data analysis. Any linear method, which can be seen as a *straight line regression* can be represented in the form of (2.15), but it also possible to represent operational equations that may not appear to yield a straight line regression in this form. Computationally there are advantages to linearity and the GLM parameterisation of the operational equation in terms of parameter estimation:

- The estimation of coefficients β is a one step, non-iterative procedure, which only has one solution.
- The expected error variance associated with the estimated parameters can be directly calculated.
- Because the estimation procedure is not iterative, it is fast enough to be applied to individual pixels to calculate *parametric images*.
- If the GLM is applied at the pixel level, then because of the linear properties pixel estimates of the parameters may be pooled after estimation. This has advantages when pooling to reduce noise or apply smoothing during statistical mapping procedures.

2.8.3 GLM parameter estimation

Equation (2.15) can be extended to the practical measurement situation by adding a vector **e** to account for random error:

$$\mathbf{c} = \mathbf{X}\boldsymbol{\beta} + \mathbf{e} \tag{2.16}$$

The best estimator of β in a least squared sense (Press et al. 1987) (Johnson & Witchern 1998)is given by:

$$\boldsymbol{\beta} = (\mathbf{X}'\mathbf{X})^{-1}\mathbf{X}'\mathbf{c} \tag{2.17}$$

This result shows that the parameters can be estimated in a one step procedure, which involves the inversion of the matrix containing the basis functions describing the model. If the uncertainty of the measurement is variable, then a weighting term can be introduced. The estimated (co-)variance associated with the estimates can also be estimated:

$$\sigma_{\boldsymbol{\beta}}^2 = \sigma_c^2(\mathbf{X}'\mathbf{X})^{-1} \tag{2.18}$$

This is a very important result since it shows that the uncertainty in the estimates of the parameters β is directly proportional to the uncertainty in the measurement of the data.

2.9 Parametric images

PET data consists of both a spatial and a temporal component. The spatial element can be removed from the data set by choosing a region of interest and the models in this course

will be based on such data. However, it is very important not to neglect the spatial domain, since it also contains much of the information.

One way to retain the spatial information in the data is to apply pharmacokinetic models at the finest spatial scale, determined by the image digitisation matrix - the pixel. By estimating a parameter at each pixel, a map of the parameters spatial distribution can be made - *a parametric image*. This parametric image then contains the most complete, yet succinct summary of the data. Parametric images can be used with image statistical techniques to test the spatial difference in parameter distribution between two conditions e.g. two study groups or longitudinally.

As has been noted in the previous sections the GLM has desirable properties within which to implement methods to calculate parametric images. Part of the modelling effort is to develop models and methods, which lead to parametric images, and so linearisations will be discussed in detail. Under certain conditions, it is even possible to apply models before reconstruction, which has advantages in terms of statistical efficiency and reconstruction times.

2.10 References

Beck, J. & Arnold, J. 1977, *Parameter estimation in engineering and science* Wiley, New York.

Bittinger, M. L. 1981, *Calculus a modeling approach* Addison-Wesley, Reading, USA.

Blomquist, G. 1990, "Maps of receptor binding parameters in the human brain - a kinetic analysis of PET measurements", *Eur.J Nucl Med.*, vol. 16, pp. 257-265.

James, F. & Roos, M. 1976, "Minuit, A System for Function Minimization and Analysis of the Parameter Errors and Correlations," CERN, Geneva.

Johnson, R. A. & Witchern, D. W. 1998, *Applied multivariate statistical analysis*, 4 edn, Prentice-Hall, London.

Landaw, E. E. & DiStefano III, J. J. 1984, "Multiexponential, multicompartmental, and noncompartemental modeling. II. Data analysis and statistical considerations", *Am.J.Physiol.*, vol. 246, p. R666.

Levenberg, K. 1944, "A Method for the solution of certain problems in least squares", *Quart.Appl.Math.*, vol. 2, pp. 164-168.

Maguire, R. P., Spyrou, N. M., & Leenders, K. L. 2000, "Variance in parametric images: Direct estimation from parametric projections", *Physics in Med.Biol.*, vol. 45.

Marquardt, D. W. 1963, "An Algorithm for Least-Squares Estimation of Nonlinear Parameters", *J Soc.Indust.Appl.Math.*, vol. 11, pp. 431-441.

Nelder, J. A. & Mead, R. 1965, "A simplex method for function minimization", *Comput.J.*, vol. 7, pp. 308-313.

Patlak, C. S., Blasberg, R. G., & Fenstermacher, J. D. 1983, "Graphical evaluation of blood-to-brain transfer constants from multiple-time uptake data", *J Cereb.Blood Flow Metab*, vol. 3, pp. 1-7.

Press, W. H., Flannery, B. P., & Teukolsky, S. A. 1987, *Numerical Recipies in C (The Art of Scientific Computing)*, 2 edn, Cambridge University Press, Cambridge.

Ralston, M. L. & Jennrich, R., I 1978, "Dud, a derivative-free algorithm for nonlinear least squares", *Technometrics*, vol. 20, pp. 7-14.

3. Basic pharmacokinetic concepts

K.L. Leenders, GNIP Project, Groningen, The Netherlands.

3.1 Introduction

In this section, some basic concepts of brain uptake of a radiotracer from blood are discussed. The water phase of plasma will be considered as the source of the radioactivity that is taken up. This is the physiological space from which the PET signal is supplied to the brain and in which the time course of the brain input signal can be measured. Using this starting point also allows utilisation of well-known concepts and quantitative measures used in clinical pharmacokinetics. It is worthwhile to underline that the PET scanner intrinsically measures radioactivity per volume (units: $Bq.ml^{-1}$), whereas organ size is defined in terms of mass units (g) to avoid conversion to volume using density. This remains a possible source of confusion when reading the literature.

Depending on the transport rate of the radiotracer across the blood-brain barrier or its interaction with the brain parenchyma, the uptake of signal represents either: information concerning the blood-brain barrier transport, or specific brain tissue binding mechanisms, or both. Only tracers that cross the blood-brain barrier rapidly are suitable for regional perfusion measurements.

3.2 Flow and perfusion

In physics and engineering texts the expression, 'flow rate' means 'volume flux' (SI units of $l \cdot s^{-1}$, litres per second). Many biological phenomena take place on a time scale of min. and volumes are of the order of ml. Systemic blood flows (volume fluxes) are therefore normally in units $ml \cdot min^{-1}$. The symbol Φ will be used in this text to denote **volume flux**.

Delivery of substrates to tissue, however, depends on the volume flux per unit tissue volume. Consider the supply of oxygen to tissue. The amount of oxygen with a concentration c_a in arterial blood supplied to the tissue sample per unit time is c_a times Φ. However, the oxygen requirements of the tissue sample depend on its volume. A sample with a larger volume will require more oxygen per unit time to sustain it than a sample with a smaller volume. So in order to assess the sufficiency of supply of oxygen (or any other nutrients) we use the concept of **perfusion** (volume flux / tissue volume).

In the literature on PET, **perfusion is often simply called 'blood flow'**. Since an aim of this manual is to introduce the student to current PET literature, the term **'blood flow' will be used to describe perfusion with the symbol F throughout this text. Volume flux and e.g. systemic circulation 'blood flow', will be designated by the symbol Φ.** Since these concepts are often confused in publications, it is important to check the direct or implied definition each time.

3.3 Equilibria

One definition of equilibrium given by Webster's dictionary is "an Equality of weight or force; an equipoise or a state of rest produced by the mutual counteraction of two or more forces." This definition concurs analogously with the thermodynamic definition of equal

temperatures. Closer to the definition which will be used in this text is the concept of equilibrium in a chemical reaction. (Le Châtelier's principle).

In the case of exchange between compartments in a pharmacokinetic model, a condition of equilibrium can theoretically be defined as having been reached when the rate of change of the concentration in the compartments is zero. The conditions for equilibrium can also be defined mathematically by setting the rate of change in the differential equations describing the system to zero (Delforge et al. 1993). However, this idealised situation is not normally encountered in PET since the system is not closed and tracer is normally being continuously lost e.g., by kidney clearance. Different terms for equilibria between plasma and tissue activity concentrations are used:

Secular equilibrium: Equilibrium conditions where the net rate of exchange between the compartments is small and total loss from the system is zero (two orders of magnitude smaller than the rate constants). This is the practical equivalent of the theoretical equilibrium definition above.

Pseudo-equilibrium: Net exchange between the plasma compartment and the tissue-compartments is small but the tracer loss from the plasma compartment is not negligible. The plasma curve has a small negative slope. In this situation, the ratio of tissue to plasma concentration will be slightly higher than in the true equilibrium situation.

Transient equilibrium: With reference to neuroreceptor binding studies this is a term used for the maximum turning point of the total tissue curve. Although at this point the change of concentration in tissue is zero, there may still be exchange between tissue and blood compartments and the total loss from the system is not negligible (loss from non-specific binding). The ratio of tissue to plasma concentration will be higher than at true equilibrium.

Steady state: Can best be defined in terms of a single compartment, rather than between compartments as for equilibria. The net flux of tracer through the compartment under study is stable; there is a constant turnover. The total amount leaving is identical to the total amount entering the system. However this compartment may receive or supply other compartments with which it is not in equilibrium. e.g. The free compartment in a two tissue-compartment, irreversible binding model, when it is in equilibrium with plasma.

3.4 Partition coefficient and volume of distribution

The partition coefficient between two compartments is defined as the ratio of their equilibrium concentrations (see 3.3). However, the concept of volume of distribution which is numerically identical to partition coefficient, as determined in in-vitro systems, warrants extra discussion.

The term "volume of distribution" (Ganong 1991) is used in pharmacology to denote the ratio of the dose administered divided to the concentration of a substance in the systemic circulation at equilibrium. The unit of this quantity is a real volume (normally expressed in litres) and is conceptually the total volume of all the compartments in which the injected substance is distributed. The pharmacological volume of distribution can easily be greater than the total body volume (circa 70 l) for organs where the substance builds up.

The term "volume of distribution" used in the PET literature is not the same as the pharmacological volume of distribution. It is defined as the ratio of the volume occupied by the tracer at equilibrium to the total tissue volume and is **unitless.** The term is used since it allows easy access to some of the conceptual ideas associated with the pharmacological term. A large volume of distribution is then equivalent to a large partition coefficient between the compartments. Again PET volumes of distribution can be much larger than 1.0. The following figures seek to illustrate the meaning of partition coefficient and volume of distribution based on two examples. Note that the real space occupied by the tracer is unknown (and perhaps irrelevant). Conceptual "volumes" are derived from the measurement of concentration ratios:

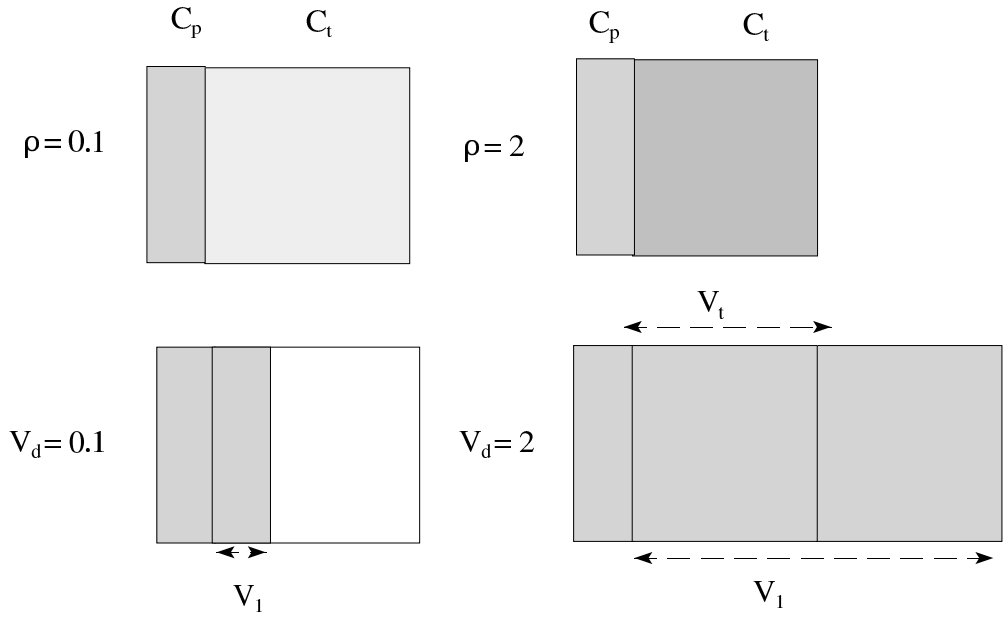

Figure 3-1. Graph illustrating V_d and ρ. Upper left: the lighter colour in tissue represents a lower concentration than in blood. Upper right: An example where the tissue concentration is higher than in blood (tissue box is darker). Lower left: The equivalent conceptual volume of distribution representation of the situation upper left. V_1 is a fraction of the total volume V_t. Lower right: Equivalent to upper right; V_1 is greater than V_t.

This volume is a virtual volume and therefore it is often called the “apparent” volume of distribution: the “volume” the tracer would occupy, if the tracer were to adopt the same concentration in the tissue as in the blood. For a value of $V_d = 0.1$ the tissue space would have to “diminish”. For a value of $V_d = 2$ it would need to “expand” beyond the real tissue volume. In PET studies, the idea of V_d is borrowed from clinical pharmacokinetics. In steady-state PET studies, the V_d is easily derived. In dynamic PET studies we do not measure concentrations, but activities and rate constants (see below) between kinetic compartments are then estimated. From the rate constants, the distribution volume can be derived as shown i.e. in section 8.6

The exchange of substances between various physiological or biochemical states or spaces has led to the concept of compartmental models. It must be kept in mind that kinetic compartments are not necessarily identical to physical spaces. The kinetic model only attempts to describe the exchange of substance between kinetically defined

"compartments" by using rate constants (*k*'s). Without knowing the concentration of the substance in the various compartments the degree of substance exchange (such as transport through one or more membranes, enzymatic conversions or binding to specific sites) can be quantified by estimating the fraction of substance moving "from one compartment into another". Often rate is confused with rate constant. The former actually designates an amount of substance being processed over a period, which is dependent on both substance concentration and the turnover constant, whereas the latter directly relates to the degree of "system response".

3.5 Measures of tracer uptake into brain

Many entities have been used to describe quantification of substance exchange between blood and brain. The most well-known are:

Table 2. Pharmacokinetic parameters used in *describing blood-brain barrier transport.* Note that the definitions here refer to blood-brain barrier transport only. For example, the partition coefficient given here is the tissue-arterial concentration ratio. (See also table of symbols and glossary).

Parameter	Symbol	Definition	Unit
Relative volume of Distribution	V_d	Apparent volume divided by the total volume - see text. Numerically equivalent to partition coefficient.	Unitless or $l \cdot kg^{-1}$
Perfusion	F	Flow per unit volume = $\frac{\Phi}{V}$ or Flow per unit tissue mass	$ml \cdot 100g^{-1} \cdot min^{-1}$ or min^{-1}.
Partition coefficient	ρ	Tissue concentration over plasma concentration $\frac{c_t}{c_a}$ (as measured in vitro).	Unitless
Extraction (Net)	E	Fraction of substance moving from blood into tissue during a single capillary passage.	Unitless
Plasma to tissue rate constant	K_1	Product of perfusion and extraction = F E	min^{-1} or $ml \cdot g^{-1} \cdot min^{-1}$
Physical flow	Φ	The volume flux of a fluid.	$l \cdot min^{-1}$
Permeability	P	A measure of how easily substances cross a barrier. e.g. a membrane	$cm \cdot min^{-1}$
Surface	S	Area available for passage per unit volume of tissue.	$cm^2 \cdot g^{-1}$
Permeability surface product	PS		$ml \cdot g^{-1} \cdot min^{-1}$

Methods for determination of blood-brain barrier passage are described in (Pardridge 1998).

3.6 The Renkin-Crone-model

The Renkin-Crone equation relates (Crone 1964;Renkin 1959) the entities permeability, flow, and extraction. For the formula and graphical representation of the relationships see the figures below. It is important to realise that blood flow (perfusion) influences the brain extraction of a substance and this is, in turn, related to the total amount of substance crossing the blood-brain barrier.

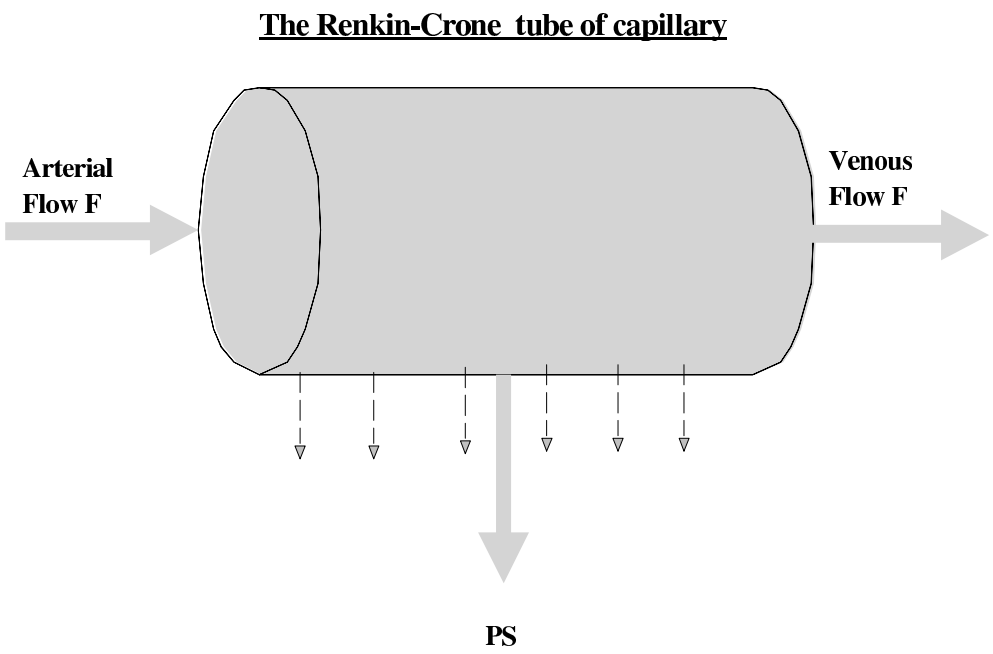

Figure 3-2: The Renkin-Crone rigid tube model of capillary.

Extraction (*E*) can be expressed by the Renkin-Crone formula which relates *E* to *F* and *PS*:

$$E = 1 - e^{-\frac{PS}{F}} = \left.\frac{c_a - c_v}{c_a}\right|_{c_t=0} \tag{3.1}$$

Where c_a and c_v is the arterial and venous concentration, respectively. This equation is only true at t=0, when the tissue concentration c_t is zero. As soon as c_t increases, there will be an increase in c_v, but the extraction will remain constant. At secular equilibrium c_a and c_v are equal, however extraction is still the same as at t=0. The rate constant for the blood brain barrier transport is then:

$$K_1 = EF \tag{3.2}$$

3.7 Graphical examples of how the Renkin-Crone model relates *PS* to *E*, K_1 and F

The permeability surface area product (PS) is a composite constant that uniquely describes the extractive properties of the capillary bed.

High PS. (e.g. water or butanol). If *PS* is high then the extraction is 100% i.e. 1.0 (Fig. 3-3), even if perfusion is high (i.e. the time that the molecule spends in the capillary is short = short transit time (*T*) of the blood $F = 1/T$ note the units min^{-1}). Under common physiological conditions of perfusion extraction is independent of perfusion only if *PS* is greater than 3. The amount of substance crossing the blood-brain barrier is directly proportional to perfusion, when *PS* is high see Fig. 3-4. Examples of high PS tracers are [O-15]water, [O-15]butanol, [C-11]flumazenil.

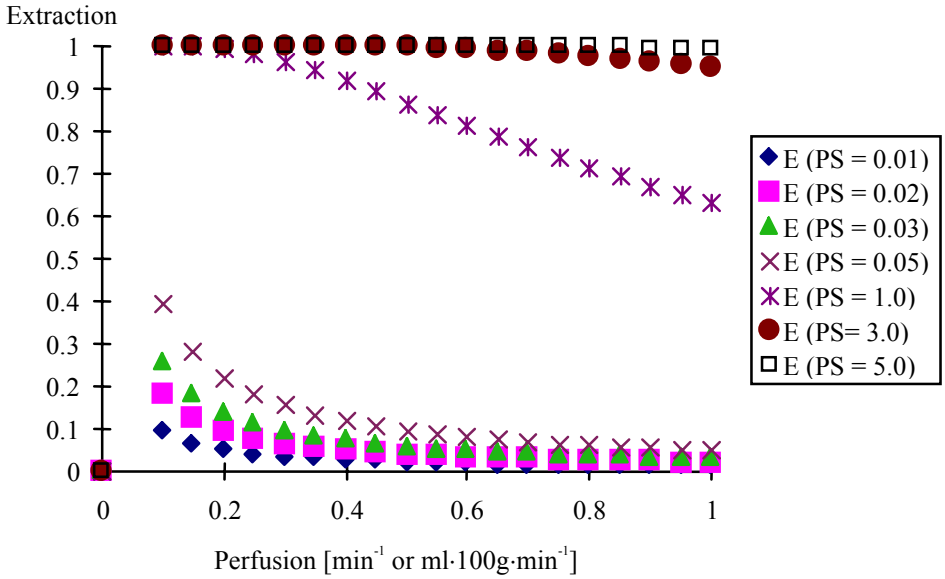

Figure 3-3. Relationship between perfusion *F*, extraction fraction *E* and Permeability Surface Product *PS*.

Low *PS*. Extraction is low because during one capillary passage a small amount of substance can cross the blood-brain barrier. However, if perfusion is low then extraction can still be high in spite of a relatively low *PS* (Fig. 3-3). K_1 is low if *PS* is low and K_1 is completely independent of perfusion under these circumstances. [F-18]Fluorodopa with (K_1 = 0.03 $ml \cdot g^{-1} \cdot min$) is an example of a low *PS* product tracer.

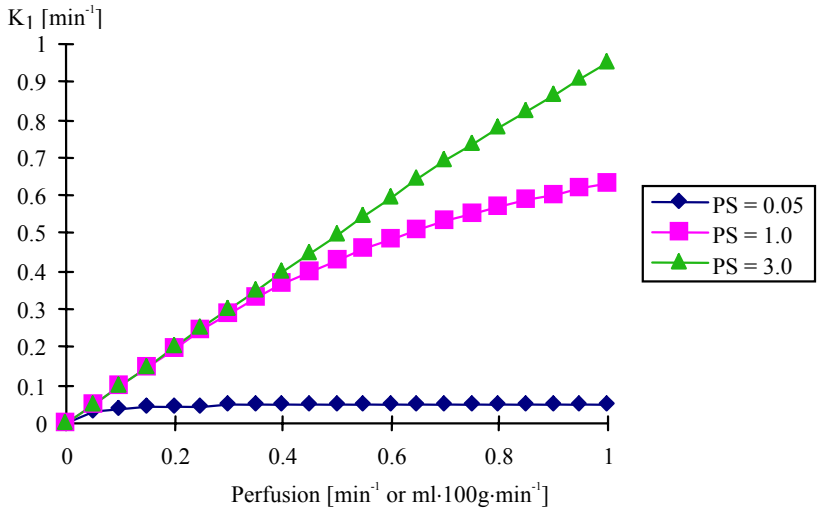

Figure 3-4. Relationship between perfusion F, K_1 and *PS*-Product

3.8 References

Crone, C. 1964, "The permeability of capillaries in various organs as determined by use of the indicator diffusion method", *Acta physiol scand*, vol. 58, pp. 292-305.

Delforge, J., Syrota, A., Bottlaender, M., Varastet, M., Loc'h, C., Bendriem, B., Crouzel, C., Brouillet, E., & Maziere, M. 1993, "Modeling analysis of [11C]flumazenil kinetics studied by PET: application to a critical study of the equilibrium approaches", *J.Cereb.Blood Flow Metab* , vol. 13,no. 3, pp. 454-468.

Ganong, W. F. 1991, *Review of Medical Physiology* Appleton & Lange, East Norwalk, Connecticut.

Pardridge, W. M. 1998, *Introduction to the blood-brain barrier. Methodology, Biology and Pathology.* Cambridge University Press, Cambridge.

Renkin, E. M. 1959, "Transport of Potassium-42 from Blood to Tissue in isolated Mammalian Skeletal Muscles", *Am J Physiol* , vol. 197, pp. 1205-1210.

4. Cerebral blood flow -single-tissue-compartment model

R.P. Maguire, Pfizer, USA.

4.1 Introduction

Of the total cardiac output of circa 5 $l \cdot min^{-1}$, some 14% (700 ml/min) of the blood flow goes to the brain which has only around 2% of the total body mass. This delivery system constantly supplies the brain with oxygen and other substrates of metabolism, which enter the brain by crossing the blood brain barrier. The neuronal activation studies, which have been reported in the last decades in the scientific and popular press, are based on the measurement of changes in regional cerebral perfusion and local large vessel blood flow. From these experiments, it is easy to see that changes in neuronal activity are very closely coupled with perfusion, although the exact mechanisms for the changes are not fully understood (Fox et al. 1988). Note that the term perfusion is used advisedly here to distinguish the blood flow per unit tissue from the physical flow in (ml/min), although in fact the term *flow* is used freely to denote both in the literature. This section aims to introduce the models that are the basis for regional cerebral flow determination with PET.

4.2 Flow tracers

In the late 1940's Kety and Schmidt (Kety & Schmidt 1948) developed a cerebral blood flow model, based on the Fick principle that the change in the amount of a substance in tissue is given by the arterio-venous concentration difference times the flow. It was noted in the previous chapter that, where a tracer has a high permeability surface product, the uptake rate of the tracer is be proportional to the flow defining a good tracer for the measurement of flow. It was also important for the Kety-Schmidt experiment, that the tracer is freely diffusible, so that the concentration of tracer in tissue, at all times, could be estimated using the partition coefficient. (The ratio of the tissue to venous blood concentration). Examples of tracers which fulfil this criteria are, Nitrous Oxide, Xenon, Butanol, Water, Iodoantipyrine. In PET [O-15]Water is the most widely applied blood flow tracer. This section will concentrate on methods for quantifying regional cerebral blood flow rCBF using this tracer.

4.3 Partition coefficient

The partition coefficient ρ, in the context of high extraction tracers, is the ratio of the tissue to venous blood concentration and was originally defined by Kety. A partition coefficient can be defined very generally as the ratio of the equilibrium concentrations between two compartments. In PET the partition coefficient nearly always refers to the concentration ratio between any compartment and arterial blood at equilibrium when $c_a=c_v$. The absolute value for water should depend on the water content of tissue and the water content of blood. It is important, however, to consider the units of measurement when comparing calculated values. (Herscovitch & Raichle 1985) quotes a value of 0.9 ml/g based on whole brain and blood water measurements equivalent to a value of 1.05 ml brain/ml blood, calculated by applying the densities. This should be close to the value measured by PET, much lower values have however been observed, (Iida et al. 1993) 0.77 ml/ml due to partial volume effects and many investigators have assumed the value 1.00. The effects of

an incorrectly assumed partition coefficient are most apparent for studies of long >120 s duration, so that the exact value may not be important (Kanno et al. 1991).

4.4 Kety - Schmidt model and operational equations for PET

The Fick principle, which is the basis of the Kety-Schmidt method is expressed in equation (4.1).

$$\frac{dq_t}{dt} = \Phi c_a - \Phi c_v \qquad (4.1)$$

q_t is the amount of tracer in tissue (mole)

Φ is the physical blood flow (ml/min).

In this equation, the symbol Φ has been used for flow to emphasise that this quantity has units ml/min and differs from the perfusion. The equation expresses a mass balance between the delivery, washout and accumulation of tracer in tissue. The ratio of the tissue activity concentration to the venous concentration is the volume of distribution (V_d):

By dividing the equation on both sides by the volume of tissue perfused and applying the, the more familiar form of equation (4.2) can be derived.

$$\frac{dc_t}{dt} = Fc_a - \frac{F}{V_d}c_t \qquad (4.2)$$

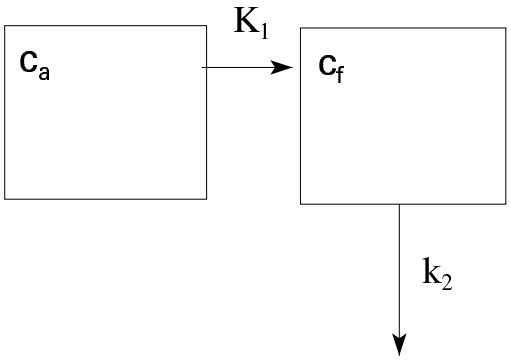

Figure 4-1. Single-tissue-compartment model for high extraction tracers (flow model)

F is the perfusion in units of min^{-1}.

V_d is the volume of distribution.

By solving equation (4.2) for C_t, the operational equation (4.3) for PET can be derived. See also the notes on delay and dispersion below.

$$c_t = Fe^{-\left(\frac{F}{V_d}\right)t} \otimes c_a \tag{4.3}$$

4.5 Decay

The half-life of O-15 is 123 s (decay constant 0.338). Note that the equations here as in other parts of this text are written in terms of the decay corrected tissue and blood activity concentrations. If equation (4.2) is rewritten for data which is not decay corrected, then an extra term appears on the right hand side to account for the fractional loss due to decay. Since the half-life of O-15 is comparable with the tissue delivery and washout constants, the effects of the decay are easily observable. Indeed the accurately known half-life of O-15 can be used as an internal standard. This is the basis for the steady state (Frackowiak et al. 1980) and weighted integration (Carson et al. 1986) methods.

4.6 Parameter estimation methods

There are a variety of methods for quantification of blood flow based on the equations (4.3). It can be used to directly fit measured data to the single-tissue-compartment model. This method has been used, with extensions to the model to account for delay and dispersion in order to determine these values for the whole brain. It also gives reasonable estimates for large individual regions of interest. Parametric images of flow (images in which the pixel values are proportional to flow) can be generated by assuming fixed delay and dispersion for the whole brain and applying equation (4.3) to generate an activity concentration vs. flow lookup table which is then used to convert integrated images between two time points (Lammertsma et al. 1990) .

Note that although the use of flow measurement to indicate neuronal activity was mentioned in the introduction, modelling methods are often not used to generate scaled flow images. Instead, integral images of the activity distribution in the cortex for 120 s after application of [O-15]Water are acquired. These are monotonically, though not linearly related to blood flow, so that regions with a higher flow will have a higher pixel value. It is claimed that the statistical methods used to determine the significance of observed changes are insensitive to the non-linear relationship between flow and pixel value.

4.7 Delay and dispersion

As previously noted, flow tracers and [O-15]Water are extracted from blood in the first passage through the capillary bed. It is important therefore to measure the time base of the input signal accurately (automatic blood sampling). The short delay of ~10 sec and the dispersion of the blood signal also become important. Accordingly, the operational equations given above must be modified to account for these effects. The dispersion can be modelled by a single compartment model, the relationship between the measured and actual arterial concentration time courses is given by equation (4.4):

$$\frac{dc_a^*(t)}{dt} = \frac{1}{\tau_d}\left(c_a(t-\Delta t) - c_a^*(t)\right) \tag{4.4}$$

Where c^*_a is the measured arterial concentration

c_a is the true arterial concentration

Δt is the delay in units of time.

and τ_d is the dispersion constant in units of min.

This equation can be solved and substituted into the previous operational equations to allow fitting for delay and dispersion. It can also be used to correct the delay and dispersion of the measured arterial concentration time course if τ_d and Δt are known.

4.8 Cerebral blood volume component

As will be shown later in the text, modelPaul.s of tracers with low extraction commonly include a term to account for the small intravascular blood component in the PET region of interest. In the human circulation, 54% of blood is in the veins and venules and around 14% in the arteries, arterioles and capillaries at any one instant (Ganong 1991). If a tracer exhibits 100% extraction then the venous blood will be in equilibrium with tissue so that the component of the blood volume will be indistinguishable from the tissue signal. Although an initial signal attributable to arterioles can be observed, its inclusion in the model is debatable.

4.9 References

Carson, R. E., Huang, S.-C., & Green, M. V. 1986, "Weighted integration method for local cerebral blood flow measurements with positron emission tomography", *J Cereb Blood Flow Metab*, vol. 6, pp. 245-258.

Fox, P. T., Raichle, M. E., Mintun, M. A., & Dence, C. 1988, "Nonoxidative glucose consumption during focal physiologic neural activity", *Science*, vol. 241,no. 4864, pp. 462-464.

Frackowiak, R. S., Lenzi, G. L., Jones, T., & Heather, J. D. 1980, "Quantitative measurement of regional cerebral blood flow and oxygen metabolism in man using 15O and positron emission tomography: theory, procedure, and normal values", *J.Comput.Assist.Tomogr.*, vol. 4,no. 6, pp. 727-736.

Ganong, W. F. 1991, *Review of Medical Physiology* Appleton & Lange, East Norwalk, Connecticut.

Herscovitch, P. & Raichle, M. E. 1985, "What is the correct value for the brain--blood partition coefficient for water?", *J.Cereb.Blood Flow Metab*, vol. 5,no. 1, pp. 65-69.

Iida, H., Jones, T., & Miura, S. 1993, "Modeling approach to eliminate the need to separate arterial plasma in oxygen-15 inhalation positron emission tomography", *J.Nucl.Med.*, vol. 34,no. 8, pp. 1333-1340.

Kanno, I., Iida, H., Miura, S., & Murakami, M. 1991, "Optimal Scan time of O-15 labelled Water injection method for measurement of cerebral blood flow", *J Nucl Med*, vol. 32, pp. 1931-1934.

Kety, S. S. & Schmidt, C. F. 1948, "The Nitrous Oxide Method for the Quantitative Determination of Cerebral Blood Flow in Man: Theory, Procedure and Normal Values", *J Clin Invest.*, vol. 27, pp. 476-483.

Lammertsma, A. A., Cunningham, V. J., Deiber, M. P., Heather, J. D., Bloomfield, P. M., Nutt, J., Frakowiak, R. S. J., & Jones, T. 1990, "Combination of Dynamic and integral methods for generating reproducible functional CBF images", *J Cereb Blood Flow*, vol. 10, pp. 675-686.

5. Energy metabolism (FDG) and the general two tissue compartment model

W. Müller-Schauenburg, University of Tübingen, Germany.

5.1 Introduction

This chapter deals with the important two-tissue-compartment model. It will concentrate on measurement of energy metabolism using the most common of these tracers 2-fluoro-2-deoxy-D-glucose (FDG).

5.2 The FDG model

FDG is an analogue of glucose that is extracted from arterial plasma and crosses the blood brain barrier into a free pool in tissue. In contrast to the previous section, the extraction from blood is low (Extraction: about 20%) so that the signal associated with K_1 depends more on permeability surface product than on perfusion. The substance is subsequently trapped by being metabolised in the mitochondria to FDG-6-PO4 by the action of the enzyme hexokinase. If the measurement time of the study is less than 1 hour, dephosphorylation (k_4) of the FDG-6-PO4 is not observed in the brain (Lucignani et al. 1993), corresponding to a condition k_4=0 in Fig. 5-1, the Sokoloff model for FDG (Sokoloff 1978).

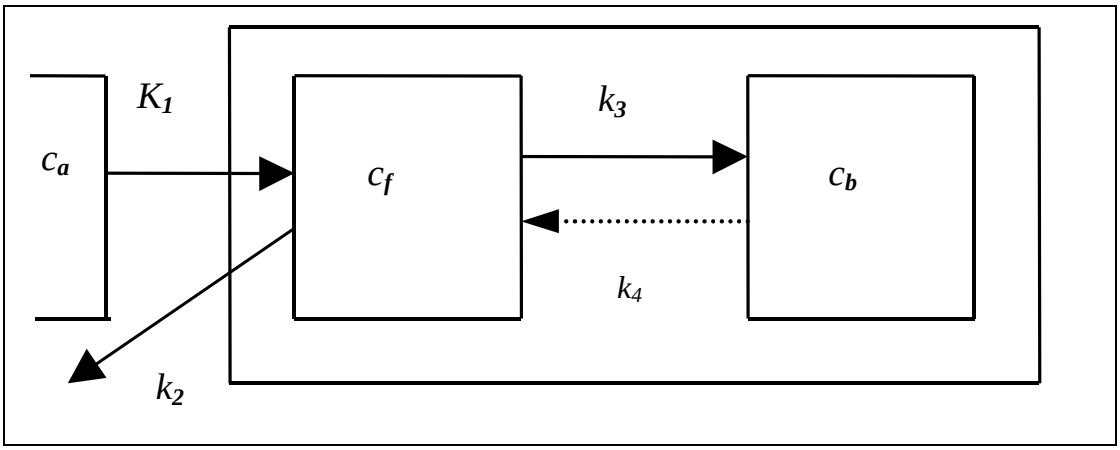

Figure 5-1: The standard FDG two-tissue-compartment model for the concentrations of arterial C_a, free C_f and bound FDG C_b The box around c_f and c_b reflects the PET-pixel summing c_f and c_b. The box around all could not be eliminated and may be interpreted as a PET-pixel including fractional blood volume.

The following equations correspond to.Figure 5-1

$$\frac{dc_f}{dt} = K_1 c_a - (k_2 + k_3) c_f + k_4 c_b \qquad \frac{dc_b}{dt} = k_3 c_f - k_4 c_b \tag{5.1}$$

Although the tracer is an analogue of glucose, it behaves different:
1. It becomes trapped after phosphorylation.
2. The influx/uptake of FDG is only proportional to the influx/uptake of glucose not numerically identical. The constant of proportionality is called the lumped constant *LC*, converting the metabolic rate constant K_i of FDG to the rate constant of glucose. Finally this rate constant is multiplied by the concentration of (inactive) glucose in blood c_p^{glu} , to obtain the (e.g.cerebral) metabolic rate for glucose:

$$CMR_{glu} = K_i\left(\frac{c_p^{glu}}{LC}\right) \tag{5.2}$$

The influx rate constant for FDG K_i

$$K_i = \frac{K_1 k_3}{(k_2 + k_3)} \tag{5.3}$$

may be understood intuitively by regarding the flow K_1 of tracer entering the free pool and being subdivided into two fractions, a metabolised/bound/irreversible fraction $k_3/(k_2+k_3)$ and a returning/reversible fraction $k_2/(k_2+k_3)$. This is a branching of the primary influx K_1 according to the relative speed of irreversible binding or phosphorylation (k_3) and venous clearance (k_2). The branching works for a stationary flow as well as for any individual tracer amount.

The description of the standard FDG-system ($k_4=0$) is obtained by solving equations (5.1) for $k_4=0$. This is done in two steps: 1. We investigate the system after a tracer amount proportional to K_1 has entered the first compartment, assuming $c_a = 0$ during the time of observing the system. We thus study a *response function* $IRF(K_1,k_2,k_3,t)$ (= IRF = impulse response function) describing the behaviour of the two tissue-compartments. 2. Subsequently we regard the full input time course c_a , i.e we decompose the input into many tiny tracer amounts and sum up all responses, i.e. we convolve the system response with the plasma input function:

$$c_{tis} = IRF(K_1, k_2, k_3, t) \otimes c_a \tag{5.4}$$

5.3 "The system behaviour" (IRF) of the two-tissue-compartment model for k_4=0.

Figure 5-1 and (5.1) for $k_4=0$ and $c_a = 0$ tell us that any tracer amount entering the free FDG-pool will be cleared exponentially with $-(k_2 + k_3)$. If we call the amount entered for shortly "K_1" the free FDG than decreases according to

$$c_f = K_1 e^{-(k_2+k_3)t} \tag{5.5}$$

Next we calculate c_b from c_f via (5.1)

$$c_b = k_3 \int_0^t c_f(\tau) d\tau = k_3 \int_0^t K_1 e^{-(k_2+k_3\tau)} d\tau = \frac{K_1 k_3}{(k_2+k_3)} \left(1 - e^{-(k_2+k_3)t}\right) \qquad (5.6)$$

The total signal ($c_f + c_b$) (as measured by PET) can then be decomposed in two ways:

$$K_1 \left(e^{-(k_2+k_3)t} + \frac{k_3}{(k_2+k_3)} \left(1 - e^{-(k_2+k_3)t}\right) \right) = \text{free+ bound} = \; c_f + c_b \qquad (5.7)$$

or equivalently (by summing up the two exponential terms and using 1-$k_3/(k_2+k_3)=k_2/(k_2+k_3)$, reflecting the fact that the reversible fraction $k_2/(k_2+k_3)$ and the irreversible fraction $k_3/(k_2+k_3)$ add up to unity)

$$K_1 \cdot \left(\frac{k_2}{(k_2+k_3)} e^{-(k_2+k_3)t} + \frac{k_3}{(k_2+k_3)} \right) \quad = \text{exponential + const} \qquad (5.8)$$

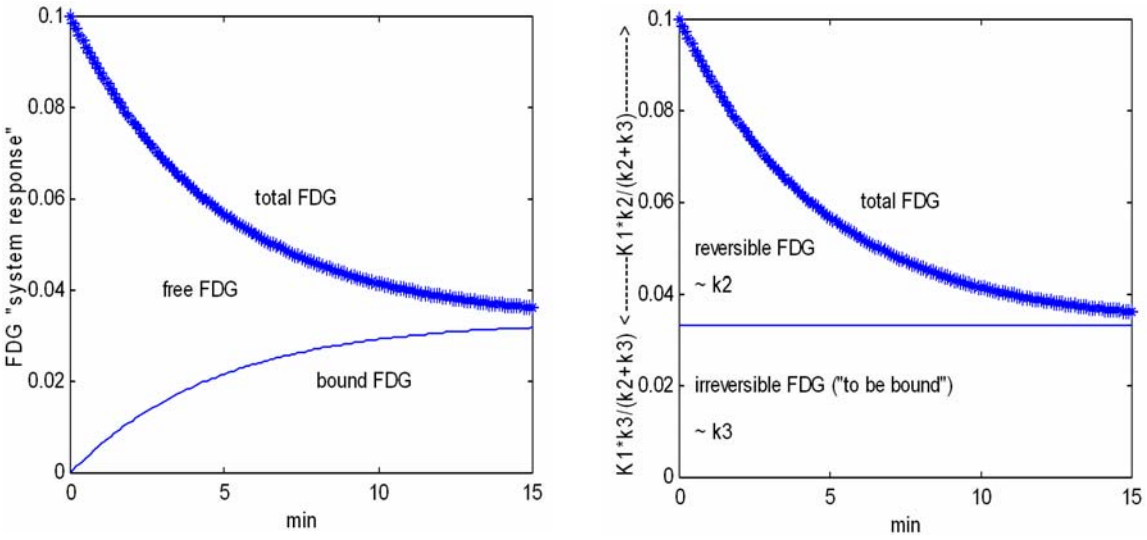

Figure 5-2: Sketch of equation (5.7) and (5.8) for $[K_1,k_2,k_3]=[0.1,0.14,0.07]$ min^{-1}.

5.4 The operational equation for FDG including k_4

The derivation in section 5.3 introduced the concept of dividing the response function into components, which are related to compartments of the original model. A derivation of the rigorous solution to the model for FDG uptake which includes k_4 (important in the liver for FDG and a basis for receptor modelling) will be cited first as a result (Phelps, Mazziotta, & Schelbert 1986, derivations in the following section, the fractional blood volume V_b being omitted in the derivations):

$$c_{tis} = \frac{K_1}{(\alpha_2 - \alpha_1)}\left[(k_3 + k_4 - \alpha_1)e^{-\alpha_1 t} + (\alpha_2 - k_3 - k_4)e^{-\alpha_2 t}\right] \otimes c_a + V_b c_a \tag{5.9}$$

$$\alpha_1 = \frac{(k_2 + k_3 + k_4) - \sqrt{(k_2 + k_3 + k_4)^2 - 4k_2k_4}}{2} \tag{5.10}$$

$$\alpha_2 = \frac{(k_2 + k_3 + k_4) + \sqrt{(k_2 + k_3 + k_4)^2 - 4k_2k_4}}{2} \tag{5.11}$$

Similarly we present an expression for the rCMRglu which will be derived afterwards. By assuming literature values for the rate constants, an estimate of the rate of glucose utilisation can be calculated based on a measurement c_t or c_{tis} made some time after equilibration of the plasma and free compartments.

$$CMR_{glu} = \frac{c_p^{glu}\left\{c_t - \frac{K_1}{(\alpha_2 - \alpha_1)}\left[(k_4 - \alpha_1)e^{-\alpha_1 t} + (\alpha_2 - k_4)e^{-\alpha_2 t}\right] \otimes c_a\right\}}{LC\frac{k_2 + k_3}{\alpha_2 - \alpha_1}\left(e^{-\alpha_1 t} - e^{-\alpha_2 t}\right) \otimes c_a} \tag{5.12}$$

(c_t=c_{tis} in 5.12 and 5.13, a formula editor problem, c_t=c_{tis}=c_{tissue}=c_g=c_{Gewebe})
(5.12) may be understood as

$$CMR_{glu} = \frac{c_p^{glu}}{LC}\frac{\left\{c_t^{meas} - c_f^{calc}\right\}}{\left(\frac{c_b^{calc}}{K_i^{calc}}\right)} \tag{5.13}$$

A first step to understand (5.13) is done by omitting the difference between measured and calculated: then c_{tis} -c_f = c_b in the nominator cancels with the c_b in the denominator, and K_i from denominator of the denominator gets to the nominator. This looks as if we put the constants K_1 to k_4 into the equation to get them out afterwards. But that isn't true. It is just opposite: The normalisation of the calculated c_b by the calculated K_i in the denominator eliminates part of its dependency on the k-values inserted from the literature. Especially the dependence of this ratio in the denominator of (5.13) on K_1 is completely eliminated. (The dependency of the calculated c_f on K_1 in the nominator of (5.13) remains.)

The normalisation gets even more transparent if we apply (5.13) to the case k_4=0 (including α_1=0 and α_2=k_2+k_3). Then the denominator of (5.13) reads as

$$\frac{c_b^{calc}}{K_i^{calc}} = \left\{1 - e^{-(k_2 + k_3)t}\right\} \otimes c_a \tag{5.14}$$

If we go even a step further and neglect the latest free FDG entered the free FDG-pool "for large *t*" the influence of the k-values form the literature disappear completely:

$$\frac{c_b^{calc}}{K_i^{calc}} = \int_0^t c_a \tag{5.15}$$

In summary: K_1 to k_4 from the literature eventually enter only in small correction terms.

An excellent review on the various methods of measuring glucose consumption was recently given by Wienhard 2002. He does not only cover single scan approaches of type (5.13) but as well the alternative line following

$$CMR_{glu} = \frac{c_p^{glu}}{LC} \frac{\left\{c_t^{meas}\right\}}{\left(\frac{c_t^{calc}}{K_i^{calc}}\right)} \tag{5.16}$$

described 1984 by Hutchins and 1983 as K-normalisation by Heiss et al., and its simplifying normalisation to the integral of c_a similar to (5.15) by Rhodes 1983, as well as the full dynamic evaluations. (For details of the literature see Wienhard 2002). Comparing the approaches (5.16) and (5.13) it is worth mentioning that pure variations in K_1 give exact results in the approach (5.16) while the varying ("wrong", non-literature) K_1 spoils at least a little bit the calculated correction-term c_f in (5.13). One may argue that pure variations in K_1 are academic because of physiologic covariations of K_1 and k_2, but one gets at least some insight into the mathematical structure of the approaches.

5.5 The full derivation of the 2-tissue compartment system

Solving the equations (5.1) means that we look for the system response to a sharp input that results in a start value c_f proportional to K_1. We assume for simplicity c_f(t=0)= K_1, and c_b(t=0)=0:

$$\frac{dc_f}{dt} = -(k_2 + k_3)c_f + k_4 c_b \qquad \frac{dc_b}{dt} = k_3 c_f - k_4 c_b \tag{5.17}$$

(The general solution for any c_a will then be given by the convolution of this system response IRF with c_a similar to (5.4).)

It will be shown that we get from (5.17) for c_f and c_b sums of two exponentials. As an intermediate step we have to look at solutions which contain only one single exponential term. We can be motivated to regard these funny solutions by looking at real time courses at late times, when the faster of the two exponentials has already disappeared. If we regard such mono-exponential terms for c_f and c_b we have a complete solution for (5.17) starting at t=0 with some values, where c_b is not zero. (These slowest exponential terms form

together a so-called *pseudoequlibrium*. This is a general name for the situation where we have *constant ratios* between the compartments, following the *slowest exponential* of the whole system considered, mostly an exponential originating from a slow decrease in the blood.). And we will see that even the two faster exponentials (with identical exponents in c_f and c_b) are a solution of (5.17). We will further see that by regarding these mono-exponential solutions, we get the equation for the exponents: a quadratic equation giving the two exponential constants α_1 and α_2 as its two solutions. The simplicity of the solution is based on the fact that for a mono-exponential term $e^{-\alpha t}$ the time derivative is just a multiplication by $-\alpha$, converting the differential equations (5.17) into ordinary equations, which get very simple, because the common exponential factor drops out (it can't be zero).

Let us start to consider the funny mono-exponential solutions and insert them into (5.17). In order to have a strict orientation, in which compartment I am, I want to be so free as to call the factors of the exponentials in the free compartment F and in the bound compartment B, i.e. $c_f = F\, e^{-\alpha t}$ and $c_b = B\, e^{-\alpha t}$ (sorry for the confusion with flows and Bmax). Now (5.17) reads as

$$-\alpha c_f = -\left(k_2 + k_3\right) c_f + k_4 c_b \qquad -\alpha c_b = k_3 c_f - k_4 c_b \tag{5.18}$$

or by reordering $\left(k_2 + k_3 - \alpha\right) c_f = k_4 c_b$ $\qquad k_3 c_f = +(k_4 - \alpha) c_b$ (5.19)

Since both equations in (5.19) must give consistent ratios c_b/c_f we get the predicted equation for α

$\left(k_2 + k_3 - \alpha\right) / k_4 = k_3 / (k_4 - \alpha)$ or better (avoiding denominators)

$\left(k_2 + k_3 - \alpha\right)(k_4 - \alpha) = k_3 k_4$ which reads in a sorted way as

$$\alpha^2 - \alpha\left(k_2 + k_3 + k_4\right) + k_2 k_4 = 0 \tag{5.20}$$

(5.20) has the solutions (5.10) and (5.11) and reflects two conditions

$$\alpha_1 + \alpha_2 = k_2 + k_3 + k_4 \qquad \alpha_1 \alpha_2 = k_2 k_4 \tag{5.21}$$

which are very helpful in converting different versions of equations from the literature.

We now have to bring to an end the construction of the solution of (5.17) starting from our two mono-exponential solutions $c_f = F_1 e^{-\alpha_1 t}, c_b = B_1 e^{-\alpha_1 t}$ and $c_f = F_2 e^{-\alpha_2 t}, c_b = B_2 e^{-\alpha_2 t}$ with

$$k_3 F_1 = (k_4 - \alpha_1) B_1 \quad \text{and} \quad k_3 F_2 = (k_4 - \alpha_2) B_2 \tag{5.22}$$

i.e. a rigid coupling of (F_1, B_1) and (F_2, B_2) from (5.19), and the initial conditions

$$F_1 + F_2 = K_1 \quad \text{and} \quad B_1 + B_2 = 0 \tag{5.23}$$

(5.22) and (5.23) are 4 equations for the 4 unknown constants F_1, F_2, B_1, B_2, It is now straightforward to start from a F_1, calculate $F_1 \rightarrow B_1 \rightarrow B_2 \rightarrow F_2$ as proportional to F_1, apply the initial condition $F_1 + F_2 = K_1$ to obtain F_1 and subsequently go for $F_1 \rightarrow B_1 \rightarrow B_2 \rightarrow F_2$ In detail this path reads as

$B_1 = F_1 k_3 / (k_4 - \alpha_1)$ from the coupling (5.22),

$B_2 = -B_1 = -F_1 k_3 / (k_4 - \alpha_1)$ via initial condition (5.23),

$F_2 = B_2 (k_4 - \alpha_2) / k_3 = -F_1 (k_4 - \alpha_2) / (k_4 - \alpha_1)$ via the coupling (5.22).

From the initial condition $F_1 + F_2 = K_1$ we then get

$$F_1 = K_1 \frac{k_4 - \alpha_1}{\alpha_2 - \alpha_1} \text{ and subsequently } B_1 = K_1 \frac{k_3}{\alpha_2 - \alpha_1} \ , \ B_2 = -K_1 \frac{k_3}{\alpha_2 - \alpha_1} \ , \ F_2 = K_1 \frac{\alpha_2 - k_4}{\alpha_2 - \alpha_1} \tag{5.24}$$

Now we have all parts and write down immediately the components of (5.9) and (5.12)

$$c_f = \frac{K_1}{\alpha_2 - \alpha_1} \left[\left(k_4 - \alpha_1 \right) e^{-\alpha_1 t} + \left(\alpha_2 - k_4 \right) e^{-\alpha_2 t} \right] \ , \ c_b = \frac{K_1 k_3}{\alpha_2 - \alpha_1} \left(e^{-\alpha_1 t} - e^{-\alpha_2 t} \right) \tag{5.25}$$

$$c_t = \frac{K_1}{\left(\alpha_2 - \alpha_1 \right)} \left[\left(k_3 + k_4 - \alpha_1 \right) e^{-\alpha_1 t} + \left(\alpha_2 - k_3 - k_4 \right) e^{-\alpha_2 t} \right] \tag{5.26}$$

It is a good and easy exercise to verify the initial conditions $c_f(0) = c_t(0) = K_1$, $c_b(0) = 0$ and to specialise (5.25) and (5.26) to $k_4 = 0$, using $\alpha_1 = 0$ and $\alpha_2 = k_2 + k_3$.

5.6 References

Lucignani, G., Schmidt, K. C., Moresco, R. M., Striano, G., Colombo, F., Sokoloff, L., & Fazio, F. 1993, "Measurement of Regional Cerebral Glucose Utilization with Fluorine-18-FDG and PET Heterogeneous Tissues: Theoretical Considerations and Practical Procedure", *J.Nucl.Med.*, vol. 34, pp. 360-369.

Phelps, M. E., Mazziotta, J. C., & Schelbert, H. R. 1986, *Positron Emission Tomography and Autoradiography (Principles and Applications for the Brain and Heart)* Raven, New York.

Sokoloff, L. 1978, "Mapping Cerebral Functional Activity with Radioactive Deoxyglucose", *Trends Neurosci.*, vol. 1, pp. 75-79.

Wienhard K 2002, "Measurements of glucose consumption using [^{18}F]fluorodeoxyglucose", *Methods,* vol 27, pp 218-225. (you may get the article via www.academicpress.com)

6. Linearisations

J. Van den Hoff, MHH, Hannover, Germany

6.1 Introduction

Compartment models describe the exchange of substances between the compartments with coupled linear differential equations. For these differential equations an analytical solution can be derived which represents the tissue's impulse response by a sum of exponential functions. Because all model parameters (with the exception of the influx parameter K_1) enter the solution in the exponents of the e-functions, the determination of the parameters from the evaluation of experimental data requires non-linear fitting procedures. Up to now, these procedures are too time-consuming if pixel-by-pixel estimates of the parameters are to be done. Alternative data evaluation schemes are thus called for.

The term "linearisation" will be used in the following discussion for all methods that enable the use of linear least-squares fitting procedures for the parameter estimation. These methods can be divided in two groups:

1. methods which are in principle exact and allow the determination of the complete set of transport constants of the model,

2. methods which make use of asymptotic properties of the tissue response and provide only restricted information, e.g. volumes of distribution V_d or metabolic rates.

The present discussion will be limited to the two most important models (as far as PET is concerned), namely the single-tissue-compartment model (including the Kety-Schmidt model) and the two-tissue-compartment model with irreversible binding (e.g. FDG) or reversible binding (e.g. radioligands).

6.2 Linearisation of the Kety-Schmidt model (CBF)

In order to facilitate comparisons with results given in the following sections, the equations are written with the standard symbols of the single-tissue-compartment model - influx rate is K_1, and washout rate is k_2. For a freely diffusible tracer, K_1 equals perfusion and the ratio $\rho = K_1/k_2$ represents the tissue-blood partition coefficient (ρ).

Integration of the model equation $\frac{dc_t}{dt} = K_1 c_a - k_2 c_t$ between zero and a (variable) time t yields:

$$c_t = K_1 \int_0^t c_a d\tau - k_2 \int_0^t c_t d\tau \qquad (6.1)$$

This is not really a solution of the model equation because the tissue concentration appears on both sides of the equation. Nevertheless, input and response can simply be treated as quantities that are known from the measurement. Therefore, equation (6.1) allows the

determination of the transport parameters from a linear two-parameter fit which can easily be performed even on a pixel-by-pixel basis. As far as the calculations are concerned, equation (6.1) should be used directly instead of one of several possible reformulations. With respect to a graphical visualisation of the results, however, it is advantageous to transform Eq. (6.1) to the equation of a straight line.

If equation (6.1) is divided on both sides by the time dependent integral of the arterial plasma concentration (Van den Hoff et al. 1993) the equation

$$y(t) = K_1 - k_2 x(t) \tag{6.2}$$

is obtained with

$$y = \frac{c_t}{\int_0^t c_a d\tau} \quad \text{and} \quad x = \frac{\int_0^t c_t d\tau}{\int_0^t c_a d\tau} \tag{6.3}$$

The following figure illustrates this transformation: on the left hand, one can see an idealised bolus injection for a freely diffusible tracer and the calculated tissue response for the indicated values of the parameters. A sampling rate of 5 seconds is assumed for both curves. On the right, one can see the transformed data according to Eq. (6.3).

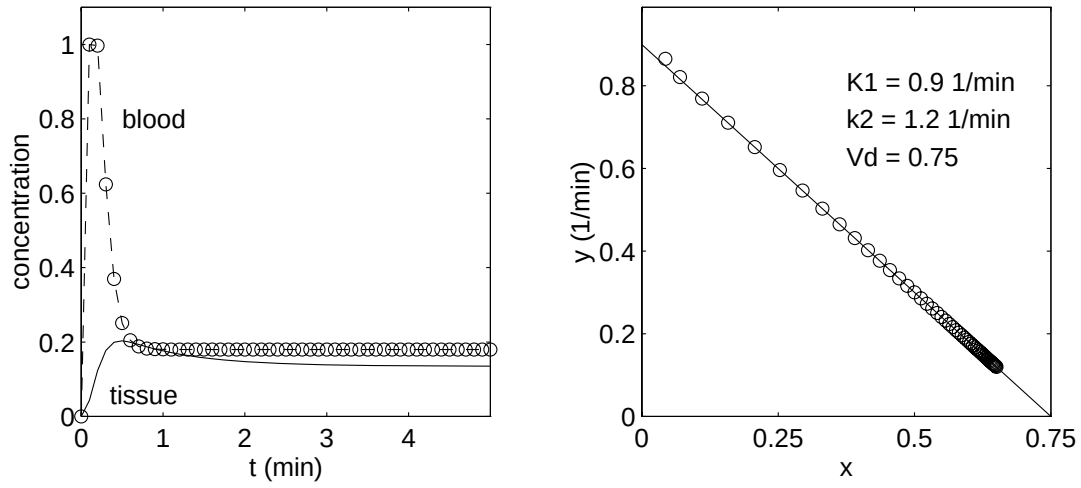

Figure 6-1. Linearisation of the single-tissue-compartment system

Obviously, the data follows the straight line perfectly (with the exception of the first two points, which are affected by small inaccuracies of the numerical integration of the time activity curves). The resulting straight line intercepts the y-axis at $y = K_1$ and the x-axis at

$$x = V_d = \frac{K_1}{k_2} \tag{6.4}$$

6.3 Linearisation of the FDG-model (Blomquist approach)

The linearisation procedure described for the single-tissue-compartment model can be extended to the general two-tissue-compartment model. For the case of irreversible binding (e.g. FDG) this has been demonstrated by Blomquist (Blomquist 1990). The derivation of this linearized form directly from the model equation is more difficult and will not be given here. Instead, use will be made of the known analytical solution:

$$c_t = c_f + c_b = \frac{K_1}{k_2 + k_3}\left(k_2 e^{-(k_2+k_3)t} + k_3\right) \otimes c_a \tag{6.5}$$

This equation shows that as far as the total tissue response is concerned the FDG-model is equivalent to a system of two independent ("decoupled") compartments u_1 and u_2:

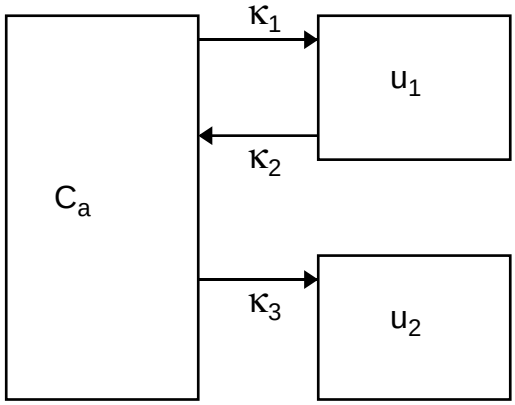

Figure 6-2. The decoupled model which is equivalent to the FDG model

From the analytical solution given above it follows that the transport constants of this new model are related to the parameters of the FDG model by

$$\kappa_1 = \frac{K_1 k_2}{(k_2 + k_3)} \tag{6.6}$$

$$\kappa_2 = k_2 + k_3 \tag{6.7}$$

$$\kappa_3 = \frac{K_1 k_3}{(k_2 + k_3)} \tag{6.8}$$

With these definitions one has, for all times, the identity:

$$c_t \equiv c_f + c_b \equiv u_1 + u_2 \tag{6.9}$$

that is, the measurement of c_t alone does not allow the two model configurations to be distinguished, namely the "true" FDG model with compartments c_f and c_b and the "decoupled" model with compartments u_1 and u_2. All properties of the total tissue concentration may therefore be derived from any of the two models.

The decoupled model now allows the following derivation of the Blomquist formula:

Because the reversible component u_1 represents a one compartment system it is treated with the linearisation derived in section 6.2. Similarly, the time dependence of the trapping component u_2 is simply defined by the integral influx:

$$\begin{aligned} u_1 &= \kappa_1 \int_0^t c_a d\tau - \kappa_2 \int_0^t u_1 d\tau \\ u_2 &= \kappa_3 \int_0^t c_a d\tau \end{aligned} \tag{6.10}$$

Moreover, $u_1 = c_t - u_2$. Substituting for u_2 the expression from Eq. (6.10) and integration yields

$$\int_0^t u_1 d\tau = \int_0^t (c_t - u_2) d\tau = \int_0^t c_t d\tau - \kappa_3 \int_0^t \int_0^\tau c_a d\tau' d\tau \tag{6.11}$$

From these relations the following formula for c_t is found:

$$\begin{aligned} c_t &= u_1 + u_2 \\ &= \kappa_1 \int_0^t c_a d\tau - \kappa_2 \int_0^t u_1 d\tau + \kappa_3 \int_0^t c_a d\tau \\ &= (\kappa_1 + \kappa_3) \int_0^t c_a d\tau - \kappa_2 \left(\int_0^t c_t d\tau - \kappa_3 \int_0^t \int_0^\tau c_a d\tau' d\tau \right) \\ &= K_1 \int_0^t c_a d\tau - (k_2 + k_3) \int_0^t c_t d\tau + K_1 k_3 \int_0^t \int_0^\tau c_a d\tau' d\tau \end{aligned} \tag{6.12}$$

This is the Blomquist formula. For the special case $k_3=0$ the Blomquist formula reduces to the linearisation of the single-tissue-compartment model. Contrary to the one compartment case the rate constants are no longer identical with the linear parameters of the equation. Therefore, the parameter estimation is performed by first determining the linear parameters (p_1-p_3) in front of the integrals in Eq. (6.12) with a linear three-parameter fit. In the second step the rate constants are determined:

$$c_t = p_1 \int_0^t c_a d\tau - p_2 \int_0^t c_t d\tau + p_3 \int_0^t \int_0^\tau c_a d\tau' d\tau \tag{6.13}$$

with $K_1 = p_1$, $k_3 = \frac{p_3}{p_1}$ and $k_2 = p_2 - \frac{p_3}{p_1}$

6.4 Linearisation of the FDG-model (Gjedde-Patlak Plot)

The linearisation method presented here has been described by (Gjedde 1982) in general terms and more specifically by (Patlak et al. 1983). Because the method is usually simply called the “Patlak plot", this terminology is adopted here.

The Patlak approach is a description of the behaviour of the FDG-model when the free FDG in tissue has reached its steady state so that the ratio of concentrations c_t/c_a becomes time independent. This approach therefore can only provide restricted information. The simplest derivation makes use of the decomposition into independent components, which has been discussed in section 6.3. If one looks at sufficiently late time points after the bolus passage of the tracer, the reversible component u_1 (which must not be confused with the free FDG pool in tissue, c_f) will also approach steady state with the tracer in the blood pool:

$$u_1 \to \frac{\kappa_1}{\kappa_2} c_a \tag{6.14}$$

The last equation is valid in a strict sense only if c_a becomes constant later. It is approximately valid if the variations of c_a are very slow in comparison to the time constant $1/\kappa_2$ of the reversible component, u_1.

Together with Eq. (6.10) this leads to

$$c_t = u_1 + u_2 \to \frac{\kappa_1}{\kappa_2} c_a + \kappa_3 \int_0^t c_a d\tau \tag{6.15}$$

This equation allows the determination of κ_3 as well as of the ratio κ_1/κ_2 from a linear fit. Dividing Eq. (6.15) by c_a on both sides results asymptotically in the equation of a straight line:

$$\frac{c_t}{c_a} \to \frac{\kappa_1}{\kappa_2} + \kappa_3 \frac{\int_0^t c_a d\tau}{c_a} = \frac{K_1 k_2}{(k_2 + k_3)^2} + \frac{K_1 k_3}{k_2 + k_3} \frac{\int_0^t c_a d\tau}{c_a} \tag{6.16}$$

A representation of the data in this form is called a Patlak-plot. It allows easily to assess whether the asymptotic regime of the tissue response has already been reached, cf. Fig. 6-3:

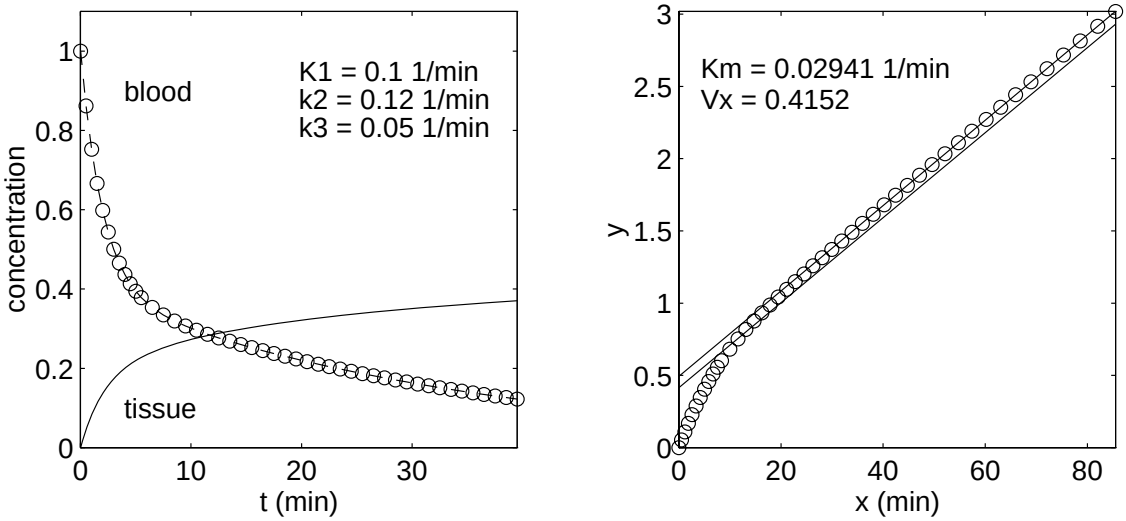

Figure 6-3. Time activity curves (left) and Patlak-plot (right). In the Patlak-plot two straight lines are indicated. The first one results from a least squares fit to the linear portion of the data points. The second one is the straight line expected from Eq. (6.16). The shift of the data points relative to the theoretically expected behaviour is explained by the rather rapid variations of c_a during the late phase.

In Figure 6-3 an input function is used which varies sufficiently slowly to reach steady state but the input function does **not** vary negligible slowly. Because the input actually *decreases* at late times, u_1 is *higher* than under equilibrium conditions because there must be a small net washout from the reversible component in this case. This results finally in an *increase* of the y-intercept in the Patlak-plot without modifying the interesting slope.

The time constant which controls the approach to steady state conditions is $(1/\kappa_2) = (k_2+k_3)$.

For brain investigations with FDG the time constant typically is about 5 min, so that a time of 20 minutes can be estimated for the approach to steady state. Note that this means "20 minutes after the rapid variations of c_a have stopped" and not "20 minutes after injection".

The most important parameter derived from the Patlak-plot is the metabolic rate K_i:

$$K_i = \kappa_3 = \frac{K_1 k_3}{k_2 + k_3} \tag{6.17}$$

which represents the steady state trapping rate of the tracer in tissue.

6.5 The Logan-plot

The so-called Logan-plot has been developed for evaluation of investigations with reversible radioligands (Logan et al. 1990). Its discussion will be restricted to the case of the two-tissue-compartment model. The original derivation concentrated on the behaviour of the system after steady state has been reached in the complete system. Because one of the time constants of the reversible two-tissue-compartment model is usually very long, this would be a rather strong limitation for a valid use of the Logan-plot. The

measurements would be either impractical, or simply impossible because of the limited half-life of the tracer. In practice, however, the Logan-plot can be applied before steady state in the whole system is obtained.

We will concentrate on the important special case where the rate of release from the metabolic compartment is much faster than the washout from tissue, that is we assume $k_4 >> k_2$.

Now, if one looks (again!) at the equivalent decoupled model:

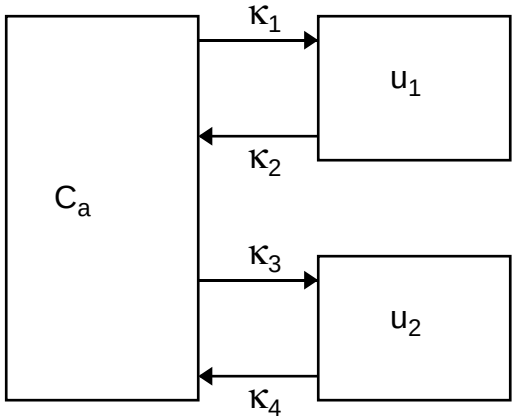

Figure 6-4. The decoupled model which is equivalent to the two-tissue-compartment model with reversible binding

The system response is given by:

$$c_t = \kappa_1 e^{-\kappa_2 t} + \kappa_3 e^{-\kappa_4 t} \tag{6.18}$$

The rate constants κ_2, κ_4 and the influx rates κ_1, κ_3 are fixed according to the analytical solution. In the presently investigated case (large k_4) the rate constants are approximately given by

$$\begin{aligned} \kappa_2 &= \frac{k_2 k_4}{k_2 + k_3 + k_4} \\ \kappa_4 &= (k_2 + k_3 + k_4) - \kappa_2 \end{aligned} \tag{6.19}$$

That is, κ_4 is much larger than κ_2. Now, it turns out that the influx κ_3 into the rapidly exchanging component u_2 approaches zero in the investigated limit of a large k_4. At the same time, the influx into the slowly exchanging component approaches the true influx K_1. Therefore, the total tissue response is essentially identical with u_1, and u_2 is approximately zero at all times. In other words: the system reacts as a single-tissue-compartment system and can therefore be treated analogous to section 6.2.

The identifiable parameters are

$$\kappa_1 \approx K_1, \text{ and } \kappa_2 \approx \frac{k_4}{k_3 + k_4} k_2$$

which is the effective washout of tracer from tissue (k_2 has been neglected in the denumerator). Because of the reversible transfer into a bound form the washout is reduced with respect to the true washout rate k_2. The ratio of the two parameters is obviously the total volume of distribution of the tracer:

$$V_d = \frac{\kappa_1}{\kappa_2} \approx \frac{K_1}{k_2} \frac{k_3 + k_4}{k_4} \tag{6.20}$$

which is identical to the expression which is obtained directly from the inspection of the original compartment model.

In the form originally proposed by Logan et al. the linearized equation is not plotted in the form that has been discussed in section 6.2 but rather by plotting:

$$\frac{\int_0^t c_t d\tau}{c_t} = -\frac{1}{\kappa_2} + V_d \frac{\int_0^t c_a d\tau}{c_t} \tag{6.21}$$

In this case, V_d can be identified with the slope of the resulting straight line. Two examples of Logan-plots are given in Fig. 5

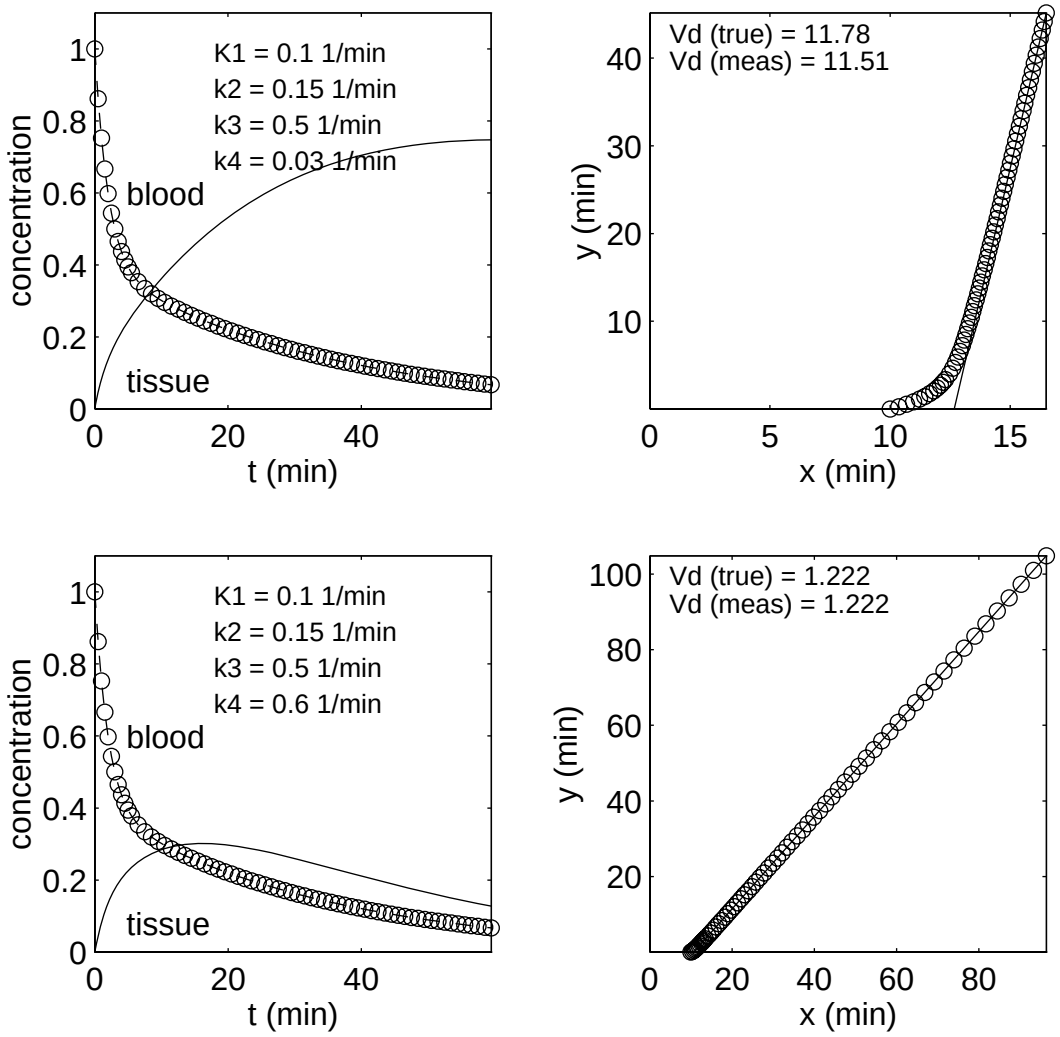

Figure 6-5. Logan plot for small k_4 (upper graph) and large k_4 (lower graph).

As has been mentioned in section 6.2 it is not advantageous to use such "graphical" representations for the numerical calculations instead of the original form.

In the first case (upper row) k_4 is very small. The plot becomes linear only at late times and the slope is not exactly identical with the volume of distribution. Nevertheless the linear behaviour is observed well before the system reaches steady state (the slow time constant being 2.5 hours in this example!). In the second case (lower row) k_4 is four times as large as k_2. This is the special case discussed above. Here, the plot is linear at **all** times which demonstrates that this case cannot be distinguished from a true single-tissue-compartment model. In terms of the decoupled model, this behaviour is explained by the approximately vanishing influx into the rapidly exchanging component u_2. In terms of the original model, the behaviour is explained by a cancellation effect of the contributing fast e-functions when adding up the contributions of free and bound tracer. The time dependence in the individual pools is by no means describable as a steady state situation.

6.6 References

Blomquist, G. 1990, "Maps of receptor binding parameters in the human brain - a kinetic analysis of PET measurements", *Eur.J Nucl Med.*, vol. 16, pp. 257-265.

Gjedde, A. 1982, "Calculation of cerebral glucose phosphorylation from brain uptake of glucose analogs in vivo: a re-examination", *Brain Res Rev*, vol. 4, pp. 237-274.

Logan, J., Fowler, J. S., Volkow, N. D., Wolf, A. P., Dewey, S. L., Schlyer, D. J., MacGregor, R. R., Hitzemann, R., Bendriem, B., Gatley, S. J., & Christman, D. R. 1990, "Graphical Analysis of Reversible Radioligand Binding from Time-Activity Measurements Applied to [N-[C-11]-methyl-(-)-Cocaine PET Studies in Human Subjects", *J.Cereb.Blood Flow Metab.*, vol. 10, pp. 740-747.

Patlak, C. S., Blasberg, R. G., & Fenstermacher, J. D. 1983, "Graphical evaluation of blood-to-brain transfer constants from multiple-time uptake data", *J Cereb.Blood Flow Metab*, vol. 3, pp. 1-7.

Van den Hoff, J., Burchert, W., Müller-Schauenburg, W., Meyer, G. J., & Hundeshagen, H. 1993, "Accurate local blood flow measurements with dynamic PET: Fast determination of input function delay and dispersion by multilinear minimization", *J Nucl Med*, vol. 34, pp. 1770-1777.

7. *In vivo* PET imaging understood from the perspective of *in vitro* receptor binding

Robert B. Innis, MD, PhD, National Institute of Mental Health, Bethesda, Maryland, USA

7.1 Introduction.

The purpose of this chapter is to better understand *in vivo* receptor binding based on *in vitro* receptor binding theory. This explanation may be particularly helpful for individuals, like myself, who were trained with *in vitro* receptor methods and receptor-oriented pharmacology and then wish to apply similar methods to the *in vivo* situation.

The following basic concepts will be explained:

1) *In vitro* receptor binding concepts will be explained from a mathematical perspective to calculate:

a) density of receptor sites: B_{max}

b) affinity of each receptor: $1/K_d$

c) product of density and affinity: BP (binding potential) = B_{max}/K_d.

2) Two basic *in vitro* methods will be described (equilibrium and kinetic approaches) as well as the concept that the kinetic rate constants can be used to predict equilibrium values.

3) A two-chamber device with a semi-permeable membrane will be used as a simple model of *in vivo* receptor binding. Similar to the *in vitro* methods, both kinetic and equilibrium methods will be used to estimate BP.

For an excellent review of *in vitro* receptor binding methods and data analysis, see (Wharton & Polak 1993).

7.2 Derivation of "Michaelis-Menten" equation from Law of Mass Action.

The theory of *in vitro* receptor binding derives from earlier studies of enzyme kinetics in which a substrate binds to an enzyme and is converted to a product. For receptor studies, a radioligand is used instead of a substrate, and just the binding itself of the ligand to the receptor is viewed as the product. For this reason, quotation marks will be used to refer to the equivalent of the "Michaelis-Menten" equation for receptor binding which will now be derived.

The Law of Mass Action for ligand binding is described as follows:

$$L + R \underset{koff}{\overset{kon}{\rightleftharpoons}} LR \qquad (7.1)$$

The binding described above is reversible. The ligand (L) does not form a covalent bond with the receptor (R). Instead, it is adsorbed to the receptor and attracted by non-covalent forces, such as electrostatic interactions, hydrogen bonding, and similar lipophilicity. Binding of L and R forms the ligand-receptor complex (LR). The ligand can both "bind to" and "unbind from" the receptor. The terms for these two processes are "association" and "dissociation." The rate constant of association is termed k_{on}; and the rate constant of dissociation is k_{off}.

$$\text{Rate of association} = k_{on}\,[L]\,[R] \tag{7.2}$$

$$\text{Rate of dissociation} = k_{off}\,[LR] \tag{7.3}$$

where [] is used to demote molar concentration – e.g., nM or nmol/L. It's useful to review the units of these equations. Rate is measured as a change in concentration per unit time – e.g., nM min^{-1}. By rearranging the equations, we can see that units of the rate constants are:

$$k_{on}: nM^{-1}\ min^{-1}$$

$$k_{off}: min^{-1}$$

Please note that the rates can change over time, but the rate constants (k_{on} and k_{off}) are just that: constant over time. One easy way to understand these rate constants is to consider the meaning of $k_{off} = 0.1\ min^{-1}$. This value corresponds to 10% per min - and means that if the free concentration of L was kept close to zero, then the concentration of LR would constantly decrease by 10% per minute of whatever is present at that time.

When ligand L is mixed with receptor R, the rate of association is initially greater than the rate of dissociation, since [LR] is initially 0, and the rate of dissociation would, therefore, equal 0. Over time, the concentration of L and R will decrease, and, thus, the rate of association will decrease. Conversely, the concentration of LR will increase, and the rate of dissociation will increase. At some point, the rates of association and dissociation will be equal, and that special condition is called a dynamic equilibrium. The equilibrium is dynamic, because both the association and dissociation rates are >0. That is, although equilibrium has been reached, the ligand continues to bind and rebind to the receptor, but with no net change in the concentration of L, R, or LR.

Equilibrium implies: Rate of association = Rate of dissociation

$$k_{on}\,[L]\,[R] = k_{off}\,[LR] \tag{7.4}$$

With rearrangement:

$$\frac{koff}{kon} = \frac{[L][R]}{[LR]} = K_d \tag{7.5}$$

This ratio of two rate constants must also be a constant and is defined as K_d, the dissociation constant. Please note that the units of K_d are those of concentration (nM).

At this point, we must re-define terms into the units typical of the "Michaelis-Menten" equation for receptor binding. The total concentration of receptors (B_{max}) equals those with ligand bound and those that are not bound.

$$B_{max} = [LR] + [L] \tag{7.6}$$

Furthermore, we will re-define [LR] as the concentration of bound ligand (or B), and the [L] will be referred to as the free concentration of ligand F.

$$\text{Let } [LR] = B \quad \text{and} \quad [L] = F \tag{7.7}$$

Thus:

$$B + [R] = B_{max} \tag{7.8}$$

$$[R] = B_{max} - B \tag{7.9}$$

Define a new term:

$$B_{max}' = B_{max} - B \tag{7.10}$$

B_{max}' is referred to as the concentration of "available" receptors. That is, a receptor that already has a ligand bound to a sole site is no longer available to bind another ligand.

From equation (7.5),

$$K_d = \frac{k_{off}}{k_{on}} = \frac{F\,B_{max}'}{B} \tag{7.11}$$

substituting from (7.10) and rearranging:

$$K_d = \frac{F(B_{max} - B)}{B} \tag{7.12}$$

$$K_dB = F(B_{max} - B) = FB_{max} - FB \tag{7.13}$$

$$K_dB + FB = FB_{max} \tag{7.14}$$

$$B(K_d + F) = FB_{\max} \tag{7.15}$$

$$B = \frac{B_{\max} F}{K_d + F} \tag{7.16}$$

The plot of the Michaelis-Menten equation as B vs. F (Bound vs. Free) is hyperbolic with an asymptote at B_{max}. That is, if enough ligand is added to saturate all receptors, then bound ligand will equal the maximal concentration of receptors B_{max}. Another important point on this curve is the Free concentration at 50% B_{max} (shown on Figure 7-1). When B = 50% of B_{max}, then equation (7.16) can be solved to show that F = K_d. In another words, K_d equals the concentration of free ligand required to saturate 50% of receptors. We can now understand why affinity is inversely related to K_d. If the affinity of the ligand is high for a particular receptor, then only a low concentration is needed to bind many the receptors. In this manner, affinity = $1/K_d$; and the ratio of B_{max} / K_d is equivalent to B_{max} * affinity.

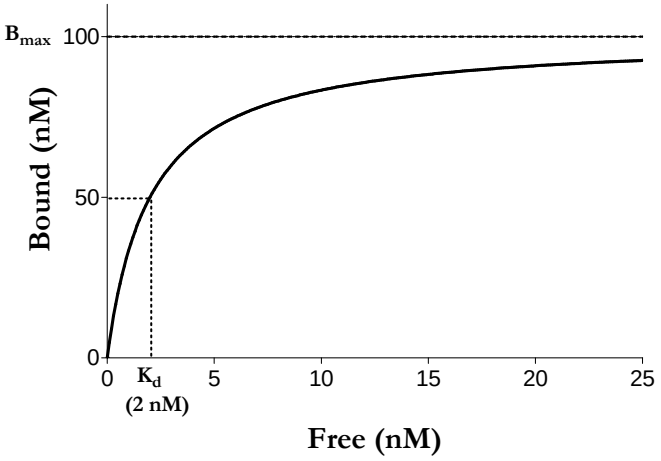

Figure 7-1. Saturation binding curve. As the concentration of Free ligand is increased, more and more of the receptors become bound with the ligand. When all receptor sites are saturated, Bound = B_{max}. In addition, the dissociation constant K_d equals the Free ligand concentration at 50% of maximal binding. For this hypothetical situation, B_{max} = 100 nM and K_d = 2 nM.

Equation (7.16) can be simply rearranged to provide the slope of the saturation curve – i.e., B/F.

$$\frac{B}{F} = \frac{B_{\max}}{K_d + F} \tag{7.17}$$

At low concentrations of free ligand (i.e., when F<<K_d):

$$\frac{B}{F} = \frac{B_{max}}{K_d} = B_{max} * affinity \qquad (7.18)$$

where affinity = $1/K_d$.

7.3 Binding Potential.

The slope (B/F) of the initial portion of the curve (Figure 7-2) is a special constant that reflects the ratio of B_{max} / K_d. Please note that a sizeable portion of the initial binding curve is, in fact, linear. That is, if the free level is doubled, then the bound level is doubled. Most PET neuroreceptor studies are performed at minuscule free levels of radiotracer so that the ratio of bound to Free is a constant. As shown above, this special constant can also be viewed as the product of B_{max} and affinity. Although not commonly considered with *in vitro* studies, this number is particularly important for *in vivo* imaging. In PET, this number is termed the "binding potential" or BP. If two individuals differ in binding potential for a particular ligand, the one with a higher binding potential could have either more receptors (B_{max}) or higher affinity or both. In general (but not always), we assume the affinity is the same and that differences in BP reflect differences in B_{max}.

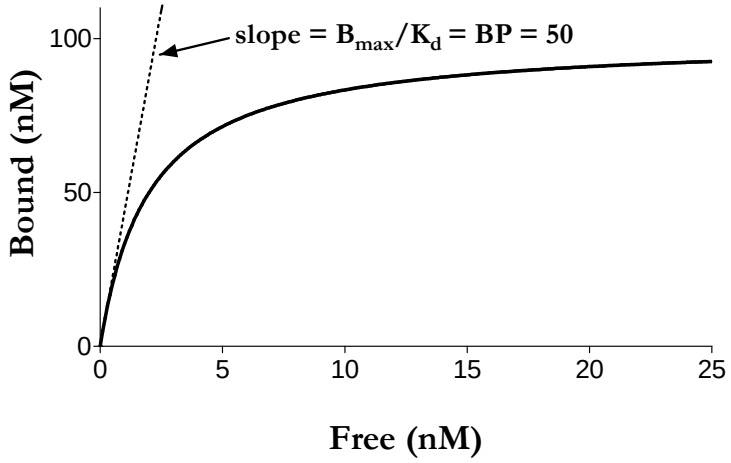

Figure 7-2. Initial slope of the saturation-binding curve. The slope (or derivative) of this curve is B/F. The initial slope is quite linear until about 20% Bound. When B and F are quite low, the initial slope B/F = B_{max} / K_d.

Binding Potential is much more commonly used term in PET studies than *in vitro* research, because the ligand is administered in "tracer" doses from a pharmacological perspective. The tracer occupies only a small percentage of receptors. Although Bound and Free are quite low, their ratio is a constant. Thus, even if the dose were doubled or cut in half, the ratio of Bound to Free should be constant. *In vitro* studies commonly study multiple concentrations of Free and can thereby derive separate estimates of B_{max} and K_d. At tracer doses typically used in PET, only the ratio of these two values (i.e., BP) can be measured.

Another important point with regard to the Michaelis-Menten equation is to understand the difference between B_{max} and K_d. B_{max} refers to the total number of receptors, and K_d refers to the affinity of any single receptor. That is, K_d is a property of the receptors, and for most PET studies, all receptors are assumed to have same affinity. This equality of affinity can be demonstrated by a linear Scatchard plot (see below). Thus, changes in binding potential are typically interpreted as changes in B_{max}, although additional evidence supporting this interpretation is always helpful.

7.4 Scatchard Plot: linearisation of the "Michaelis-Menten" equation.

The saturation binding curve generated from the Michaelis-Menten equation is a curved line – specifically, an hyperbola. The equation can be re-arranged into a linear form and its graph is called a Scatchard plot. Rearranging the Michaelis-Menten equation provides:

$$\frac{B}{F} = \left(\frac{-1}{K_d}\right)B + \frac{B_{max}}{K_d} \qquad (7.19)$$

This linear equation has the general form of y = mx + b, where y = B/F, m (slope) = (-1/K_d), and b (y-intercept) = B_{max}/K_d. Thus, the y-intercept of the Scatchard plot is BP.

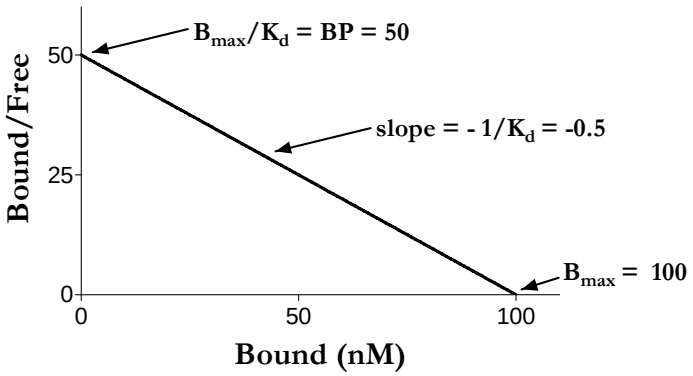

Figure 7-3. Scatchard Plot. The hyperbolic saturation binding curve can be re-plotted as a straight line via the Scatchard plot. The x-intercept is B_{max}; slope = -1 / K_d; and the y-intercept= B_{max} / K_d = BP.

7.5 Radiotracer methods.

The term "tracer" has distinct and yet overlapping meanings in nuclear medicine and pharmacology. In the nuclear medicine field, a radio-"tracer" is used to monitor a larger group process. The fate of the radiotracer reflects the fate of the larger group. George de Hevesy received the Nobel Prize in Medicine in 1943, in large part because of work to develop the radiotracer method. A perhaps apocryphal story is told concerning Dr. de Hevesy during his days as a junior scientist living in a cheap boarding room that included meals. He strongly suspected that the beef hash served on Friday was merely recycled

from the roast beef served on Monday. Although the cook denied this and said the hash was made with fresh beef Dr. de Hevesy decided to test his hypothesis. He is said to have added radioactivity to the roast beef on Monday and recovered some of the activity in the hash on Friday, thereby confirming the recycling of the meat. Whether true or not, this story can be used to illustrate the radiotracer method. Let's assume that he uniformly distributed the radioactivity in the roast beef on Monday. If he recovered 50% of the activity on Friday, then he would conclude that the cook had recycled 50% of the beef. The recovery of the tracer is not the important point. Instead, the relevant target is the amount of beef that has been recycled. By using uniform distribution of the radiotracer, the system was established whereby the percentage recovery of the tracer reflected the percentage recycling of the beef. That is, the nuclear medicine usage of the term tracer is that the radioactive label is used to monitor a larger group process. For PET neuroreceptor studies, the radiotracer is used to monitor all the targeted receptors. Even though only a small percentage (perhaps <1%) of receptors are occupied, PET provides numbers that reflect the total pool of receptors. For example, baseline studies provide measures of BP, which as described above reflect the total number of receptors (B_{max}). In addition, if a subject is imaged twice, changes in the ligand uptake are thought to reflect the total pool of receptors. For example, if a subject is imaged at baseline and then following administration of a non-radioactive drug that binds to the receptor, then changes in the tracer reflect occupancy of the receptor by the drug. For example, if drug treatment reduces tracer uptake by 50% (for example, from labelling of 1 % of receptors to 0.5% of all receptors), then we conclude that the non-radioactive drug occupies 50% of all the receptors.

The pharmacological use of "tracer" refers to doses of the drug that are so low that they lack pharmacological effects. For example, if the minimally effective dose of a drug must occupy at least 5% of the receptors, then doses lower than that would be considered tracer doses. Nuclear medicine uses the term "tracer" for an agent that reflects the fate of a larger group of homogeneous targets, and pharmacology uses "tracer" for a minuscule dose that lacks pharmacological effects. Both uses of term apply in PET neuroreceptor imaging. In fact, each use of "tracer" is a sine qua non for the other. As described above, in order for the typical Binding Potential value to be a constant for a particular subject, then F and B levels must be low – i.e., tracer pharmacological doses must be administered. Moreover, when tracer pharmacological doses are used, the radiotracer will provide a meaningful and reproducible measure that reflects the disposition of all the target receptors.

In summary, the term "tracer" has the meaning in pharmacology of a dose so low that it lacks pharmacological effects. Its typical meaning in nuclear medicine is a dose that is low enough so that the disposition of the tracer reflects that of all the targets. That is, the mass dose is not high enough to interfere with or modify the target itself. Let's consider the specific situation of PET receptor studies. When the tracer is administered, a small percentage of the ligand is usually radiolabelled, with the vast majority of ligand non-radioactive. A typical ^{11}C-labeled radioligand may have only 1 in 1,000 molecules with ^{11}C, and the other 999 have ^{12}C. These non-radioactive ligand molecules are called carrier". If the specific activity of the radiotracer is low, then it will have an even higher percentage of non-radioactive ^{12}C-labeled molecules. So, for the injection of equal amount so activity, the preparation with lower specific activity will have a higher mass dose of non-radioactive compounds. In the extreme, with extraordinarily low specific activity, all the carrier molecules will occupy / saturate the receptors and no radioligand will bind. That is, there will be no specific binding to be measured with PET. How much total mass dose can be

tolerated for neuroreceptor studies so that it is still a "tracer" dose that will reflect the disposition of entire pool of receptors? This question has no clear cut-off and depends upon how much error can be tolerated in the specific study. For in vitro binding, a commonly used guideline is that tracer conditions are achieved if <10% of receptors are bound. That is, most in vitro experimenters are happy to be 90% correct. The in vivo situation is more complex, has several sources of error, and may not tolerate significant receptor occupancy as yet another source of variability. Again without clear consensus, many PET neuroreceptor investigators would say that >10% receptor occupancy is clearly unsatisfactory; <5% occupancy is acceptable; and <1% is ideal.

7.6 Kinetic vs. equilibrium measurements.

It is important to understand that we've discussed two different ways of determining K_d and B_{max}: kinetic and an equilibrium methods. Furthermore, the kinetic parameters can be used to predict what the equilibrium values would be if the system were allowed to reach equilibrium. Let's review each method.

7.6.1 Association

The central equations for the kinetic methods are described in equations (7.2),(7.3) and (7.4). The association data are generated by mixing ligand and receptor together and then measuring the concentration of L and LR over time. If the experiment uses tracer doses of the radioligand, then only a small percentage of receptors become bound to ligand. That is, the available receptors [R] are essentially constant during the course of the association experiment and equal to B_{max}. L and LR are typically separated at various times after initial incubation by filtration, in which the free ligand L goes through the filter and LR is retained by the filter. Since this experiment measures the rate of association as well as [L] and [R], the association rate constant k_{on} can then be calculated (equations (7.2) and (7.3)). Please note that the filtration method is based on the fact that receptors are much larger than the ligand and often come with chucks of surrounding tissue membrane. Thus, when the solution is passed through a porous filter, water and the small ligand pass through, but the receptor (both R and RL) are trapped and retained by the filter, and the retained radioactivity can be measured.

7.6.2 Dissociation

For the dissociation experiment, L and R are incubated together until binding reaches equilibrium. At time 0 of the dissociation, excess non-radioactive displacer is added to the test tube to occupy all the receptors. [LR] is measured after filtration at various times after beginning the dissociation. This design assumes that whenever a bound ligand comes off the receptor, it never binds again, because the large excess of non-radioactive displacing agent will occupy and block the site for a radiolabelled compound. Since the rate of dissociation is then measured as well as [LR] over time, the dissociation rate constant can then be calculated according to equations (7.2) and (7.3).

These two kinetic experiments generate the association and dissociation rate constants: k_{on} and k_{off}. As described in equation (7.5), the ratio of these two constants is the equilibrium dissociation constant, which itself is inversely related to affinity. Thus, equilibrium values can be predicted from kinetic rate constants. Furthermore, if the kinetic experiments are

performed at varying concentrations of ligand (F), then B_{max} can also be estimated from kinetic experiments.

7.7 Summary of *in vitro* methods.

Binding Potential is the most common outcome measure for PET neuroreceptor studies, because the radioligand is administered at "tracer" doses, in both the nuclear medicine and pharmacological senses. At these low doses, only the ratio of B_{max} to K_d can be measured. Thus, PET seeks to measure the initial slope of the saturation binding curve (Figure 7-2), which is equivalent to y-intercept of the Scatchard plot (Figure 7-3). The next section will show how these *in vitro* methods can be extended to *in vivo* receptor binding using a simple two-chamber device.

7.8 Two-chamber model of *in vivo* receptor binding.

Consider the following two-chamber model with a semi-permeable membrane in the middle. The volumes of each chamber are identical, and the membrane will be permeable to small ligands like radioligands but not to large proteins such as albumin. What would happen if we instantaneously added a tracer at 4 nM concentration into chamber and at a well-mixed uniform concentration? Let C1 be the concentration of tracer in chamber 1, and C2 the concentration of tracer in chamber 2. Of course, the tracer would diffuse equally in both chambers and ultimately reach a concentration of 2 nM on both sides. The concentration gradient would drive the rate of exchange between the two chambers. When equilibrium is achieved, the concentrations of tracer are the same on both sides of the membrane, and no further net flow will occur. However, note that this is a dynamic equilibrium, so that tracer flows from chamber 1 to chamber 2 and vice versa, but the rate of flow is the same in both directions.

Similar to the *in vitro* equations (7.2) and (7.3) above:

Forward rate (from chamber 1 to chamber 2) = $k_1 C_1$

Reverse rate (from chamber 2 to chamber 1) = $k_2 C_2$

Equations of this type are first order and follow an exponential process, as shown in Figure 7-4. The equilibrium value for both chambers is 2 nM. Because it's an exponential process, the concentration will reach half way to its equilibrium value in one half-life ($T_{1/2}$). Thus, after one $T_{1/2}$, C_1 will go from 4 to 3 nM – i.e., half the way to 2 nM. Similarly, in the next $T_{1/2}$, C_1 will go from 3 to 2.5 nM – i.e., half the way from 3 to 2 nM.

Exp #1: Initial Conditions:

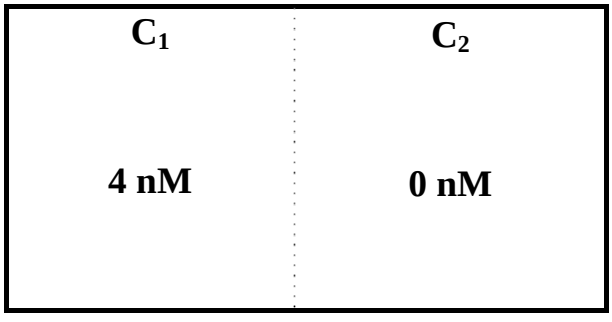

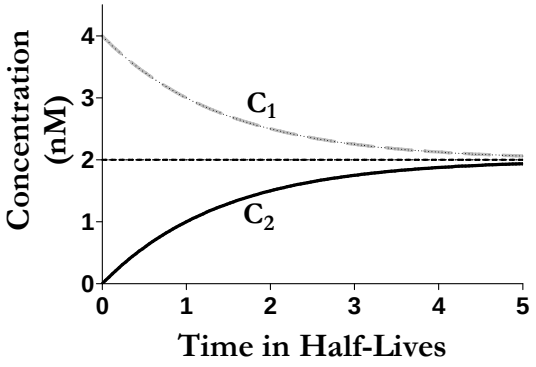

Figure 7-4. Time course to reach equilibrium. The volumes of both chambers are the same. Thus, the final concentration of tracer will be 2 nM distributed equally in both chambers. The concentrations in both chambers change in an exponential fashion – i.e. they reach half way to the equilibrium goal within the subsequent $T_{1/2}$.

Now let's consider a slightly different situation in which albumin is added to chamber 2 at a concentration such that it will bind 2/3rds of the tracer. That is, within the right hand chamber, 1/3 of the tracer will be free, and 2/3 will be bound to albumin. When equilibrium is achieved, the level of Free tracer (not total tracer) will be the same on both sides of the membrane. That is, the component of the ligand that will have the same concentration is the one that is available to cross the membrane – i.e., the Free tracer. Since albumin cannot cross the membrane, then the tracer bound to albumin is bound up and thereby removed from the concentration gradient that drives the flow of tracer from one side to the other. To understand this new situation, we'll need nomenclature to describe the free and bound component of tracer. In addition to C_2 as a measure of the Total concentration of tracer in chamber 2, we will also need a term for the concentration of Free tracer, as well as the fraction of Total tracer that is Free.

F_1 = concentration of Free tracer in chamber 1

F_2 = concentration of Free tracer in chamber 2

f_1 = fraction of Total tracer in #1 that is free

f_2 = fraction of Total tracer in #2 that is free

$$F_1 = f_1 C_1 \tag{7.20}$$

$$F_2 = f_2 C_2 \tag{7.21}$$

In this particular situation, $f_1 = 1$ (or 100% free) and $f_2 = 1/3$ (or 33%). The equilibrium concentration of tracer in chamber 2 will be 3 nM, and that in chamber 1 will be 1 nM. Under equilibrium conditions, $F_1 = F_2 = 1$ nM.

$$F_1 = f_1 C_1 = 1 * 1 \text{ nM} = 1 \text{ nM}$$

$$F_2 = f_2 C_2 = 1/3 * 3 \text{ nM} = 1 \text{ nM}$$

Under equilibrium conditions, the forward and reverse rates are the same, but are the transfer rate constants k_1 and k_2 also the same? From equation (7.4):

Forward rate = Reverse rate

$$k_1 C_1 = k_2 C_2 \tag{7.22}$$

$$\frac{k_1}{k_2} = \frac{C_2}{C_1} = \frac{3}{1} \tag{7.23}$$

Thus, the rate constants (expressed relative to total concentration) are inversely related to the Total concentration of tracer. Although the equilibrium value of C_2 is three times that of C_1, its reverse rate constant is 1/3 that of the forward rate constant – leading to equal overall forward and reverse rates.

Exp #2: Initial Conditions:

C_1	C_2
4 nM	**0 nM**
$f_1 = 1$	$f_2 = 1/3$

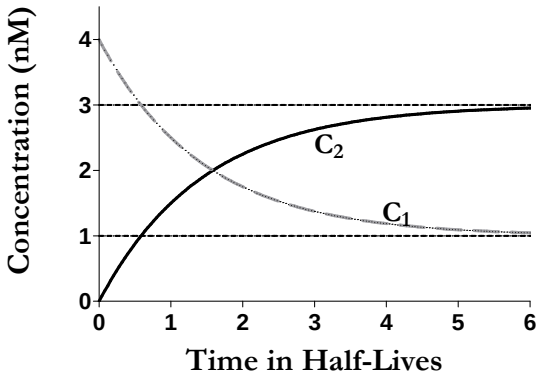

Figure 7-5. Time course to reach equilibrium with albumin in chamber 2. The volumes of both chambers are the same, but albumin adsorbs Ligand in chamber 2 until 2/3rds is bound. Tracer will continue with a net flow into chamber 2 until Free levels are equal on both sides of the semi-permeable membrane.

NOTE: As described in the section on nomenclature, the number of compartments in a model is determined by how many exist in the tissue with the exclusion of the vascular compartment. Following this consensus, the simple model described above might be referred to as a one-compartment model. However, in this situation, neither chamber has

been identified as tissue or vasculature. So, for this unrealistic but heuristic example, the device is referred to as a "two-chamber" model.

7.9 Binding Potential.

What is the Binding Potential of the albumin? As shown for *in vitro* techniques, BP = B/F at equilibrium (equation (7.18)). So, within chamber 2, the ratio of B/F = 2/1 = 2. Please note that the TOTAL concentration of tracer in chamber is 3 nM, with the components of B = 2 nM and F = 1 nM. Furthermore, if this binding is performed under tracer conditions, then $B/F = B_{max} / K_d$ (equation (7.18)). Thus, Binding Potential of this tracer for albumin would also be 2.

7.10 Summary of *in vivo* model.

This two-chamber simplified model is a heuristic "stepping stone" between *in vitro* receptor binding and *in vivo* PET measurements. The *in vivo* equations are analogous to the *in vitro* situation and demonstrate the concordance between kinetic predictions and actual equilibrium values. Although an over simplification, the purpose of most modelling described in this course is to use portions of the kinetic curves to estimate equilibrium values. As applied to this two-chamber model, the task could be understood as follows. If you were provided with only a small portion of the initial curve of Figure 7-2, could you predict the final equilibrium ratio of 3 : 1 for $C_2 : C_1$? The answer is yes, since as soon as the rate constants can be determined within the noise of the measurements, then their ratio is the inverse of the ratio of the equilibrium concentrations (equation (7.23)). Thus, this two-chamber device is a heuristic model, but one that is overly simplistic for several reasons. First, as stated, the data provided here are perfectly accurate and have no noise. Secondly, C_1 was described as having a fixed initial amount of tracer. For *in vivo* situations, this chamber will become the blood pool, which is continuously replenished with new circulating blood of variable concentrations. Finally, this model has only one tissue chamber (C_2), whereas multiple tissue chambers will be reviewed in this course.

7.11 Reference

Wharton, J. & Polak, J. M. 1993, *Receptor autoradiography principles and practice* Oxford University Press, Oxford.

8. Receptor kinetics - modelling and practical approach

A.A.Lammertsma, PET Centre VUmc, Amsterdam, The Netherlands.

8.1 Introduction

An important aspect of PET is its flexibility. Measurements of blood flow and glucose consumption are only two of the possibilities of PET. Of course, together with the measurements of oxygen utilisation, they have been the backbone, on which PET has been accepted as a quantitative imaging technique of regional (patho)-physiology. However, although the study of these parameters is important in many instances (e.g. stroke, epilepsy, ischaemic heart disease, and tumours), they only give an overall assessment of the tissues.

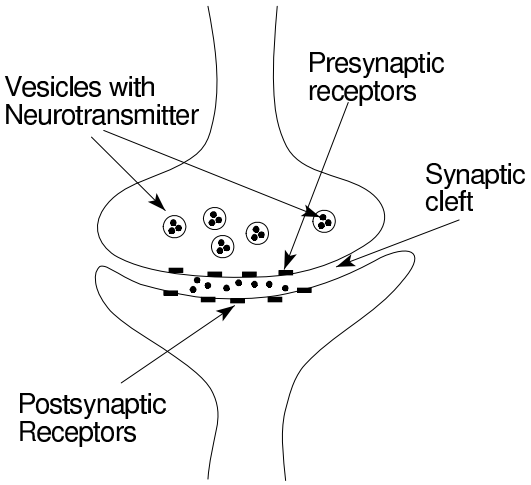

Figure 8-1. A schematic view of a synapse in the brain, representing a general neurotransmitter system.

Many diseases are thought to be connected to specific neurotransmitter systems. In order to gain further insight into the underlying pathophysiology, methods to assess these systems are required. PET provides an opportunity by the multitude of labelled tracers that have been developed over recent years. Tracers have been developed to study different aspects of neurotransmission. For example, for the dopaminergic system (implicated in movement disorders such as Parkinson's and Huntington's disease), labelled tracers (or ligands) have been developed for the synthesis of the transmitter dopamine itself ([F-18]-6-L-fluorodopa), as well as for post-synaptic receptors ([C-11]raclopride for D2, [C-11]SCH-23390 for D1) and pre-synaptic receptor transporters ([C-11]nomifensine, [C-11]-CFT, [F-18]FP-beta-CIT).

8.2 Standard ligand-receptor model

To describe the time course of the uptake of a ligand in tissue, a model is required that distinguishes between the different components contributing to the externally detected (total) signal. These are free ligand in plasma, free ligand in tissue, ligand in tissue that is not specifically bound, and finally, ligand specifically bound to the receptor under study. Note, that with a PET scanner the total activity is measured, including the first three "contaminating" signals.

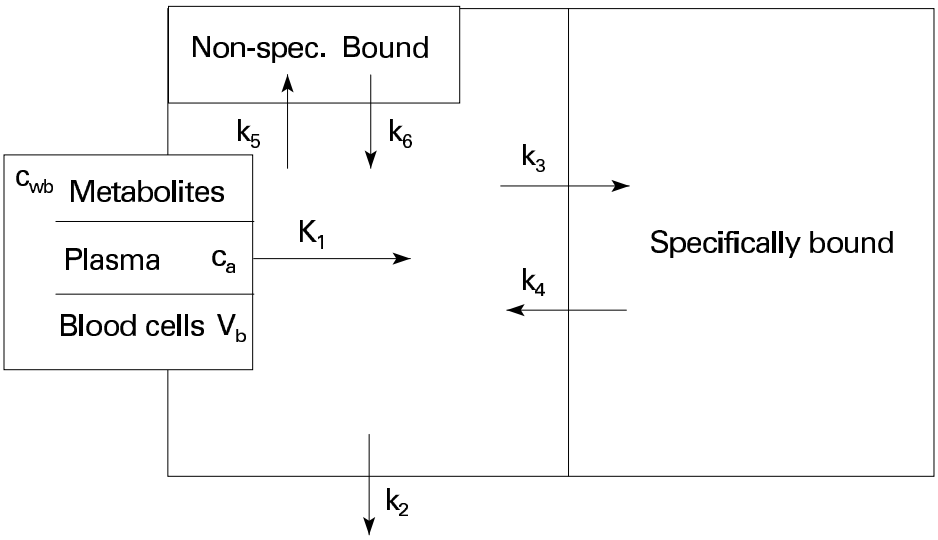

Figure 8-2. Schematic diagram of a three tissue-compartment model. The left block indicates the input function, illustrating the corrections that are required to obtain the metabolite-corrected plasma curve.

K_1 and k_2 describe the transport of ligand from plasma to tissue and vice versa, k_3 and k_4 that between free and specifically bound ligand in tissue, and k_5 and k_6 that between free and non-specifically bound ligand. Note, that the units of all rate constants (k_2 - k_6) are min^{-1}, except for K_1, which is (ml plasma)/(ml tissue)/min.

Note also, that the input to the tissue is that of the parent tracer (i.e. non-metabolised) in plasma. The labelled metabolites could have entirely different kinetics and should not be included in the input function. In fact, in the standard model it has been assumed that the (labelled) plasma metabolites do not enter the tissue. This is often the case for ligands used in brain studies, where the metabolites usually do not cross the blood brain barrier. When metabolites do cross the blood brain barrier or for body studies, the standard model is not valid.

Finally, note the parameter V_b, which is included to account for intra-vascular activity. This is needed, since a region of interest defined on a PET scan will contain a small fraction of blood vessels, which also contribute to the total signal. The contribution from these vessels, however, is not related to the plasma concentration, but to the concentration of whole blood including metabolites.

The above model contains 7 parameters (6 rate constants and blood volume). The model equations become rather complicated and, in the majority of cases, no reliable fits can be

obtained. In practice, errors of individual parameters would be far too large. The most common way to deal with this problem is to simplify the model further. It is usually assumed, that the kinetics of the non-specific component are fast, i.e. there is a rapid equilibrium between free and non-specific compartments. This implies that one would not be able to distinguish between the two compartments and the availability of free ligand for specific binding would be the same as for a system without non-specific binding. This simplification results in the following model, which is in general use.

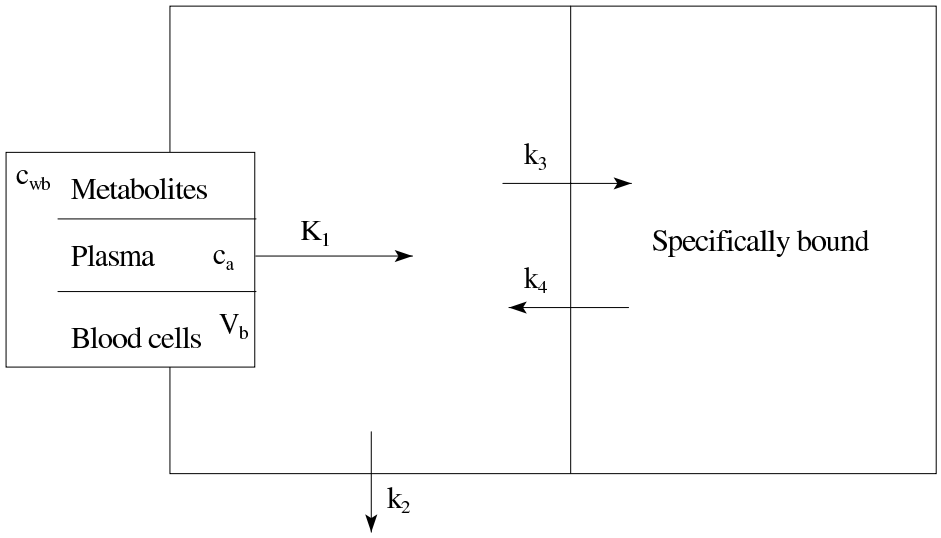

Figure 8-3. Schematic diagram of the standard two tissue-compartment model, assuming that the free and non-specific bound compartments reach equilibrium rapidly.

8.3 Input functions

The diagram of the standard model illustrates the two measurements involved. An ROI (or pixel) defined on a dynamic PET scan provides the tissue time-radioactivity curve. In addition, the input function to the tissue (metabolite corrected plasma) and the time course of the vascular component (uncorrected whole blood) need to be measured. It should be noted that a composite measurement is as strong as its weakest component. Therefore, attention should be paid to the measurement of the input functions.

The traditional method to measure a blood curve is to collect sequential discrete blood samples. It is clear, that in the case of PET measurements where the input to the tissues has to be measured, these samples have to be taken from an artery, usually the radial artery. These samples are then used to measure whole blood and plasma concentrations of radioactivity and the fraction of labelled metabolites in plasma.

Following a bolus injection, initial changes in both blood and tissue are rapid. To be able to fit for delay (between blood sampling and tissue), blood volume V_b and K_1, the early frames after injection should be short, e.g. 5 seconds per frame. During the course of the scan, the frame duration can be progressively prolonged, sometimes up to 10 minutes for the last frames. However, the fast frames at the beginning of the scan are only useful if the blood samples are collected at a rate which is at least as fast as the frame rate. Therefore, collection of the blood curve using continuous withdrawal and on-line detection is

recommended, at least during the first 5 to 10 minutes of a study. The withdrawal rate is a compromise between high delay and dispersion and excessive loss of blood. In practice, a flow rate of 5 ml/min over the first 10 minutes and 2.5 ml/min thereafter can be used. The tubing should be of non-sticking material such as polytetra fluoroethylene (PTFE) and the internal diameter should be small (e.g. 1 mm). In addition to the on-line curve, a limited number of discrete samples are still required (e.g. 5 during a 1 hour scan), as described below. This can be achieved by interrupting the continuous withdrawal for a few seconds. This also allows for flushing the blood lines with heparinised saline. It is, however, important that the on-line curve is not interrupted during the first 5 minutes, in order to measure the peak of the bolus as accurately as possible.

Once an on-line blood curve has been collected, a few operations have to be performed to extract the two input functions required for modelling. First, of course, corrections for detector dead time and possible background from a previous run have to be carried out depending on the system employed. Secondly, the blood curve has to be calibrated, i.e. scaled to the same units as the PET scanner. The detector set-up could be cross-calibrated against the scanner on a regular basis and a fixed calibration factor (independent of the scan) could be used. However, to allow for some variation in the actual diameter of the tubing it is probably better to use an individual calibration factor based on the whole blood concentrations of the discrete samples (measured in a cross-calibrated well counter). At this stage the whole blood time-activity curve has been obtained which, in the fitting process, is used to estimate the blood volume component V_b.

For the model, also the metabolite corrected plasma curve is required. This is obtained as follows. First, the ratio of plasma to whole blood concentrations of the discrete samples are plotted as a function of time and fitted with a multi-exponential function, the number of exponentials depending on the actual curve. When the whole blood curve is multiplied with this multi-exponential function, the total plasma curve is obtained. Secondly, the fraction of metabolites is plotted as a function of time and fitted to a multi-exponential. When the total plasma curve is multiplied with one minus this multi-exponential (parent + metabolite = 1), the metabolite corrected plasma curve is obtained. This curve, of course, is the more important input function for the model. An alternative approach to the last step is not to fit the metabolite fraction with a multi-exponential, but instead to fit the absolute level of metabolites in plasma using compartmental analysis. This method does not produce an exponential description, but rather an exponential convolution, which is a more physiological description.

8.4 Model equations

The simplified standard ligand-receptor model (Fig. 8-3) is described by the following equations:

$$C_{PET} = (1 - V_b)\ C_t + V_b\ C_{wb} \tag{8.1}$$

with

$$C_t = C_f + C_b \tag{8.2}$$

$$\frac{dC_f}{dt} = K_1 C_p - k_2 C_f - k_3 C_f + k_4 C_b \tag{8.3}$$

$$\frac{dC_b}{dt} = k_3 C_f - k_4 C_b \tag{8.4}$$

Each frame in a dynamic PET scan provides a measurement of C_{PET} for a given time. Non-linear regression can then be used to find the best fit to the data points, resulting in best estimates for the five parameters K_1, k_2, k_3, k_4 and V_b.

Note the difference between c_p (metabolite corrected plasma) and c_{wb} (uncorrected whole blood). The reason for this difference has been explained in the previous section.

Note also, that only the starting equations have been given above. The explicit solutions of the differential equations for c_f and c_b have not been given. The final solution can be found in the literature . In fact, the solution is the same as that for the FDG model (chapter 5) with finite k_4.

8.5 Relationship with pharmacological parameters

With respect to better known pharmacological parameters, the following relationships apply:

$$k_3 = k_{on} f_{ND} \left(B_{max} - \frac{C_b(t)}{SA} \right) \tag{8.5}$$

$$k_4 = k_{off} \tag{8.6}$$

where

B_{max} = Receptor concentration

k_{on} = Bimolecular association rate constant

k_{off} = Dissociation rate constant

SA = Specific activity of injected ligand

f_{ND} = free fraction of ligand in non-displaceable tissue compartment

The ratio c_b/SA gives the concentration of receptors occupied by the ligand. The specific activity SA is required here, since the receptors can be occupied by both labelled and unlabelled ligand. When the specific activity is low, the amount of co-injected unlabelled ligand is high and more receptors are occupied. B_{max} - c_b/SA represents the concentration of free receptors (total - bound).

For a tracer alone study, i.e. when the specific activity is high, the c_b/SA is small compared to B_{max} and the equation for k_3 simplifies to:

$$k_3 = k_{on} f_{ND} B_{max} \tag{8.7}$$

Since the equilibrium dissociation constant K_d is defined by:

$$K_d = \frac{k_{off}}{k_{on}} \tag{8.8}$$

it follows that, for high specific activity:

$$\frac{k_3}{k_4} = f_{ND} \frac{B_{max}}{K_d} \tag{8.9}$$

The ratio of k_3 over k_4 is often referred to as binding potential (BP, (Mintun et al. 1984), which for tracer alone is:

$$BP_{ND} = \frac{k_3}{k_4} = f_{ND} \frac{B_{max}}{K_d} \tag{8.10}$$

It should be noted from the equations that it is not possible to obtain B_{max} and K_d separately from a single study. Only their ratio (BP_{ND}) can be estimated. To measure B_{max} and K_d individually, at least two separate studies need to be performed, one with tracer alone, the other with a lower specific activity or during infusion of unlabelled ligand.

For low specific activity, k_3 becomes dependent on c_b, which itself is a function of time. It follows that, in this case, first order kinetics do not apply any more. Consequently both equations and solutions become complicated.

For most ligands, k_3 and k_4 can not be obtained with any degree of accuracy. This is due to the presence of a strong correlation between various fitting parameters. The presence of noise in the scan data then results in estimates of the parameters with high associated standard errors. For example, noise in the data often results in two local minima, one with high k_2 and low k_3, the other with low k_2 and high k_3. However, the ratio of k_3 and k_4, the binding potential BP, tends to be more stable.

Sometimes even BP_{ND} can not be measured accurately. In that case, it is only possible to fit for the total volume of distribution V_d (see also next section):

$$V_d = \left(\frac{K_1}{k_2}\right)\left(1 + \frac{k_3}{k_4}\right) \tag{8.11}$$

which is still related to B_{max}/K_d.

As mentioned previously, the model assumes that labelled metabolites do not enter the tissue. If they do, at least one more parallel compartment, describing the fate of the metabolites has to be implemented. For this approach to be successful, in most cases, additional information about the kinetics of the metabolites has to be obtained.

8.6 Volume of distribution

In this section the relationship between the volume of distribution and various k values will be derived, based on the definition that the volume of distribution V_d is equal to the ratio of tissue (c_t) and plasma (c_p) concentrations at true equilibrium:

$$V_d = \frac{C_t}{C_p}$$
$$\frac{dC_t}{dt} = \frac{dC_p}{dt} = 0 \qquad (8.12)$$

The differential equation for a single-tissue-compartment model is given by:

$$\frac{dC_t}{dt} = K_1\, C_p - k_2\, C_t \qquad (8.13)$$

At equilibrium:

$$K_1\, C_p - k_2\, C_t = 0 \qquad (8.14)$$

and it follows, that

$$V_d = \frac{K_1}{k_2} \qquad (8.15)$$

For a two tissue-compartment model, the equations are as given in section 8.4:

$$C_t = C_f + C_b \qquad (8.16)$$

$$\frac{dC_f}{dt} = K_1 C_p - k_2 C_f - k_3 C_f + k_4 C_b \qquad (8.17)$$

$$\frac{dC_b}{dt} = k_3 C_f - k_4 C_b \qquad (8.18)$$

At equilibrium, also dc_f/dt and dc_b/dt will be zero. From

$$\frac{dC_b}{dt} = k_3 C_f - k_4 C_b = 0 \tag{8.19}$$

it follows that

$$C_b = \frac{k_3}{k_4} C_f \tag{8.20}$$

Therefore

$$V_d = \frac{C_t}{C_p} = \left(\frac{C_f + C_b}{C_p} \right) = \left(1 + \frac{k_3}{k_4} \right) \frac{C_f}{C_p} \tag{8.21}$$

From

$$\frac{dC_f}{dt} + \frac{dC_b}{dt} = K_1 C_p - k_2 C_f = 0 \tag{8.22}$$

it follows that

$$C_f = \frac{K_1}{k_2} C_p \tag{8.23}$$

and V_d simplifies to

$$V_d = \left(\frac{K_1}{k_2} \right) \left(1 + \frac{k_3}{k_4} \right) \tag{8.24}$$

Similarly, if one takes into account non-specific binding with rate constants k_5 and k_6, it can be derived that

$$V_d = \left(\frac{K_1}{k_2} \right) \left(1 + \frac{k_3}{k_4} + \frac{k_5}{k_6} \right) \tag{8.25}$$

8.7 Practical approach

In this section a possible skeleton procedure for a first pass analysis of data obtained with a new ligand is given. No refinements are provided. They always depend on the specific properties of the ligand in question.

1. Generate metabolite corrected plasma curve and uncorrected whole blood curve. Check that labelled metabolites do not cross the blood brain barrier.

2. Fit whole brain ROI or total count rate of the scanner (good statistics) for a two tissue-compartment model, including a blood volume component and delay of the blood curve. Alternatively, fit only the early part of this curve using a single tissue compartment model, including blood volume and delay.

3. Fix the delay for all subsequent fits of small ROIs. Alternatively, shift the whole blood and plasma curves.

4. Calculate the weighting factors for all frames (see section 8.9). These weighting factors take into account differences in count rate and frame duration. Note that the weighting factors should take into account the original counts for the frame (not corrected for decay), and the decay correction factor for the frame (the statistics are based on the original counts).

5. Fit a regional tissue time-radioactivity curve (i.e. a region that is expected to have a high degree of specific binding) for a single tissue-compartment model. Always include a blood volume component. This gives K_1, k_2 or V_d, and V_b.

6. Fit again for a two tissue-compartment model. Try both setting k_4 to zero (irreversible binding) and with floating k_4 (reversible binding). Again, for both fits include a blood volume component. This gives K_1, k_2, k_3, k_4 and V_b. For reversible binding, V_d and BP can also be obtained.

7. Use Akaike (Akaike 1974) and Schwarz (Schwarz 1978) criteria and F-test (Cunningham 1985;Landaw & DiStefano III 1984) to establish which model gives the best fit. Do not use the sum of squares: they are always smaller for more parameters. Also, check standard errors of possible parameters of interest (see next section).

8. Repeat steps 1 to 6 for a series of normal volunteers to check variability of possible parameters of interest (see next section).

It is obvious, that the results should be compared with in vitro or ex vivo animal data and that (possible lack of) selectivity, i.e. binding to different receptors, should be taken into account.

Finally, it should be clear that analysis of studies without correcting for labelled metabolites is useless. The same is true for studies where the labelled ligand is a racemic mixture. Also, in this case the true input function will not be known and it will not be possible to separate the two isomers using standard metabolite analysis techniques.

8.8 Analysis of results

This section is restricted to data obtained from single tracer alone studies. These constitute the majority of PET receptor studies. In addition, the analysis of multiple dose studies is very dependent on the actual acquisition protocol used.

As mentioned in the previous section, the first step is to check whether the two-tissue-compartment model consistently provides significantly better fits than the single-tissue-compartment model.

If this is the case, BP_{ND} values should be used, but only when they are robust (small standard errors of the fitted BP_{ND} values) and stable (small standard deviation of average BP_{ND} value for a series of normal subjects). Otherwise, V_d should be used, calculated from:

$$V_d = \left(\frac{K_1}{k_2}\right)\left(1+\frac{k_3}{k_4}\right) \tag{8.26}$$

If the two-tissue-compartment model does not provide better fits, V_d from the single tissue-compartment model should be used:

$$V_d = \frac{K_1}{k_2} \tag{8.27}$$

If a region devoid of receptors with volume of distribution $V_{dr} = K_1'/k_2'$ is available, binding potential can be calculated from

$$BP_{ND} = \frac{(V_d - V_{dr})}{V_{dr}} = \frac{\left\{\left(\frac{K_1}{k_2}\right)\left(1+\frac{k_3}{k_4}\right) - \left(\frac{K_1'}{k_2'}\right)\right\}}{\left(\frac{K_1'}{k_2'}\right)} = \left(\frac{k_3}{k_4}\right) \tag{8.28}$$

assuming the K_1/k_2 ratio is the same for target and reference tissue ($K_1/k_2 = K_1'/k_2'$). This assumption does not imply that K_1 and k_2 are the same for both regions, only their ratio. This is plausible, since any higher permeability in one direction should be accompanied with a higher permeability in the other.

Note that above calculation can also be used if the target region can only be fitted to a single-compartment model. Assuming there is specific binding (which can be tested by predosing or displacing), the failure of the fit would be due to the specific kinetics. For example, if the exchange between free and bound is fast, it is quite possible that the model can not detect the specific component as a separate compartment. However, V_d would still be increased.

If there is non-specific binding, which is assumed to be the same in target and reference tissue ($k_5/k_6 = k_5'/k_6'$), the binding potential calculated from V_d will be biased. The volumes of distribution for both tissues become

$$V_d = \left(\frac{K_1}{k_2}\right)\left(1 + \frac{k_3}{k_4} + \frac{k_5}{k_6}\right) \text{ and } V_{dr} = \left(\frac{K_1'}{k_2'}\right)\left(1 + \frac{k_5'}{k_6'}\right) \tag{8.29}$$

respectively. It then follows that

$$BP_{ND} = \frac{(V_d - V_{dr})}{V_{dr}} = \frac{\frac{k_3}{k_4}}{\left(1 + \frac{k_5}{k_6}\right)} \tag{8.30}$$

However, the bias is only a scaling factor, provided that the level of non-specific binding is relatively constant.

8.9 Weighting of fits

Time-activity curves are routinely expressed in terms of radioactivity concentrations, i.e. there has been an inherent correction for frame duration. Statistics do not depend on the actual counts within a region of interest, but more on overall counts, i.e. for calculating weighting factors one can start with the total count rate.

Suppose T total counts (trues, not corrected for dead-time and decay) are collected in a frame of duration L. Then the total count rate for that frame is R = T/L. For the total counts Poisson distribution can be assumed, i.e.

$$\text{Variance of T} = \text{Var(T)} = \text{T} \tag{8.31}$$

$$\text{SD(T)} = \sqrt{\text{T}} \tag{8.32}$$

$$\text{COV(T)} = \sqrt{\text{T}} / \text{T} = 1/\sqrt{\text{T}} \tag{8.33}$$

Since L has no error:

$$\text{COV(R)} = 1/\sqrt{\text{T}} \tag{8.34}$$

$$\text{SD(R)} = \text{R}/\sqrt{\text{T}} \tag{8.35}$$

$$\text{Var(R)} = \text{R}^2/\sqrt{\text{T}} \tag{8.36}$$

$$\text{Weight}(R) = T/R^2 = L/R = L^2/T \tag{8.37}$$

The weights given by equation (8.37) are valid for non-decay corrected data.

If the data are decay corrected, R is not equal to T/L, but

$$R = fT/L \tag{8.38}$$

where f is the decay correction factor for the frame

$$f = \lambda T/\{\exp(-\lambda T_s)-\exp(-\lambda T_e)\} \tag{8.39}$$

with T_s and T_e being start and end times of the frame

The corresponding weighting factors (for decay corrected data) are then given by:

$$\text{Weight}(R) = L^2/(f^2T) \tag{8.40}$$

8.10 Comparison of fits

As mentioned in section 8.10, three different tests are commonly used for (statistical) comparison of various fits. These are the Akaike and Schwarz criteria and the F-test (Landaw & DiStefano III 1984). The Akaike information criterion (AIC) is given by:

$$AIC = N \ln(SS) + 2P \tag{8.41}$$

where

N = number of frames

P = number of parameters

SS = residual sum of squares.

The fit with the lowest AIC is considered to be the "best" fit.

The Schwarz criterion is similar:

$$SC = N \ln(SS) + P \ln(N) \tag{8.42}$$

Again the fit with the lowest SC is considered to be the best.

Finally, the F-test is given by:

$$F = \frac{\left\{\frac{(SS_1 - SS_2)}{(P_2 - P_1)}\right\}}{\left\{\frac{SS_2}{(N - P_2)}\right\}} \tag{8.43}$$

where 1 and 2 stand for the fits with the lowest and highest number of parameters, respectively.

An F-statistic table is required to assess significance.

It is difficult to indicate which is the better test. In practice, all three tests are often used to check whether they indicate the same best fit. The Akaike (Akaike 1974) and Schwarz (Schwarz 1978) tests can easily be implemented into an (automatic) program. This is more difficult for the F-test.

8.11 Reference tissue model

In the previous section, it was shown that, if a region devoid of receptors is available, binding potential can be calculated from the volumes of distribution of the target (specific) tissue and this reference tissue.

However, if such a region exists BP can also be obtained from a reference tissue model, where the reference region is used as an indirect input function to the total target region. Fitting the target region with the reference region as indirect input function, provides estimates for R_1, k_2, k_3 and k_4 or BP_{ND}. Again only the estimates of BP_{ND} and R_1 are robust. R_1 is the ratio of K_1 for target and reference regions. This model takes into account differences in both delivery and free concentration between target and reference tissues. It avoids the need for measuring plasma concentrations and metabolites and, therefore, does not require arterial cannulation.

A schematic diagram of the reference tissue model (Hume et al. 1992) is given in Fig. 8-4, showing both, the target ("specific") and reference region.

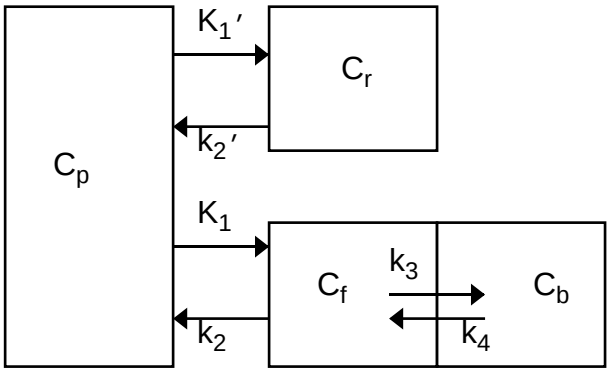

Figure 8-4. Schematic diagram of the reference tissue model. Although the plasma input function c_p is illustrated, the model does not require its measurement. Instead, the reference tissue curve c_r is used as an indirect input function.

The differential equations as function of time (t) are as follows:

$$\frac{dC_r}{dt} = K_1' C_p - k_2' C_r \tag{8.44}$$

$$\frac{dC_f}{dt} = K_1 C_p - k_2 C_f - k_3 C_f + k_4 C_b \tag{8.45}$$

$$\frac{dC_b}{dt} = k_3 C_f - k_4 C_b \tag{8.46}$$

where c_p = Metabolite corrected plasma concentration $(kBq \cdot ml^{-1})$

c_r = Concentration in reference tissue $(kBq \cdot ml^{-1})$

c_f = Concentration of free (i.e. not specifically bound) ligand $(kBq \cdot ml^{-1})$

c_b = Concentration of specifically bound ligand $(kBq \cdot ml^{-1})$

and the rate constants have the same meaning as defined previously. A 'prime' indicates a rate constant for the reference region. Note, that it is not assumed that $K_1 = K_1'$ or $k_2 = k_2'$.

As previously mentioned, only the total concentration c_t within the "specific" region can be measured:

$$C_t = C_f + C_b \tag{8.47}$$

Using $R_1 = K_1/K_1'$, and assuming that the volume of distribution of the not specifically bound tracer in both tissues is the same (i.e. $k_2' = k_2 \cdot K_1'/K_1 = k_2/R_1$), results in the following relationship between c_t and c_r (Lammertsma et al. 1996):

$$C_t = R_1 \left\{ C_r + a \cdot C_r \otimes \exp^{-ct} + b \cdot C_r \otimes \exp^{-dt} \right\} \tag{8.48}$$

with

$a = (k_3+k_4-c)\cdot(c-r)/p$

$b = (d-k_3-k_4)\cdot(d-r)/p$

$c = (s+p)/2$

$d = (s-p)/2$

$p = \sqrt{(s^2-q)}$

$q = 4k_2 \cdot k_4$

$s = k_2+k_3+k_4$

$\otimes$ = convolution integral

Using the measured tissue concentrations c_t and c_r, this equation (8.48) can now be fitted for R_1, k_2, k_3 and BP_{ND} (after substitution of $BP_{ND} = k_3/k_4$), without the need for measuring c_p. Note, that this operational equation takes into account differences in delivery between specific and reference tissue (R_1). In addition, it does not assume that c_r equals c_f.

8.12 Simplified reference tissue model

The reference tissue compartment model described in the previous paragraph provides a robust estimate of BP_{ND} , the parameter of interest in ligand studies, without measuring the arterial input function and thereby circumventing arterial cannulation. The estimates of the other linear parameters (R_1, k_2 and k_3), however, are often associated with large standard errors. In addition, convergence rates are slow. To overcome this problem, a simplified reference tissue model reducing the number of parameters from four to three was developed (Lammertsma & Hume 1996).

Simplification to a three-parameter model is possible if the tracer kinetics are such that it is difficult to distinguish between the free and specifically bound compartments. Fig. 8-5 illustrates the simplified reference tissue model where the compartments for free and bound are lumped together.

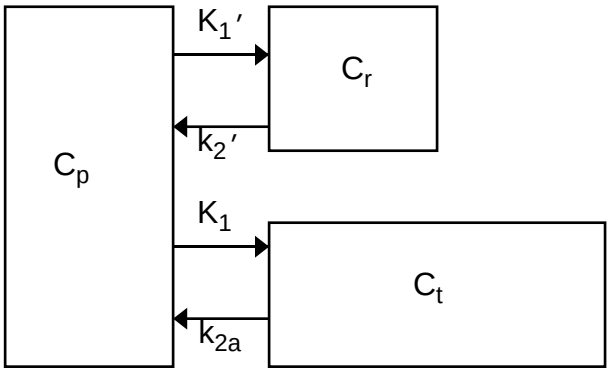

Figure 8-5. Simplified reference tissue model where the compartments of free and specifically bound are not distinguishable. k_{2a} is the apparent (overall) rate constant for transfer from the specific compartment to plasma.

The target tissue can now be described by a single differential equation:

$$\frac{dC_t}{dt} = K_1 C_p - k_{2a} C_t \tag{8.49}$$

The volume of distribution should be the same as that obtained from the four-parameter model. In other words, the apparent rate constant k_{2a} relates to the true rate constant k_2 through:

$$\frac{K_1}{k_{2a}} = \left(\frac{K_1}{k_2} \right) \cdot \left(1 + BP_{ND} \right) \tag{8.50}$$

The differential equation for the reference tissue is:

$$\frac{dc_r}{dt} = K_1^{'} c_p + k_2^{'} c_r \tag{8.51}$$

Solving for c_p using (8.50) and substituting in (8.49):

$$\frac{dc_t}{dt} = R_1 \frac{dc_r}{dt} + k_2 c_r - \frac{k_2}{1 + BP_{ND}} c_t \tag{8.52}$$

The new equation for the simplified reference tissue model can now be derived:

$$C_t = R_1 C_r + \left\{ k_2 - \frac{R_1 k_2}{(1 + BP_{ND})} \right\} C_r \cdot \otimes \exp^{-\left(\frac{k_2 t}{(1+BP_{ND})}\right)} \qquad (8.53)$$

In contrast to the original reference tissue model described in the previous paragraph, this simplified model is only based on three parameters: R_1, k_2 and BP_{ND} .

The validity of this new three-parameter model compared to the established four-parameter model was demonstrated for a variety of PET tracers both in humans and in rats. Radiotracers, such as [C-11]raclopride and [C-11]SCH-23390 with reasonably fast kinetics, provided in all cases essentially the same BP_{ND} values for both models. In addition, the three-parameter model produced small standard errors for all parameters and converged rapidly.

Nevertheless, for new tracers, the validity of the reference tissue model and especially the simplified reference tissue model should be checked prior to routine application.

8.13 Reference

Akaike, H. A new look at statistical model identification. IEEE Trans Automat Control 19, 716-723. 1974.
Ref Type: Journal (Full)

Cunningham, V. J. 1985, "Non-linear regression techniques in data analysis", *Med.Inform.(Lond.)*, vol. 10,no. 2, pp. 137-142.

Hume, S. P., Myers, R., Bloomfield, P. M., Opacka-Juffry, J., Cremer, J. E., Ahier, R. G., Luthra, S. K., Brooks, D. J., & Lammertsma, A. A. 1992, "Quantitation of carbon-11-labeled raclopride in rat striatum using positron emission tomography", *Synapse*, vol. 12,no. 1, pp. 47-54.

Lammertsma, A. A., Bench, C. J., Hume, S. P., Osman, S., Gunn, K., Brooks, D. J., & Frackowiak, R. S. 1996, "Comparison of methods for analysis of clinical [11C]raclopride studies", *J.Cereb.Blood Flow Metab*, vol. 16,no. 1, pp. 42-52.

Lammertsma, A. A. & Hume, S. P. 1996, "Simplified Reference Tissue Model for PET Receptor Studies", *Neuroimage.*, vol. 4,no. 3, pp. 153-158.

Landaw, E. E. & DiStefano III, J. J. 1984, "Multiexponential, multicompartmental, and noncompartemental modeling. II. Data analysis and statistical considerations", *Am.J.Physiol.*, vol. 246, p. R666.

Mintun, M. A., Raichle, M. E., Kilbourn, M. R., Wooten, G. F., & Welch, M. J. 1984, "A quantitative model for the in vivo assessment of drug binding sites with positron emission tomography", *Ann.Neurol.*, vol. 15,no. 3, pp. 217-227.

Schwarz, G. Estimating the dimension of a model. Ann.Statist. 6, 461-464. 1978.

9. Steady-state measurements of neuroreceptor binding

Gitte Moos Knudsen, University Hospital Rigshospitalet, Copenhagen

9.1 Introduction

The in vivo determination of the pharmacokinetic constants K_d and B_{max} of neuroreceptors requires a minimum of two studies at different occupancies. To yield accurate measures in both studies, the occupancies have to be determined with the receptors and the ligand in complete steady-state, a prerequisite which often is hampered. The pseudo-equilibrium method is based on assessing the bound/free ratio at a time when this ratio is assumed to be close to its equilibrium value (Farde et al. 1989;Pappata et al. 1988). This approach has certain limitations. First, it requires that the brain uptake (K_1) is the same for the region of interest and for the reference region. Secondly, it assumes that the free and non-specific tracer binding in the region of interest is identical to the concentration in the receptor-void reference region. For some receptor ligands, computer simulations have shown that the brain non-specific binding is higher in the reference region since receptor rich brain regions will act as a sink. For other ligands, however, this approach will work sufficiently well (Ito et al. 1998).

There are two principally different ways to create steady-state conditions; either a steady-state is obtained for the labelled tracer (the bolus-infusion principle) or it is obtained for the unlabeled ligand. This section describes how experiments can be designed to ensure steady-state conditions.

9.2 Steady-state of labelled ligand

In order to attain steady-state conditions, a constant infusion of the tracer can be given. This approach is, however, usually rather slow. To speed up the process, an initial (priming) tracer bolus injection can be given followed by a constant tracer infusion over a longer period, frequently in the order of hours, until equilibrium is obtained in plasma and brain (Figure 9-1).

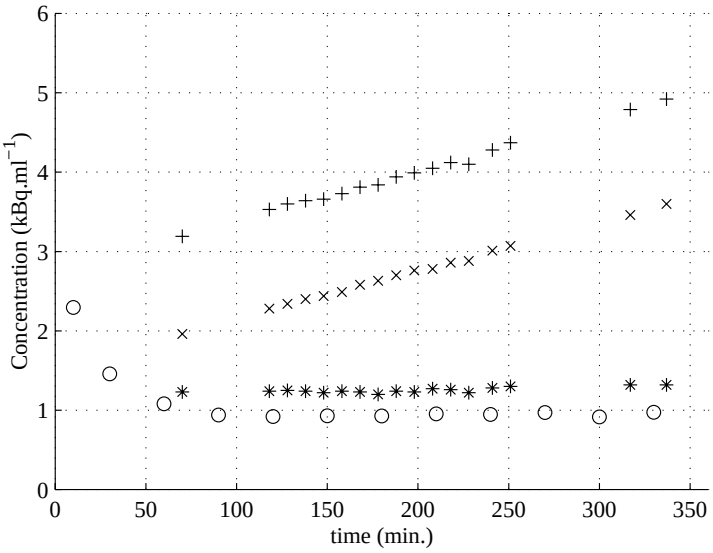

Figure 9-1 Plasma parent compound (circle) time activity curve and brain time activity curves for temporal cortex (+) and cerebellum (x) in a bolus-infusion experiment with 18F-altanserin. Specific binding (*) for temporal cortex is calculated by subtracting radioactivity in cerebellum (representing non-specific bound 18F-altanserin and 18F-metabolites in ROIs) from radioactivity in temporal cortex.

In this way, the distribution volume of the tracer can be determined from a single PET or SPECT image and one blood sample:

$$V_d = \frac{c_t(\tau)}{f_P c_p(\tau)} \tag{9.1}$$

where T denotes any time where a steady-state condition is present and f_P is the plasma free (non-protein bound) fraction of the parent compound.

Based on data from previous bolus experiments, an algorithm using conventional convolution arguments for a prediction of the outcome of a bolus/infusion (B/I) experiment can be made (Pinborg et al. 2000). This allows for designing B/I protocols, i.e., determining the ratio between the bolus and the infusion doses, that are optimally suited for that particular ligand. In cases where receptor densities vary considerably within the brain, B/I protocols may be designed for obtaining steady-state in particular brain regions.

The B/I approach is particularly well suited for studies employing long-lived tracers i.e., either SPECT studies, or PET studies with 18F-labeled ligands. The method also provides an opportunity of imaging during continuous unlabeled ligand infusion as a powerful within-scan method for determining both regional binding characteristics and receptor occupancy with tracer and cold ligand, respectively. It should be noted that unlabeled ligand may originate from both exogenous and endogenously released sources (Carson et al. 1997). Careful assessment of the sources of noise and of the correct timing in receptor imaging studies can increase the sensitivity of the B/I method for the detection of biological signals (Watabe et al. 2000).

9.3 Steady-state of unlabeled ligand

With this method, first described by Lassen (Lassen 1992), a constant plasma level of unlabeled ligand is obtained by either prolonged intravenous infusion or oral administration of the unlabeled ligand. The fraction of receptor sites not occupied by the unlabeled ligand is measured by using trace amounts of a radioactive ligand binding to the same receptor. One of the studies can be made at close to zero receptor occupancy, by administering the tracer alone. The tracer studies, i.e., one without and one (or even better, more) at constant levels of unlabeled ligand, allows calculation of the unlabeled ligand's equilibrium dissociation constant K_d. In the special case when tracer and unlabeled ligands are chemically identical, then B_{max} can also be calculated. The approach has been applied for, e.g., flumazenil (Lassen et al. 1995).

If the tracer is administered as an intravenous bolus injection, then the distribution volume, V_d can be determined from the ratio between the area under the brain and plasma time activity curves:

$$V_d = \frac{\int_0^\infty c_t dt}{f_P \int_0^\infty c_p dt} \tag{9.2}$$

In order to extrapolate the areas to infinity, the curves must be followed for so long that conventional mono-exponential extrapolation can be used. Alternatively, V_d can be determined on the basis of compartmental analysis, or from a bolus-infusion experiment as described above.

When the tracer, T, is competing for the same receptor sites as the cold ligand, L, then the concentration of bound tracer c_b^T, is determined by:

$$c_b^T = B_{\max} \frac{c_f^T}{c_f^T + K_d^T \left(1 + \frac{c_f^L}{K_d^L}\right)} \tag{9.3}$$

Likewise, the concentration of receptor bound ligand c_b^L is determined by:

$$c_b^L = B_{\max} \frac{c_f^L}{c_f^L + K_d^L \left(1 + \frac{c_f^T}{K_d^T}\right)} \tag{9.4}$$

$B_{max,}$ is the total concentration of receptor sites; c_f^T and c_f^L, the free concentrations of the two ligands in the water phase; and K_d^T and K_d^L, the corresponding affinities for T and L, respectively.

If T is given at a sufficiently high specific activity, then the denominator in Eq. (9.3) may be replaced with $K_d^T (1 + c_f^L/K_d^L)$ and in Eq. (9.4) with $c_f^L + K_d^L$. In that case, the tracer's bound/free ratio (c_b^T / c_f^T can be calculated from Eq. (9.3) if two (or more) studies are carried out, one without and one (or more) in the presence of unlabeled ligand L:

$$\left(\frac{c_b^T}{c_f^T}\right) = \frac{B_{\max}}{K_d^T} \tag{9.5}$$

$$\left(\frac{c_b^T}{c_f^T}\right) = \frac{B_{\max}}{K_d^T\left(1+\frac{c_f^L}{K_d^L}\right)} \tag{9.6}$$

From equations (9.4), (9.5) (9.6) it can be seen that, at tracer conditions (T ≈ 0), the occupancy of the cold ligands receptor binding is determined by:

$$o^L = \frac{c_b^L}{B_{\max}} \approx \frac{c_f^L}{\left(c_f^L + K_d^L\right)} = 1 - \left\{\frac{\left(\frac{c_b^T}{c_f^T}\right)\Big|_{c_f^L}}{\left(\frac{c_b^T}{c_f^T}\right)\Big|_{c_f^L=0}}\right\} \tag{9.7}$$

In the special case where tracer and cold ligand are chemically identical then rearrangement of eq. (9.5) and eq. (9.7) leads to:

$$K_d^T = c_f^L\left(\frac{1-o^L}{o^L}\right) \tag{9.8}$$

$$B_{\max} = K_d^T \left(\frac{c_b^T}{c_f^T} \right)\Bigg|_{c_f^L=0} = c_f^L \left(\frac{\left(\frac{c_b^T}{c_f^T} \right)\Big|_{c_f^L=0} \cdot \left(\frac{c_b^T}{c_f^T} \right)\Big|_{c_f^L}}{\left(\frac{c_b^T}{c_f^T} \right)\Big|_{c_f^L=0} - \left(\frac{c_b^T}{c_f^T} \right)\Big|_{c_f^L}} \right) \tag{9.9}$$

As shown in a previous section, the distribution volume of a tracer is determined by the sum of its specific binding and its (free + non-specific) binding, V_{f+ns}. Under tracer conditions, the distribution volume of the specific binding is:

$$V_d\big|_{c_f^L=0} = f_P \left(\frac{c_b^T}{c_f^T} \right)\Bigg|_{c_f^L=0} + V_{f+ns} \tag{9.10}$$

in the presence of significant amounts of cold ligand,

$$V_d\big|_{c_f^L} = f_P \left(\frac{c_b^T}{c_f^T} \right)\Bigg|_{c_f^L} + V_{f+ns} \tag{9.11}$$

Rewriting eqs. (9.7) and (9.9) then yields

$$\frac{c_b^L}{B_{\max}} = \frac{V_d\big|_{c_f^L=0} - V_d\big|_{c_f^L}}{V_d\big|_{c_f^L=0} - V_{f+ns}} \tag{9.12}$$

$$K_d^L = c_f^L \frac{V_d\big|_{c_f^L} - V_{f+ns}}{V_d\big|_{c_f^L=0} - V_d\big|_{c_f^L}} \tag{9.13}$$

$$B_{\max} = c_p^L \frac{\left(V_d\big|_{c_f^L=0} - V_{f+ns} \right)\left(V_d\big|_{c_f^L} - V_{f+ns} \right)}{V_d\big|_{c_f^L=0} - V_d\big|_{c_f^L}} \tag{9.14}$$

For ligands where V_d(f+ns) is much smaller than V_d(0), then the occupancy is well approximated by 1-V_d(L)/V_d (0). Otherwise, the occupancy can be calculated if V_d(f+ns) is inferred from either:

1. a separate study using a labelled non-specific stereo-isomer of the ligand

2. a tissue reference region devoid of the receptor in question

3. by measuring V_d^L in a condition where specific receptor binding has been completely blocked by high amounts of unlabeled ligand

4. by assuming that V_{f+ns} equals an experimentally determined value of the brain:blood partition coefficient, ρ

For ligands where reasonable and well-determined regional variations in V_d exist and assuming that these variations are solely caused by regional variations in the receptor density, B_{max}, then rewriting eq. (9.12) leads to:

$$V_d\big|_{c_f^T} = (1 - o_L) V_d\big|_{c_f^L=0} + o_L \cdot V_{f+ns} \qquad (9.15)$$

Based on this equation, by plotting regional values of $V_d(c_f^T)$ as a function of regional $V_d(c_f^L=0)$, occupancy and V_{f+ns} can be determined from the slope and the intercept of the regression line respectively.

9.4 References

Carson, R. E., Breier, A., de Bartolomeis, A., Saunders, R. C., Su, T. P., Schmall, B., Der, M. G., Pickar, D., & Eckelman, W. C. 1997, "Quantification of amphetamine-induced changes in [11C]raclopride binding with continuous infusion", *J.Cereb.Blood Flow Metab*, vol. 17,no. 4, pp. 437-447.

Farde, L., Eriksson, L., Blomquist, G., & Halldin, C. 1989, "Kinetic analysis of central [11C]raclopride binding to D2-dopamine receptors studied by PET--a comparison to the equilibrium analysis", *J.Cereb.Blood Flow Metab*, vol. 9,no. 5, pp. 696-708.

Ito, H., Hietala, J., Blomqvist, G., Halldin, C., & Farde, L. 1998, "Comparison of the transient equilibrium and continuous infusion method for quantitative PET analysis of [11C]raclopride binding", *J.Cereb.Blood Flow Metab*, vol. 18,no. 9, pp. 941-950.

Lassen, N. A. 1992, "Neuroreceptor quantification in vivo by the steady-state principle using constant infusion or bolus injection of radioactive tracers", *J.Cereb.Blood Flow Metab*, vol. 12,no. 5, pp. 709-716.

Lassen, N. A., Bartenstein, P. A., Lammertsma, A. A., Prevett, M. C., Turton, D. R., Luthra, S. K., Osman, S., Bloomfield, P. M., Jones, T., & Patsalos, P. N. 1995, "Benzodiazepine receptor quantification in vivo in humans using [11C]flumazenil and PET: application of the steady-state principle", *J.Cereb.Blood Flow Metab*, vol. 15,no. 1, pp. 152-165.

Pappata, S., Samson, Y., Chavoix, C., Prenant, C., Maziere, M., & Baron, J. C. 1988, "Regional specific binding of [11C]RO 15 1788 to central type benzodiazepine receptors in human brain: quantitative evaluation by PET", *J.Cereb.Blood Flow Metab*, vol. 8,no. 3, pp. 304-313.

Pinborg, L. H., Videbaek, C., Knudsen, G. M., Swahn, C. G., Halldin, C., Friberg, L., Paulson, O. B., & Lassen, N. A. 2000, "Dopamine D(2) receptor quantification in extrastriatal brain regions using [(123)I]epidepride with bolus/infusion", *Synapse*, vol. 36,no. 4, pp. 322-329.

Watabe, H., Endres, C. J., Breier, A., Schmall, B., Eckelman, W. C., & Carson, R. E. 2000, "Measurement of dopamine release with continuous infusion of [11C]raclopride: optimization and signal-to-noise considerations", *J.Nucl.Med.*, vol. 41,no. 3, pp. 522-530.

10. Equilibrium measurements via constant infusion

Richard E. Carson, Yale University,, USA

10.1 Introduction

Chapter 7 introduced the concept of the total volume of distribution, V_d. This physiological parameter represents the ratio *at equilibrium* of total tracer in the tissue to that in a reference fluid, usually the plasma. In many PET experiments, V_d is determined from a study including bolus injection of the tracer followed by dynamic scanning. Although equilibrium is not reached in a bolus injection experiment, V_d can be determined by the compartment model parameters (e.g., K_1/k_2 or $K_1/k_2(1+k_3/k_4)$ for one-tissue or two-tissue-compartment models, respectively), or the slope of a Logan graphical analysis. V_d has been found to be the most robust parameter to be determinable from dynamic neuroreceptor studies. In other words, although individual rate parameters can be estimated by certain analyses, they typically have larger uncertainties and are often more affected by errors in the assumptions of the model or measurements of the input function or reference region than is V_d. In neuroreceptor studies, the binding potential *BP* can be determined from the V_d values in the region-of-interest and a region without specific binding, as in equation (8.30).

A different approach to estimate V_d and *BP* is to deliver the radioactive tracer as an infusion, in order to achieve constant concentrations in the regions of interest and in the blood (Carson et al. 1993;Carson et al. 1997;Laruelle et al. 1993) . Note that the phrase "constant concentrations" does not mean compensation for radioactive decay, rather that the decay-corrected concentrations are constant over time. Multiple short scans can be acquired to demonstrate that constant radioactivity levels have been reached. Once equilibrium is achieved, V_d can then be measured directly from the concentration ratio of tissue (c_t) to plasma (c_p), i.e.,

$$V_d = \frac{c_t}{c_p} \tag{10.1}$$

If the binding potential (8.30) is calculated with respect to a reference region with no specific binding, no blood measurements are necessary as the calculation only involves tissue concentration ratios, as follows:

$$BP_{ND} = \frac{\left(V_d - V_{dr}\right)}{V_{dr}} = \frac{\left(c_t - c_r\right)}{c_t} \tag{10.2}$$

where c_r represents the radioactivity value in the reference region. This approach has the significant advantage of avoiding measurements in blood, which are often complicated by the presence of radioactive metabolites.

Because of the short half-lives of most PET tracers, it is important to reach equilibrium quickly. Therefore, the tracer is typically delivered as a bolus followed by a continuous infusion (B/I). Although ideally the infusion protocol could be more complex and could be optimised for every individual (Patlak & Pettigrew 1976), this approach would require a preliminary bolus study in each subject. Based on population values from bolus

experiments, the division of the dose into bolus and infusion components can be determined *a priori* based on an optimisation procedure (see below).

An example of time-activity data from a B/I experiment is shown in Figure 10-1 for the D_2 ligand [^{11}C]raclopride (Carson et al. 1997). Constant radioactivity levels are reached rapidly in the basal ganglia (top curve, receptor-rich region), and the cerebellum (bottom curve, devoid of receptors). BP_{ND} can then be calculated using equation (10.2), after averaging data over appropriate time intervals.

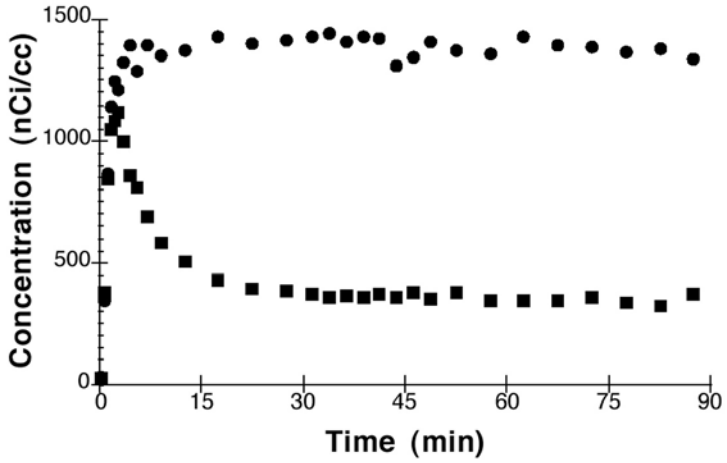

Figure 10-1 . Region-of-interest data from basal ganglia (λ) and cerebellum (ν) following combined bolus and infusion (B/I) administration of [^{11}C]raclopride

10.2 Determination of the infusion schedule

To deliver a tracer with the B/I approach, the dose must be divided into the bolus and constant infusion portions. For tracers, i.e., where the pharmacokinetic behaviour is linear, we can predict what a B/I curve will look like from knowledge of a bolus curve. Let *f(t)* be the time-activity curve for any tissue region or the plasma following a bolus administration of tracer. Define an infusion protocol H(t) as a combination of bolus plus continuous infusion over time *T*, the length of the experiment:

$$H(t) = \frac{K_{bol}}{K_{bol} + T}\delta(t) + \frac{T}{K_{bol} + T} I_T(t) \qquad (10.3)$$

where $\delta(t)$ is the Dirac delta function and $I_T(t)$ is the infusion function ($1/T$ for $0<t<T$ and 0 otherwise). The functions $\delta(t)$ and $I_T(t)$ have integrals of 1.0 and $H(t)$ is a weighted average of the two, normalised so that its integral is also 1.0. The magnitude of the bolus component is K_{bol}, which has units of time (min). A K_{bol} value of 60 min means that the bolus dose is of equal magnitude to 60 min of infusate. It is convenient to express the bolus component in this way because it is independent of the duration of the experiment.

The predicted B/I time-activity curve *g(t)* can be determined by convolution (⊗) as

$$g(t) = H(t) \otimes f(t) = \frac{K_{bol}}{K_{bol} + T} f(t) + \frac{T}{K_{bol} + T} \left(\frac{1}{T} \int_0^t f(\tau) d\tau \right) \quad (10.4)$$

Equation (10.4) shows that the predicted B/I curve is a weighted average of the bolus curve (*f(t)*) and the infusion-only curve, which is the integral of *f(t)*. The weight $K_{bol}/(K_{bol}+T)$ is the bolus fraction.

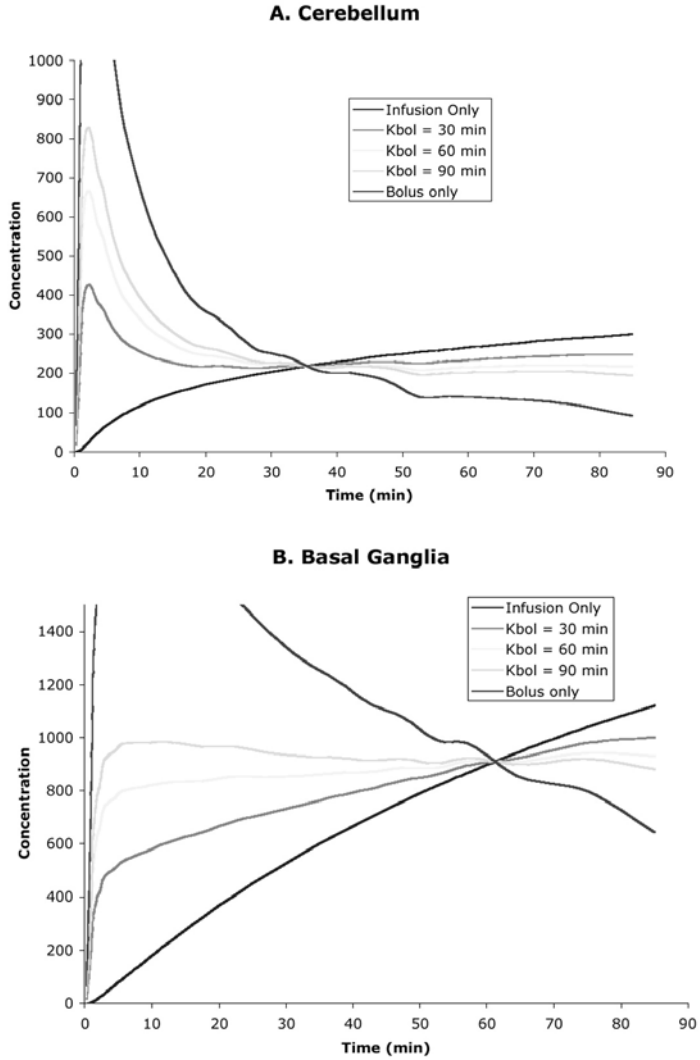

Figure 10-2. Predictions of B/I curves for a rhesus monkey [^{11}C]raclopride study based on the measured bolus curves.

An example of the process of selection of optimal K_{bol} can be seen in Figure 10-2 for a region without receptors (A. cerebellum) and with receptors (B. basal ganglia). The curves labelled Bolus only are the measured time-activity curves following a bolus injection (*f(t)*) of [^{11}C]raclopride and the remaining curves are calculated B/I curves using equation (10.4) with a range of K_{bol} values. For the cerebellum, a K_{bol} value of 30 min produces rapid equilibrium, with higher K_{bol} values producing larger overshoots in the early part of the curve. For the basal ganglia, the most rapid equilibrium is achieved with a higher K_{bol} value of 90 min. Thus, a single infusion method cannot be optimal for all regions and a compromise choice is required.

As a general rule of thumb, the region with the highest specific binding should have more weight in the selection of K_{bol} because this region has the slowest kinetics, and thus will require the longest time to reach its equilibrium level. A successful B/I result following this approach can be seen in Figure 10-1 where the infusion component has brought the basal ganglia very close to its equilibrium level at early times. Note, however, that although the total radioactivity level in the basal ganglia is nearly equal to its ultimate equilibrium level, tracer is still exchanging between free and bound compartments as they approach equilibrium; however, the total activity is nearly constant.

10.3 Transient equilibrium

V_d is the ratio at true equilibrium between the tissue concentration and plasma. For tracers that bind reversibly to tissue, often the tissue:plasma ratio and the ratio of tissue concentration values between regions become constant over time following a bolus injection. The ratios achieved in this period are *different* from those achieved during true equilibrium. When a constant tissue:plasma ratio is achieved following a bolus injection, this ratio is called the apparent volume of distribution (V_{app}) and this condition is termed "transient equilibrium", following the nomenclature of parent:daughter radioactive decay.

The source of the disagreement between the apparent and true volumes of distribution can be shown with a brief derivation. Consider the differential equation describing the tissue uptake of a reversible tracer with a single tissue-compartment:

$$\frac{dc_t}{dt} = K_1 c_p - k_2 c_t \qquad (10.5)$$

where c_t is the tissue concentration, $c_p(t)$ is the plasma input function, and K_1 and k_2 are the influx and efflux rate constants, respectively. At true equilibrium, all derivatives equal 0, Equation (10.5) shows that $V_d = c_t/c_p = K_1/k_2$. Following a bolus injection, eventually the plasma tracer activity enters a mono-exponential clearance phase with rate β, i.e., the fractional rate of change $(dc_p/dt)/c_p$ becomes -β. In other words, the plasma clears at a constant percent per minute. For reversible tracers, eventually all the tissue radioactivity levels also clear at this same fractional rate, i.e.,

$$\frac{dc_t}{dt} \to -\beta c_t \qquad (10.6)$$

At this point in time, since plasma and tissue are both clearing at the same fractional rate, the ratio between them stays constant, i.e.; transient equilibrium has been achieved. Inserting (10.6) into (10.5) , and solving for the tissue:plasma ratio yields,

$$V_{app} = \frac{c_t}{c_p} \to \frac{K_1}{k_2 - \beta} = \frac{V_d}{1 - \frac{\beta}{k_2}} \qquad (10.7)$$

Thus, the terminal plasma clearance rate β produces an increase in the measured tissue:plasma ratios so that $V_{app} > V_d$. If β is small with respect to the tissue clearance ($\beta << k_2$), then this overestimation is small. There is no overestimation under equilibrium conditions (β = 0). For regions with slower tissue clearance (e.g., due to specific receptor

binding), or for tracers with faster terminal plasma clearance rates (e.g., due to rapid peripheral metabolism), this effect can be large, producing overestimates of 100% or more. In a similar manner to that derived above, the ratios between different tissue regions are also affected by plasma clearance.

An example of this effect can be seen in Figure 10-3, where the V_{app} values for regions with high, medium, and low specific binding are plotted for the opiate antagonist [^{18}F]cyclofoxy (Carson et al. 1993). For the first 70 min, a B/I study was underway, and nearly constant radioactivity levels were achieved. At 70 min, the pump infusion was stopped, radioactivity levels in all regions dropped, and a new transient equilibrium was achieved by ~ 100 min, with much higher tissue:plasma ratios which overestimated the true equilibrium ratios. Note that the magnitude of overestimate was larger for the regions with high specific binding (smaller k_2) than those with no specific binding (larger k_2).

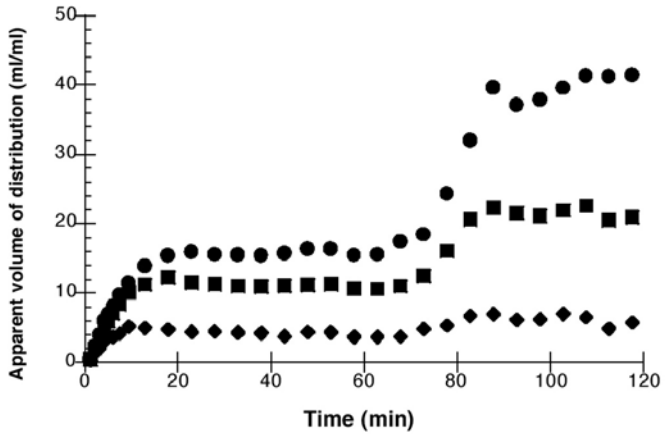

Figure 10-3. Discontinued-infusion study. [^{18}F]cyclofoxy was administered according to B/I protocol, but the infusion was discontinued at 70 min. Tissue:plasma ratios are plotted for thalamus (λ), frontal cortex (ν), and cerebellum (υ).

10.4 Infusions vs. bolus injection

The B/I methodology has a number of advantages over bolus techniques. First, the method of analysis of a constant infusion experiment is simple and is quite "model-independent" compared to some of the analysis techniques applied to dynamic bolus studies. Often, the data analysis can be accomplished without measurements in blood. If blood is to be used, at equilibrium, the arterial:venous differences may be quite small, so venous sampling may be adequate instead of the more invasive arterial sampling. For studies of changes in neurotransmitter concentrations, control and stimulus binding levels can be measured with one tracer synthesis and the total patient study time is shorter.

However, the choice of bolus or infusion paradigms is not simple. Bolus studies can also be analysed without blood measurements by use of various graphical and reference region analyses. Also, complete dynamic acquisition of data permits the estimation of more than one parameter, e.g., K_1 as a measure of blood flow; for B/I studies, if scanning is only performed at equilibrium, only V_d can be estimated. Higher levels of radioactivity must be synthesised because some will decay in the syringe while the infusion proceeds. The optimal time and duration for scanning must be determined in a B/I study. This generally

results in a trade-off between achieving equilibrium and maximising statistical counts (Watabe et al. 2000). Thus, the statistical quality of bolus studies may be better than B/I scans, particularly for short-lived PET tracers. A B/I scan is also more technically complex due to the prolonged tracer infusion. Finally, a single value of K_{bol} may not be appropriate for all individuals or for all patient categories, particularly if there are group differences in peripheral tracer metabolism.

10.5 References

Carson, R. E., Breier, A., de Bartolomeis, A., Saunders, R. C., Su, T. P., Schmall, B., Der, M. G., Pickar, D., & Eckelman, W. C. 1997, "Quantification of amphetamine-induced changes in [11C]raclopride binding with continuous infusion", *J.Cereb.Blood Flow Metab*, vol. 17,no. 4, pp. 437-447.

Carson, R. E., Channing, M. A., Blasberg, R. G., Dunn, B. B., Cohen, R. M., Rice, K. C., & Herscovitch, P. 1993, "Comparison of bolus and infusion methods for receptor quantitation: application to [18F]cyclofoxy and positron emission tomography", *J.Cereb.Blood.Flow.Metab.*, vol. 13,no. 1, pp. 24-42.

Laruelle, M., Abi-Dargham, A., Rattner, Z., al Tikriti, M. S., Zea-Ponce, Y., Zoghbi, S. S., Charney, D. S., Price, J., Frost, J. J., Hoffer, P. B., & . 1993, "Single photon emission tomography measurement of benzodiazepine receptor number and affinity in primate brain: a constant infusion paradigm with [123I]iomazenil", *Eur.J.Pharmacol.*, vol. 230,no. 1, pp. 119-123.

Patlak, C. S. & Pettigrew, K. D. 1976, "A method to obtain infusion schedules for prescribed blood concentration time courses", *J.Appl.Physiol.*, vol. 40,no. 3, pp. 458-463.

Watabe, H., Endres, C. J., Breier, A., Schmall, B., Eckelman, W. C., & Carson, R. E. 2000, "Measurement of dopamine release with continuous infusion of [11C]raclopride: optimization and signal-to-noise considerations", *J.Nucl.Med.*, vol. 41,no. 3, pp. 522-530.

11. Receptor kinetics - simplifications and limitations

R. A. Koeppe, PET Physics section, Div. of Nuc. Med. University of Michigan, Ann Arbor, USA

11.1 Model reduction

This chapter reviews the simplification methods used for analysis of receptor studies where the parameters of interest are k_3 and k_4, which give an index of receptor density in the various regions of the brain or other organs being studied. The pharmacological relationships of the model rate parameters and receptor binding densities are discussed in chapter 7.5.

We begin with a generalised kinetic model with 3-tissue-compartments, consisting of c_p, the arterial plasma concentration, c_f the concentration of free ligand in tissue, c_s the concentration of specific bound tracer in tissue and c_{ns} the concentration of non-specially bound ligand (ligand that is not available for binding to the specific receptors under investigation) (see Figure 8-2) .

K_1 and k_2 represent the blood-brain barrier (BBB) transport rate constants, k_3 and k_4 designate the rates of binding and release from specific binding sites, while k_5 and k_6 describe the transport between free and non-specifically bound compartments. It is assumed that the input function is corrected for the presence of radiolabelled metabolites, and that blood volume V_b will be taken into account although not specifically included in this general model diagram. The rate constant k_3, describing the transfer of the material from "free" to "bound" compartments is dependent on two parameters which are not identifiable from each other, k_{on} (the ligand-receptor association rate) and B_{max} density of available receptor sites. The affinity of a ligand for the receptor site, designated by the dissociation constant, K_d, is given by the ratio of k_{off}/k_{on}. The ratio of k_3/k_4, which thus becomes $k_{on} \cdot B_{max}/k_{off}$ or B_{max}/K_d, is also known as binding potential BP_{ND} .

The volumes of distribution (see section 8.6) for this 3-tissue-compartment model are as follows:

$$V_f = \frac{K_1}{k_2} \tag{11.1}$$

$$V_{ns} = \left(\frac{k_5}{k_6}\right) V_f = \left(\frac{K_1}{k_2}\right)\left(\frac{k_5}{k_6}\right) \tag{11.2}$$

$$V_{f+ns} = \frac{K_1}{k_2}\left(1 + \frac{k_5}{k_6}\right) \tag{11.3}$$

$$V_b = \frac{k_3}{k_4} V_f = \left(\frac{K_1}{k_2} \right) \left(\frac{k_3}{k_4} \right) = V_f \cdot \frac{B_{\max}}{K_d} \qquad (11.4)$$

The reduction from the three tissue-compartment to a two tissue-compartment model, where the compartments for free (c_f) and non-specifically bound (c_{ns}) ligand are lumped together as shown in Fig. 11-1 is made under the assumption of rapid equilibration between the compartments, which makes them kinetically indistinguishable.

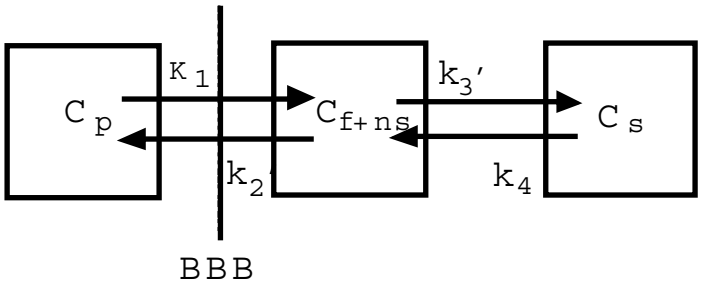

Figure 11-1. Two-tissue-compartment kinetic model configuration with 4 rate parameters (K_1 - k_4)

This simplification can be applied when the values for k_5 and k_6 from the three-tissue-compartment model are high. Model reduction, such as this, is usually necessary for use with actual measured dynamic PET data (see 11.2).

A further reduction to a single tissue-compartment model (Fig. 11-2) is possible when the values for k_3 and k_4 also are high compared to the BBB transport rates K_1 and k_2, thus allowing rapid equilibrium between free and specifically bound compartments. The description of the kinetics and the parameter estimates are identical to those of the standard flow model (e.g. the Kety-Schmidt model in section 4.4).

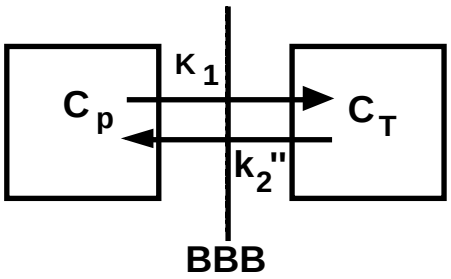

Figure 11-2. Single tissue-compartment kinetic model configuration (K_1 - k_2' ')

11.2 Trade-offs

The quality of PET data limits the number of parameters that can be measured or estimated successfully when doing kinetic fitting. For a model to be accurate, many rate parameters may be needed to describe the kinetic behaviour of the radiotracer. However, the more complex a model is, the lower the precision (due to statistical uncertainty) in the estimates of individual rate parameters. Therefore, only a limited number of rate parameters may be

estimated from the data with acceptable precision. On the other hand, when using reduced model configurations, the bias in the individual parameter estimates will increase. A trade-off between the errors due to more complex versus reduced models has to be made, which, in other words, means a trade-off between precision and bias. Adopting a more complex model, may result in decreased bias, at a loss of precision. A model simplified in the manner shown here may do the opposite: increase bias (inaccuracy) and increase precision (decrease random error). One must be very careful when simplifying models to make sure to minimise the increase in bias that occurs due to the simplification. For example, when ignoring delay or dispersion when configuring a flow model (see section 4.7), substantial bias may be introduced in the flow estimate. In actual applications, it is the task of the kinetic modellers to assess this trade-off. They need to know about the effects caused when reducing the complexity of the model in order to get more precise estimates of the rate parameters such as flow (in flow studies) or binding parameters when performing receptor studies. It is important to know the magnitudes of parameters such as blood volume V_b, dispersion or delay, and it also is necessary to know, or at least estimate, the magnitudes of the biases that will be introduced into the parameter estimates when other parameters are removed during the simplification.

11.3 Choice of model configuration

In practice, the choice of a particular model configuration is dependent on the radiotracer, the PET ligand used in a study. The following sections of this chapter focus on different ligand categories (namely reversible and irreversible) and the model configurations they are best suited for. A sensitivity analysis is needed to validate that the pertinent model parameter or parameters of an applied model are sensitive to changes in receptor density. For example, consider the case where the receptor density is changed by a factor of 10, but the estimate of an index of binding (e.g. k_3, k_3/k_4, DV) only changes by 10 %. This measure will be an extremely poor index of binding, and should be avoided. Another model configuration with a different index of binding must be found. It is important not to forget the trade-off between bias (when reducing the number of model parameters) and precision (for the individual parameter estimates) when deciding which model configuration should be applied.

11.4 Reversible Ligands

Reversible ligands, such as [C-11]flumazenil, which binds to benzodiazepine receptors and is used in the following examples, are ligands that reach equilibrium rapidly, and therefore enable short scan duration (30-60 min). Rapidly equilibrating ligands are better-suited for [C-11] tracers (which have a 20 min half-life) than for [F-18] or SPECT tracers which have longer half lives. Reversible ligands, when in true equilibrium, are well suited for use with single-tissue-compartment models or the Logan plot graphical method (see chapter 6.5). As described above, the index of binding for single-tissue-compartment models, as well as for the Logan method, is the total distribution volume of the ligand. Reversible ligands tend to be successfully applied over a larger range of ligand affinities than irreversible ligands. Non-specific binding may be problematic if there is significant binding to non-specific sites, since the free+non-specific distribution volume is included in the total distribution volume. Increased noise will propagate into the measurement, due to the presence of ligand that is not bound to specific receptor sites, and thus is not part of the "binding signal." This may require the use of a "reference region" in order to determine the

magnitude of the free+non-specifically bound component of the overall PET measure. Too rapid a clearance will also limit the statistical quality of the estimated binding index, as would be the case when the dissociation rate or reversibility is so fast that the tissue curve clears before a sufficient quantity of radioactive decay events can be recorded by the scanner.

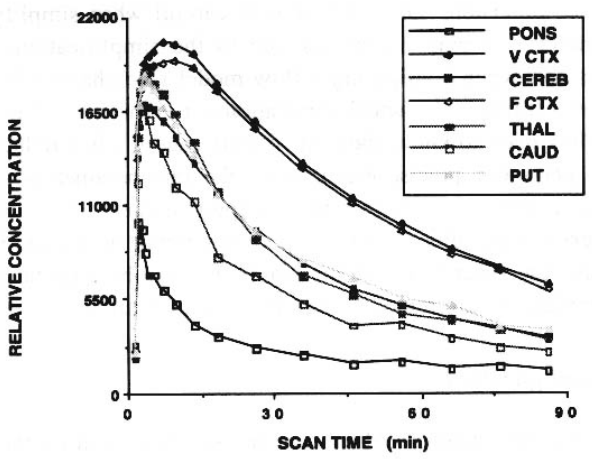

Figure 11-3. [C-11]flumazenil time-activity curves for various regions of the brain

Figure 11-3 shows tissue time activity curves in various regions of the brain, from the lowest binding density region of the brainstem (bottom-most curve), to cortical regions showed in the upper curves, which have the highest level of binding. Note the clearance of ligand for all regions, indicating reversible binding. Even in regions with high binding, such as the cortex, there is still quite rapid clearance, which suggests a high value for k_4. In this case, a single tissue-compartment model describes the shape of the curves quite well, particularly for the higher binding regions that equilibrate more rapidly.

Fig 11-4 shows a comparison of the estimates for K_1 when applying both a single-tissue and a two-tissue-compartment model. This is an example of performing a sensitivity analysis on actual [C-11]flumazenil data to demonstrate how accurately the various model parameters can be estimated. Plots show the mean and standard error of the mean (over 6 subjects) for K_1 when varying durations, up to 90 minutes, are used in the fit. The uncertainty in both single- and two- tissue-compartment models is fairly small and the estimated values are approximately the same. Note that as little as 20-30 min of data is required to yield stable results. Either model configuration could be applied successfully to the data.

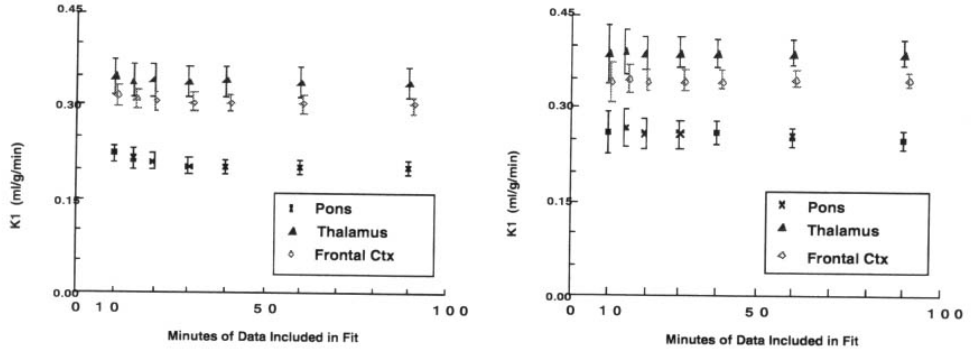

Figure 11-4. The left graph illustrates K_1 estimates in a single-tissue-compartment model whereas the right graph illustrates K_1 in a two-tissue-compartment model.

However, since the parameter of primary interest in this study would be the density of receptor sites, we are less interested in K_1 than in an index of binding. Fig. 11-5 therefore shows the estimated total distribution volume V_d for a single-tissue-compartment model (for various durations of data included in the fit) and the estimates for k_3 from a two-tissue-compartment model (for the same time durations). The standard error of the mean reflects the precision of the estimate for V_d total and k_3. The precision for V_d total from a single-tissue-compartment model estimate is considerably better than that for k_3 from a 2-tissue model, and furthermore, the single-tissue model requires only to 20-30 minutes of data to achieve stability in the results. When only 20-30 minutes of data is used for fitting, k_3 has over twice the variability as V_d because it is not possible to distinguish between the free and non-specific and the specific compartments due to the rapid equilibration. The uncertainty in the individual parameters k_3 and k_4 is quite high. However, the estimates of k_3 and k_4, although more variable, are also tightly correlated and hence, the ratio k_3/k_4 is quite stable so that either this ratio (B_{max}/K_d) or V_d could be used as an index for flumazenil binding.

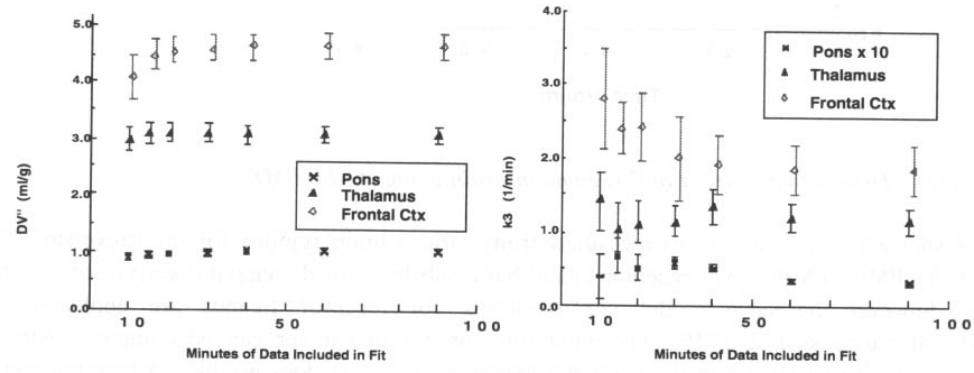

Figure 11-5. The left graph illustrates V_d estimates fitted with the single-tissue-compartment model, the right graph shows k_3 estimates obtained with the two-tissue-compartment model.

11.5 Irreversible ligands

Irreversible ligands, such as [C-11]N-methylpiperidinylpropionate (PMP) are characterised by a longer equilibration or accumulation time. Typically, these ligands are better suited for use with [F-18] labelled tracers, which have a half-life of 110 minutes, or with SPECT ligands. They are compatible with 2-tissue-compartment models rather than with single-tissue-compartment models, where k_3 and k_4 can be estimated separately (k_4 tends toward the value 0). An advantage of irreversible ligands is that they often yield high specific to non-specific concentration ratios and may allow late static imaging (as is commonly done with FDG). However, there are some disadvantages:

1. too high an affinity may produce a flow or delivery limited situation (see below);

2. the successful application of irreversible ligands tends to be limited to a narrower range of ligand affinities;

3. the slow equilibration due to irreversible or nearly irreversible binding dictates longer imaging times if the kinetic analysis is to be sufficiently sensitive to changes in binding density.

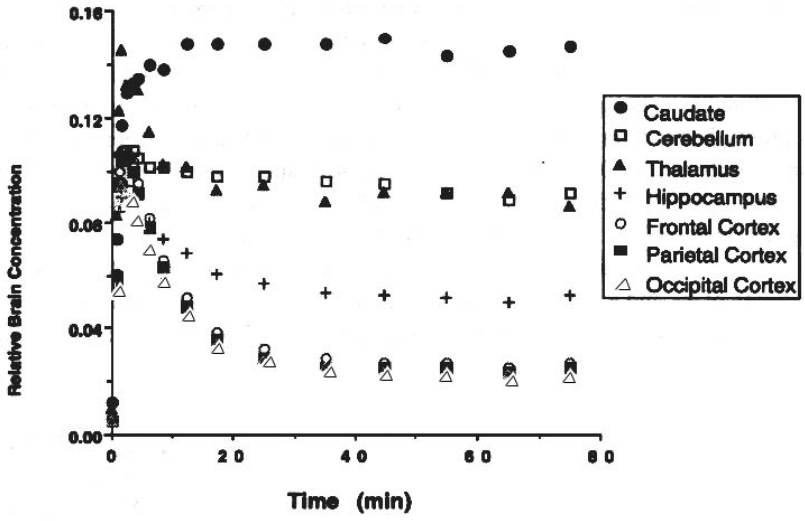

Figure 11-6. Time activity curves of 7 regions in brain using [C-11]PMP.

Fig. 11-6 shows time activity curves measured from various brain regions for the irreversible PET tracer [C-11]PMP. PMP is not a receptor ligand but a substrate for the enzyme acetylcholinesterase (AChE), however the same model configurations for receptor ligands are applicable for radiolabelled tracers such as PMP. The input function for this tracer can be compared with the input function labelled "Peak" in the computer exercises, in that it does not have a long tail caused by recirculating radiotracer. After 30 minutes, due to rapid metabolism of the tracer, the authentic level of PMP in the blood approaches 0 (less than 1%). Because this tracer is absolutely irreversible, one can see from the time activity curves that by 40 minutes everything that has entered the brain has either been trapped by the k_3 process (hydrolysis of PMP by AChE in this example) or it has been cleared from brain by the transport process, k_2. K_1 and $k_{2,}$, which depend on Blood flow,

are quite similar for the regions of the brain shown here, whereas the net accumulation, which depends both on the transport and hydrolysis, is quite different for the different brain regions. This indicates different values of k_3 for the different brain regions.

Fig 11-7 shows a 2-tissue-compartment model fit for three of the regions shown in the previous figure. The three parameters, K_1, k_2 and k_3, estimated using a standard non-linear least-squares method. One can see that a simple 3-parameter model fit to the data is quite adequate to describe the kinetics of PMP.

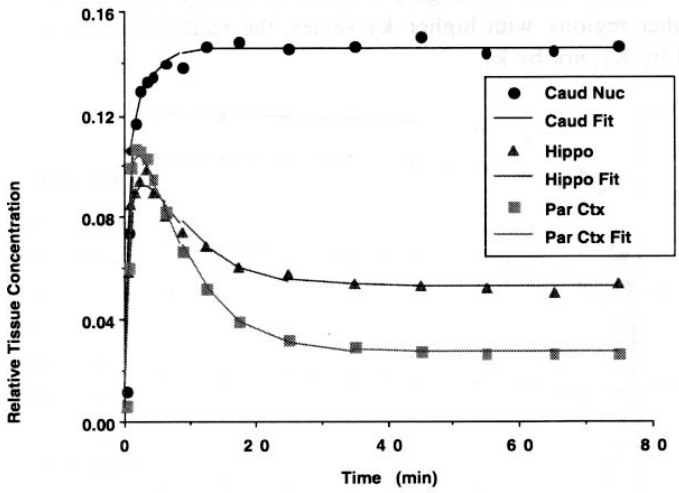

Figure 11-7. [C-11]PMP goodness-of-fit

11.6 Flow and transport limitation effects

Blood flow or transport rate across the plasma membrane may limit the net amount of tracer that is taken up by tissue. Problematic is the fact that if the affinity of a ligand is too high, especially when all tracer in tissue may be bound to specific receptor sites, the accumulation of ligand will be dependent primarily upon blood flow or tracer transport rate and not on the rate of binding or binding site density.

Recall equation **Error! Reference source not found.** that the net uptake for FDG (chapter **Error! Reference source not found.**) was defined as follows:

$$K_i = \frac{K_1 \cdot k_3}{(k_2 + k_3)},$$

we can examine the how the various rate parameters affect the net accumulation of tracer in tissue.

If k_3 is much higher than k_2 the ratio $k_3/(k_2+k_3)$ tends towards 1 and the net uptake is directly proportional to K_1, not to k_3 that is the parameter we are interested in measuring. This is what is meant by flow or transport limited uptake. The rate-limiting step is the delivery of ligand to tissue, and thus the sensitivity to changes in binding site density is

minimal. Unfortunately, this fact has been ignored often in PET, and many groups have developed tracers that have too high an affinity.

The next 3 figures demonstrate this problem. Fig. 11-8 is a simulation based on the PMP study, using an input function similar to "Peak", so that the free and non-specific concentration can be neglected. The value for k_3 changes in a way that every second step represents an order of magnitude change. For the low k_3 values, this change in magnitude can be seen clearly to produce nearly the same factor change in the tissue concentration. However, for high k_3 values, a change from 3.16 to 10 in receptor density, roughly a factor of 3, only changes the tissue concentration by about 10%. In higher regions with higher k_3 values, the relative tissue concentration is almost entirely determined by K_1, not by k_3.

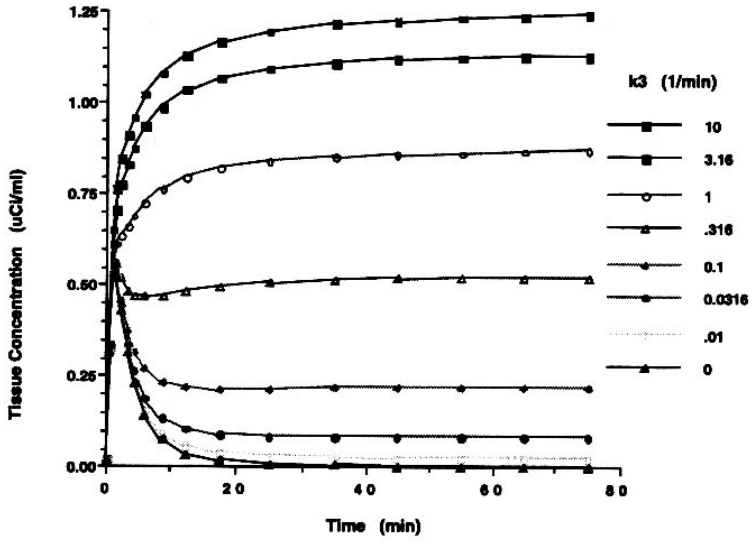

Figure 11-8. Delivery limitation effects for different k_3 values in a simulation based on a PMP study. In this simulation, free+non-specific binding does not effect signal-to-noise

Fig 11-9 shows simulated tissue curves for the same k_3 values as Fig. 11-8, but with an input function similar to the one in the exercises called "Bolus", but with a constant level in the tail of the input function curve to simulate recirculating activity in the blood. In this simulation, the free + non-specific concentration can have a significant influence on the sensitivity of the k_3 determination. Both this and the previous simulation do not have noise added to the data. Consider, however, attempting to detect a difference in receptor density if there was, for example, a 5% uncertainty in PET due to noise. Even fairly large changes in k_3, if k_3 were either too small or too large, would be "lost in the noise" and would go undetected.

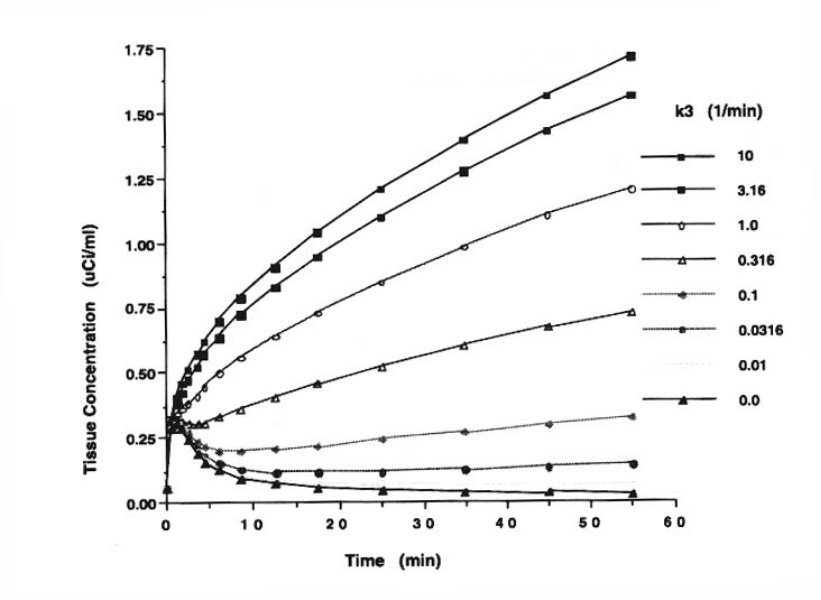

Figure 11-9. Delivery limitation effects for different k_3 values in a simulation based on a PMP study. Free+non-specific has a significant effect signal-to-noise

Fig. 11-10 shows the relative changes in PET measurement (at 50-60 min post-injection) due to the changes in k_3 values shown in the previous two simulations. Note that for latter simulation when recirculating activity is present, only k_3 values in the range of 0.03 to 0.3 would cause significant changes in the measured PET data. This plot suggests that for optimal sensitivity to changes in binding density, the value of k_3 should be between 0.05 and 0.5 of the value of k_2.

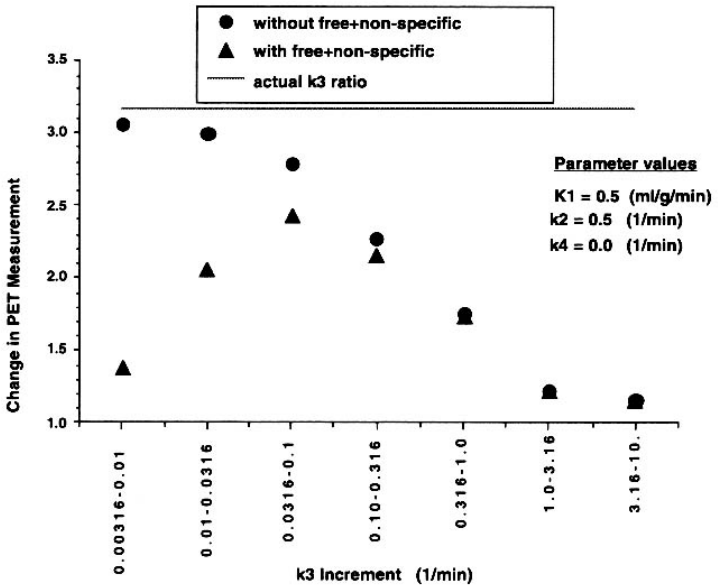

Figure 11-10. Relative changes in PET measurement at 50-60 min after injection.

11.7 Reversible versus irreversible radioligands

Sometimes tracers do not fit neatly in one of the two categories as do flumazenil (reversible) or PMP (irreversible). Often k_4 may be small but not 0, and k_3 and k_4 are not large or rapid enough to reduce the model from a two-tissue to a single-tissue-compartment model. An example for such a tracer is [C-11]dihydrotetrabenazine (DTBZ) which images binding to the vesicular monoamine transporter (VMAT2).

Fig. 11-11 shows single-tissue and two-tissue-compartment model fits for DTBZ. The density of monoamine VMAT2 is high only in the basal ganglia and low throughout the rest of the brain. The left graph shows that both regions can be well fitted with a two-tissue-compartment model. The right graph gives the residuals to the fit (i.e. the residual difference between the actual data and predicted value from the fit), demonstrating the goodness-of-fit and the appropriateness of the two-tissue-compartment configuration.

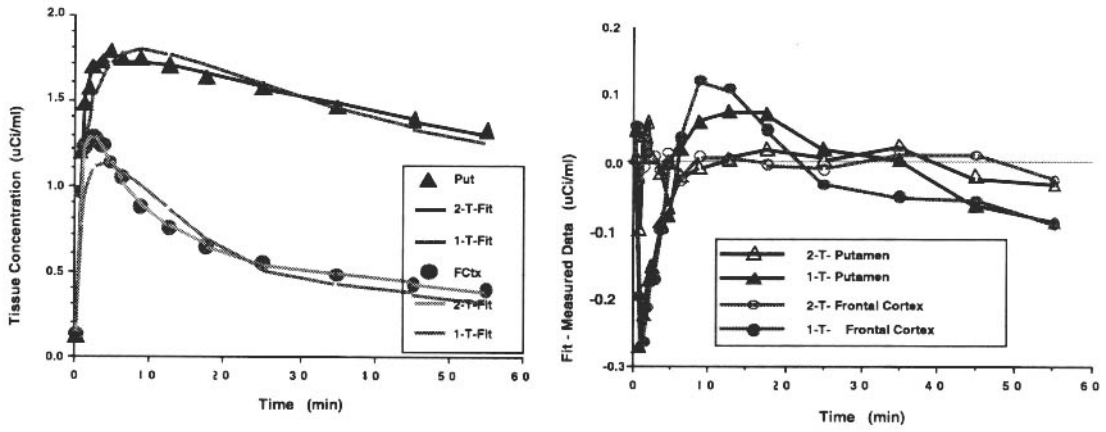

Figure 11-11. Single- and two tissue-compartment model fits for high and low binding regions in the brain investigated with DTBZ (left graph). Residuals of the DTBZ fit for single- and two-tissue-compartment model (right graph).

When estimating K_1, k_2, k_3 and k_4 with the two-tissue-compartment model, there are different indices that can be used for quantifying binding density (Fig. 11-12). As mentioned above, only the basal ganglia (caudate nucleus and putamen) have high binding to VMAT2 sites. The total distribution volume, which is estimated with high precision, includes both specific and free+non-specific components. In the basal ganglia, about 75% of the tracer is bound to specific sites while only about 25% is in the free and non-specific pool, and thus, the total distribution should provide a good index for VMAT2 binding density. In the cortex, however, well less than half of the activity is due to binding to specific sites and therefore the total V_d can not provide a reliable measure of binding. The other possible indices, k_3, k_3/k_4, and V_b do not have the free+non-specific confound, thus remove this source of bias, but yield substantially less precise estimates of binding, particularly in regions of high binding density. This is another example of a decision in how to trade-off precision vs. bias.

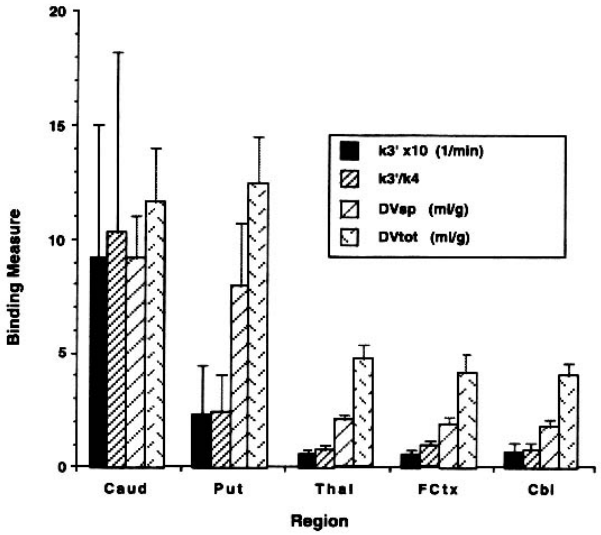

Figure 11-12. Binding estimates for several regions in the brain obtained by a two-tissue-compartment model.

In cases where there is low precision in the parameter estimates, one finds that different sets of rate parameters may equally well describe the same given tissue curve. Fig. 11-13 shows simulated time activity curves, with noise, added, having similar **total** distribution volumes, but with different fractions of the activity in the free+non-specific and specific compartments. The filled circles represent data with its fit with a specific distribution volume of 12, or 80% of the total V_d, and a free+non-specific V_d of only 3. The open circles represent data with its fit with the specific V_d of only 6.5, and a free+non-specific V_d of 7.5. Note the similarity of the two curves, with only subtle differences in their shapes and scales. When fitting curves such as those simulated here, it is often difficult to separate kinetically the free+non-specific from the specific compartment. In other words, measuring a total distribution volume V_d of 14 or 15 can be done very accurately. However, because the two compartments equilibrate quite rapidly, it can't be determined kinetically whether tracer is in the free+non-specific or in the specific compartment. Therefore, the individual estimates of the free+non-specific and the specific distribution volumes are much less precise than the estimate of their sum.

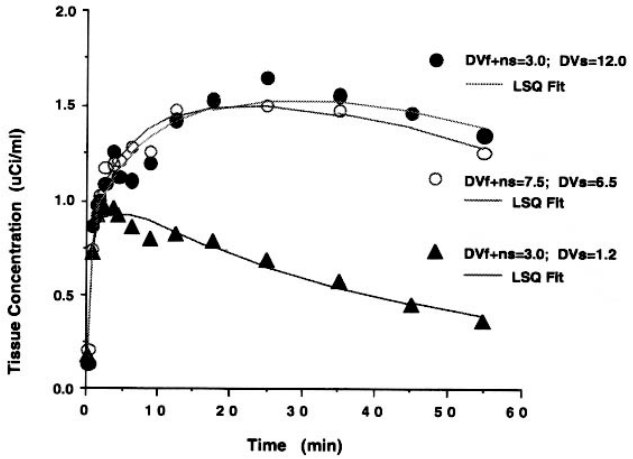

Figure 11-13. DTBZ compartment differentiability

An alternative method for estimating the total distribution volume for a **reversible** radiotracer is a graphical method usually referred to as a Logan plot (see chapter 6.5). The integral from time zero to *t* of the PET divided by the instantaneous PET value at time *t* (ordinate) is plotted versus the integral from time zero to *t* of the plasma concentration divided by the PET value at time *t* (abscissa). Note that the denominators of both axes contain the instantaneous tissue concentration measure and not the instantaneous blood measure, as does the Patlak graphical method used for estimating net uptake for **irreversible** tracers (see chapter 6.4). The slope of the straight-line portion of this plot is equal to the total distribution volume, while the negative of the ratio of the slope to the intercept yields an approximation for K_1. This approach is applicable for tracers that can be characterised either single- and multiple-tissue-compartment models. For a tracer described by a single-tissue-compartment, the plot will be linear throughout, while for multiple-tissue-compartments, there will be a non-linear portion of the graph, which must be omitted from the slope calculation. Fig 11-14 shows Logan plots for two brain regions for the ligand [C-11]DTBZ. Note the slight non-linearity at early times, indicating that a single-tissue-compartment model is not quite sufficient to describe [C-11]DTBZ kinetics. This results are in good agreement with the kinetic analysis for [C-11]DTBZ described in the preceding section. The linear portion of the curve is indicative of the time needed until sufficient equilibration has occurred between compartments.

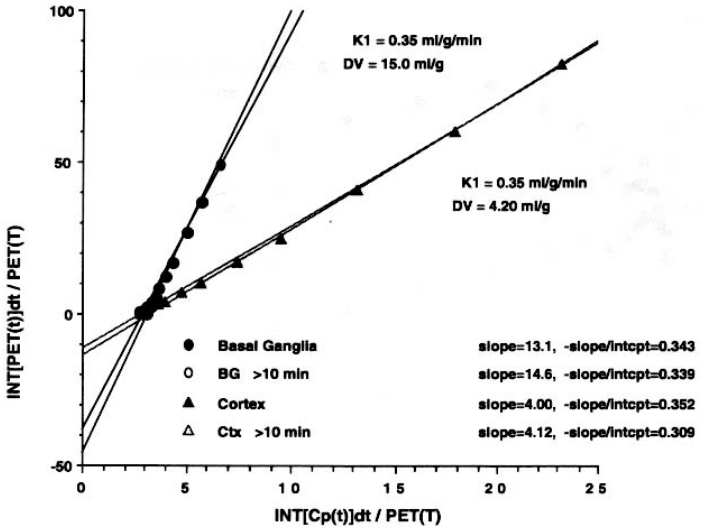

Figure 11-14. [C-11]DTBZ Logan plots of two different regions of the brain.

11.8 Alternatives for parameter estimation without acquiring arterial blood samples

Section 8.3 describes the steps needed for acquisition of arterial blood samples in order to estimate the arterial plasma concentration of authentic tracer. From this section, it becomes clear that accurate determination of the arterial plasma input function often is quite complicated as well as labour-intensive. Errors in the measured input function cause increased uncertainty in the global measures for quantitative parameter estimation (i.e. an error in the input function affects PET data from any region to nearly the same extent as any other region). Thus, if it were possible to obtain accurate parameter estimates without the use of input functions, one would choose to avoid blood-sampling altogether. This is often not possible, but in specialised cases, quantitative parameter estimates can be made from the PET data alone. Some non-invasive alternatives for parameter estimation requiring neither acquisition nor analysis of multiple blood samples are described below.

In cases where one region within the image field-of-view is devoid of specific binding sites, called a reference region, this region can be used to estimate the free+non-specific concentration of tracer. Assuming the free+non-specific distribution space to be regionally constant, estimates of parameters from this region can then be used in conjunction with a simplified model (not requiring an input function) to estimate the binding parameters in a second region which does have a significant level of specific binding (for more detailed description see 8.6).

For rapidly reversible tracers, a protocol using a constant infusion of tracer yields a tissue concentration that becomes constant later in the study. The tissue to blood ratio at steady state for later scans time points becomes identical to the total distribution volume. This ratio can be obtained without doing any arterial blood sampling and acts as a relative index of binding across the brain. For example, if one region is three times higher than another, the V_d is exactly 3 times higher as well. Fig. 11-15 shows an example of a continuous infusion study for the tracer [C-11]DTBZ. The input function for these studies is of the type from the exercise labelled “Bolus” followed by continuous infusion. After 40

minutes, the activity curves for high and low binding regions have reached stable values. Rather than estimating K_1 and k_2 in order to yield V_d, the ratio can be estimated directly from the data.

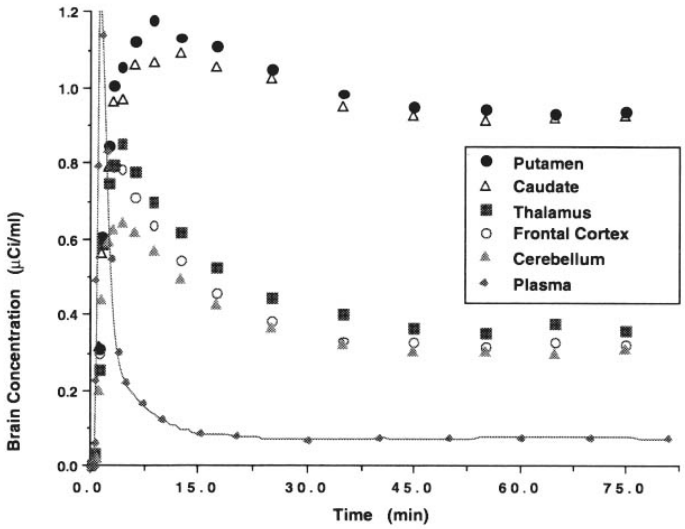

Figure 11-15. [C-11]DTBZ concentration in several regions of the brain compared to the [C-11]DTBZ concentration in plasma.

Under certain specific conditions, the k_3 value for irreversible tracers can also be estimated without the use of an input function. The following conditions must be met:

1. the input function goes to zero at some point during the study

2. k_4 must be zero (i.e. the k_3 process is completely irreversible)

3. the tissue concentration becomes constant before the end of the study.

If these conditions are met, and if the rate of transfer of tracer from the first to the second tissue-compartment is sufficiently slower than the rate of back diffusion from tissue to blood, (i.e. $k_3 < k_2$), k_3 can be measured from the shape of the tissue time activity curves alone. The calculation of k_3 requires that all radioactivity measured by PET at the start of the study is in the first tissue (precursor) compartment. This assumption can be met by acquiring sufficiently short scans immediately after injection of tracer. The calculation also requires that all activity remaining in tissue by the end of the study is in the second (product) compartment. It is this second assumption that requires the two conditions stated above to be met. All activity being in the product compartment means there is no tracer remaining in the precursor compartment, which in turn requires there to be no more delivery of tracer from the blood to tissue (i.e. the input function must go to zero). Once the input function reach zero and the radiotracer in the precursor compartment has either been cleared or trapped irreversibly in the product compartment, no further exchange between compartments is possible, and the final condition (the tissue concentration becomes constant) is achieved.

The estimation of k_3 is made as follows:

$$PET = C_{TOT} = C_{PREC} + C_{PROD} \tag{11.5}$$

For the first scan it is assumed that:

$$C_{PROD}(1) = 0 \text{ and } C_{PREC}(1) = C_{TOT}(1) \tag{11.6}$$

The product of the next and following scans will be:

$$C_{PROD}(n) = C_{PROD}(n-1) + k_3 \cdot C_{PREC}(n-1)\Delta t \tag{11.7}$$

and

$$C_{PREC}(n) = C_{TOT}(n) - C_{PROD}(n) \tag{11.8}$$

The optimal k_3 value is that which predicts an amount of product formed by the end of the study which equals the total measured PET value. If k_3 is too small, the precursor pool has not emptied completely and thus, the amount of product formed by the end of the study is less than total. When k_3 is too large, the amount of product reaches the total before the measured PET data has become constant, thus overestimating the final amount of product formed.

In this example shown in Fig. 11-16, k_3 was set to 0.03 min^{-1}. The simulated PET time activity curve (Total) is given by the large filled circles and bold solid line. The calculated precursor (open figures) and product (filled figures) contributions to the total are given for four k_3 values. Only at the correct value for k_3 does the concentration of product equal the total and the precursor concentration reaches zero at the end of the study.

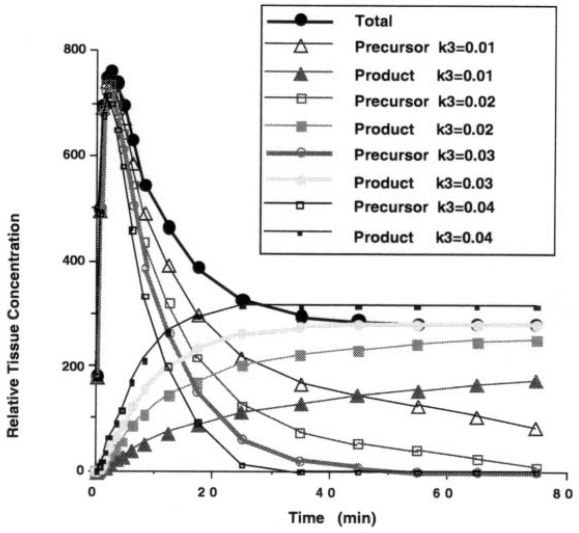

Figure 11-16. Fitting k_3 values for [C-11]PMP without input function or arterial blood sampling.

12. Data driven methods

R.N. Gunn, GSK and Oxford University, UK

12.1 Introduction

As can be seen from the previous chapters there are a range of PET modelling techniques based on a compartmental analysis of the tracer, which return biologically based parameter estimates. These techniques may be broadly divided into *model-driven* methods and *data-driven* methods. What distinguishes the two approaches is that *model-driven* methods require the a priori selection of a compartmental model, whereas the *data-driven* methods do not. The *model-driven* methods use a particular compartmental structure (see Figure 12-1) to describe the behaviour of the tracer and allow for an estimation of either micro or macro system parameters. The *data-driven* methods are based on properties of all these models that generalise to an arbitrary number of compartments and allow for the estimation of macro parameters.

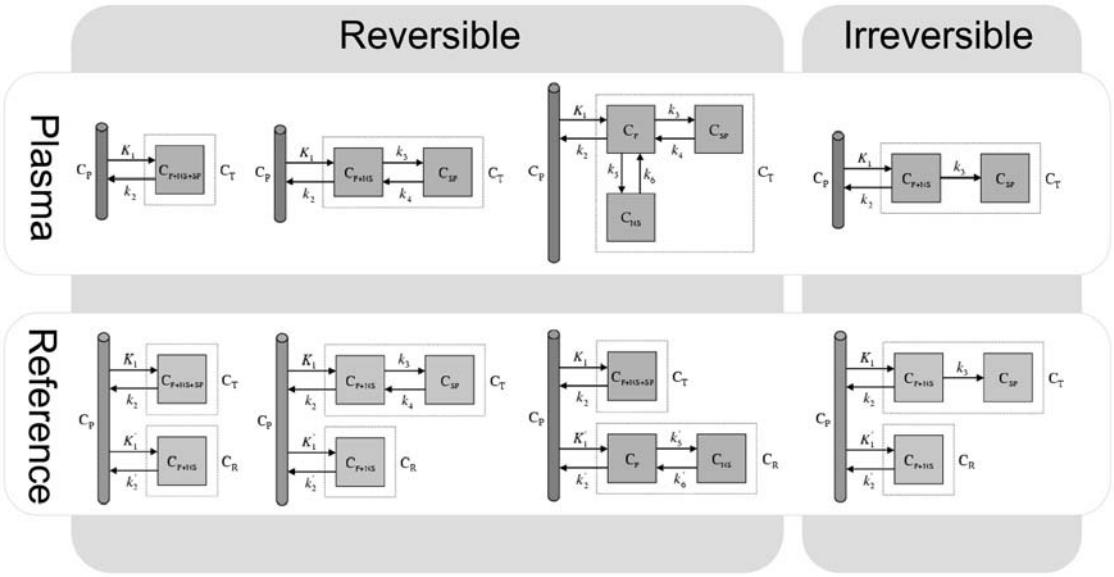

Figure 12-1: A range of PET compartmental models commonly used to quantify PET radiotracers. These include models for tracers that exhibit reversible and irreversible kinetics and models that use either a plasma or reference-tissue input function. Here, the compartments are depicted in terms of radioligand binding and constitute either free (F), non-specifically bound (NS), specifically bound (SP) radioligand or some combination of them.

There are three *data-driven* methods: graphical analysis, spectral analysis and basis pursuit. This chapter will first present the equations for a general compartmental system and then show how the *data-driven* methods are derived from this equation. First, we consider systems that use a plasma input-function for quantification. Throughout this

chapter, the contribution of blood volume to the observed signal will be neglected for simplicity.

12.2 Plasma Input Models

Let us consider a general compartmental system that is illustrated in Figure 12-2. From the

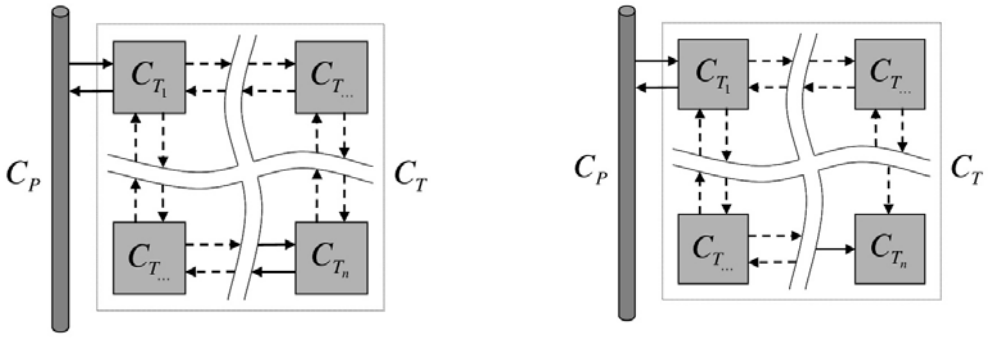

a) Reversible kinetics b) Irreversible kinetics

Figure 12-2: General compartmental model

theory of linear time invariant systems it is possible to derive the general equation for a plasma input compartmental model in terms of the systems impulse response function (IRF) which is a sum of exponentials (see (Gunn et al. 2001) for derivation),

$$IRF = \sum_{i=1}^{n} \phi_i e^{-\theta_i t} \tag{12.1}$$

where n is the total number of tissue-compartments in the target tissue, ϕ_i and θ_i are constants which are functions of the individual rate constants (the k's). As an example, for the single tissue reversible compartment model [$n = 1$, $\phi_1 = K_1$, $\theta_1 = k_2$],

$$IRF = K_1 e^{-k_2 t} \tag{12.2}$$

The simplest way to understand the impulse response function is to think of it as the tissue curve that would be observed if a true bolus (or spike of activity) could be delivered directly to the tissue. In practice, the input function is not a bolus and so the observed tissue curve becomes the convolution of the impulse response function with the plasma input function,

$$c_t = \sum_{i=1}^{n} \phi_i e^{-\theta_i t} \otimes c_p \tag{12.3}$$

The delivery of the tracer to the tissue is given by $k_1 = \sum_{i=1}^{n} \phi_i$

.

Reversible Kinetics [$\theta_i > 0$] For compartmental models which exhibit reversible kinetics the volume of distribution, V_d, which is equal to the integral of the impulse response function is given by,

$$\begin{aligned} V_d &= \int_0^\infty IRF \quad dt \\ &= \sum_{i=1}^{n} \frac{\phi_i}{\theta_i} \end{aligned} \tag{12.4}$$

Irreversible Kinetics [$\theta_{i\neq n} > 0$, $\theta_n = 0$] For compartmental models which exhibit irreversible kinetics (a single trap compartment) the net irreversible uptake rate constant from plasma, K_i, is given by,

$$\begin{aligned} K_i &= \lim_{t\to\infty} \quad IRF \\ &= \phi_n \end{aligned} \tag{12.5}$$

Equations ((12.3) (12.4) and (12.5)) are the fundamentals of all the *data-driven* methods. Let us consider how these equations are utilised by the *data-driven* methods.

12.2.1 Graphical methods

The graphical methods of Patlak and Logan have already been covered in Chapter 6, but we return to them here briefly to show that they are valid for an arbitrary number of compartments. Thus, they are classed as *data-driven* because they do not require the a-priori selection of a particular compartmental model. The graphical methods employ a transformation of the data such that, after a certain time, a linear regression of the transformed data yields the macro system parameter of interest.

Logan Plot (Reversible Kinetics) The Logan plot with a plasma input (Logan et al. 1990) allows for the estimation of the total volume of distribution (V_d) and is given by,

$$\frac{\int_0^t c_t \quad dt}{c_t} \cong V_d \frac{\int_0^t c_p \quad dt}{c_t} \quad + \quad c \tag{12.6}$$

From the general expression for a reversible plasma input system the equation for the target tissue is given by equation (12.3) and the volume of distribution by (12.4). Without loss of generality an ordering on the θ's is imposed such that $\theta_1 > \theta_2 > \ldots > \theta_n$. Substituting equation (12.3) into the left hand side of equation (12.6) yields,

$$\frac{\int_0^t c_t \quad dt}{c_t} = \frac{\int_0^t \sum_{i=1}^{n} \phi_i e^{-\theta_i t} \otimes c_p \quad dt}{c_t} \tag{12.7}$$

$$= \frac{\sum_{i=1}^{n} \frac{\phi_i}{\theta_i} \left(1 - e^{-\theta_i t}\right) \otimes c_p}{c_t} \tag{12.8}$$

$$= \frac{\sum_{i=1}^{n} \frac{\phi_i}{\theta_i} \otimes c_p}{c_t} - \frac{\sum_{i=1}^{n} \frac{\phi_i}{\theta_i} e^{-\theta_i t} \otimes c_p}{c_t} \tag{12.9}$$

$$= \sum_{i=1}^{n} \frac{\phi_i}{\theta_i} \frac{\int_0^t c_p \quad dt}{c_t} - \frac{\sum_{i=1}^{n} \frac{\phi_i}{\theta_i} e^{-\theta_i t} \otimes c_p}{c_t} \tag{12.10}$$

Substitution of equation (12.4) gives,

$$= V_d \frac{\int_0^t c_p dt}{c_t} - \frac{\sum_{i=1}^{n} \frac{\phi_i}{\theta_i} e^{-\theta_i t} \otimes c_p}{\sum_{i=1}^{n} \phi_i \, e^{-\theta_i t} \otimes c_p} \tag{12.11}$$

For suitably large *t*,

$$\frac{\int_0^t c_t \quad dt}{c_t} \cong V_d \frac{\int_0^t c_p \quad dt}{c_t} \quad - \quad \frac{1}{\theta_n} \tag{12.12}$$

Patlak Plot (Irreversible Kinetics) The Patlak plot with a plasma input (Patlak et al. 1983) allows for the estimation of the irreversible uptake rate constant from plasma (K_i) and is given by,

$$\frac{c_t}{c_p} \cong K_i \frac{\int_0^t c_p \quad dt}{c_p} + c \tag{12.13}$$

From the general expression for an irreversible plasma input system the equation for the target tissue is given by,

$$c_t = \left(\sum_{i=1}^{n-1} \phi_i e^{-\theta_i t} + \phi_n \right) \otimes c_p \tag{12.14}$$

and the irreversible uptake rate constant from plasma,

$$K_i = \phi_n \tag{12.15}$$

Substituting equation (12.14) into the left hand side of equation (12.13) yields,

$$\frac{c_t}{c_p} = \frac{\left(\sum_{i=1}^{n-1} \phi_i e^{-\theta_i t} + \phi_n \right) \otimes c_p}{c_p} \tag{12.16}$$

$$\frac{c_t}{c_p} = \phi_n \frac{\int_0^t c_p \quad dt}{c_p} + \frac{\left(\sum_{i=1}^{n-1} \phi_i e^{-\theta_i t} \right) \otimes c_p}{c_p} \tag{12.17}$$

Substitution of equation (12.15) gives,

$$\frac{c_t}{c_p} = K_i \frac{\int_0^t c_p \quad dt}{c_p} + \frac{\left(\sum_{i=1}^{n-1} \phi_i e^{-\theta_i t} \right) \otimes c_p}{c_p} \tag{12.18}$$

For suitably large *t*,

$$\frac{c_t}{c_p} \cong K_i \frac{\int_0^t c_p \quad dt}{c_p} + \sum_{i=1}^{n-1} \frac{\phi_i}{\theta_i} \tag{12.19}$$

12.2.2 Spectral Analysis

Spectral analysis (Cunningham & Jones 1993) characterises the systems impulse response function (IRF) as a positive sum of exponentials and uses non-negative least squares to fit a set of exponential basis functions to the data. The macro system parameters of interest are then calculated as functions of the *IRF*. Spectral analysis also returns information on the number of tissue-compartments evident in the data and is defined as a *transparent* technique. For the majority of plasma input models the observation of all compartments leads to only positive coefficients (Schmidt 1999), and as such the spectral analysis solution using non-negative least squares is valid. Returning to our general equation for the plasma input system (12.3). If we consider a discrete spectrum of values for θ, then this equation can be expressed as an expansion on a basis,

$$c_t = \sum_{j=1}^{N} \phi_j \psi_j \tag{12.20}$$

where

$$\psi_j = e^{-\theta_j t} \otimes c_p \tag{12.21}$$

A set of N values for θ_j may be pre-chosen from a physiologically plausible range $\theta_{min} \leq \theta_j \leq \theta_{max}$. Here, the θ_j values are spaced in a logarithmic manner to elicit a suitable coverage of the kinetic spectrum. For data that has not been corrected for the decay of the isotope θ_{min} may be chosen as (or close to the decay constant ($\theta_{min} = \lambda\ min^{-1}$) for the radioisotope and θ_{max} may be chosen as a suitably large value ($\theta_{max} = 6\ min^{-1}$). For reversible systems, where the calculation of V_d is the goal, the choice of θ_{min} which is slightly bigger than λ can suppress the calculation of infinite V_d values from noisy data. An example set of basis functions is shown in Figure 12-3.

a) Plasma input basis b) Normalised plasma input basis

Figure 12-3: Set of Basis Functions (Ψ) for a plasma input

PET measurements are acquired as a sequence of (F) temporal frames. Thus, the continuous functions must be integrated over the individual frames and normalised to the frame length to correspond to the data sampling procedure. The tissue observations, y, already exist in this form and correspond to,

$$\begin{aligned} y &= \left[y_1 \ \cdots \ y_T \right]^T, \\ y_k &= \frac{1}{t_k^e - t_k^s} \int_{t_k^s}^{t_k^e} c_t \ \ dt \end{aligned} \tag{12.22}$$

and the matrix of kinetic basis functions (or dictionary), Ψ are pre-calculated as,

$$\Psi = \begin{pmatrix} \psi_{11} & \cdots & \psi_{N1} \\ \vdots & \vdots & \vdots \\ \psi_{1F} & \cdots & \psi_{NF} \end{pmatrix}, \qquad \psi_{jk} = \frac{1}{t_k^e - t_k^s} \int_{t_k^s}^{t_k^e} e^{-\theta_j t} \otimes c_p \, dt \tag{12.23}$$

where t^s_k and t^e_k are the sequences of start and end frame times ($k = 1,\ldots, F$). For all practical purposes (i.e. choosing a large enough value for N to obtain a good coverage of the kinetic spectrum), this leads to an overcomplete basis ($N > F$) which by definition is non-orthogonal. Thus, conventional least squares techniques are not applicable. To determine the fit to the data it is necessary to solve the underdetermined system of equations,

$$\mathbf{y} \cong \mathbf{\Psi} \boldsymbol{\phi} \tag{12.24}$$

Spectral analysis uses non-negative least squares (NNLS) to solve this undetermined system of equations which corresponds to minimising the following function,

$$\min_{\phi} \left\| \mathbf{y} - \mathbf{\Psi} \boldsymbol{\phi} \right\|_2^2 \tag{12.25}$$

subject to $\phi_j \geq 0$. The system macro parameter may then be directly calculated using equation (12.4) for reversible systems (V_d) and equation (12.5) for irreversible systems (K_i).

In addition to parameter estimation, spectral analysis allows us to obtain information on the number of compartments and the kinetics involved. The number of peaks within the spectrum corresponds to the total number of compartments. The position of these peaks gives information on the kinetics; a peak at the left corresponds to very fast kinetics which represent a vascular contribution, peaks in the middle corresponds to reversible compartments and a peak at the right correspond to an irreversible compartment (see Figure 12-4).

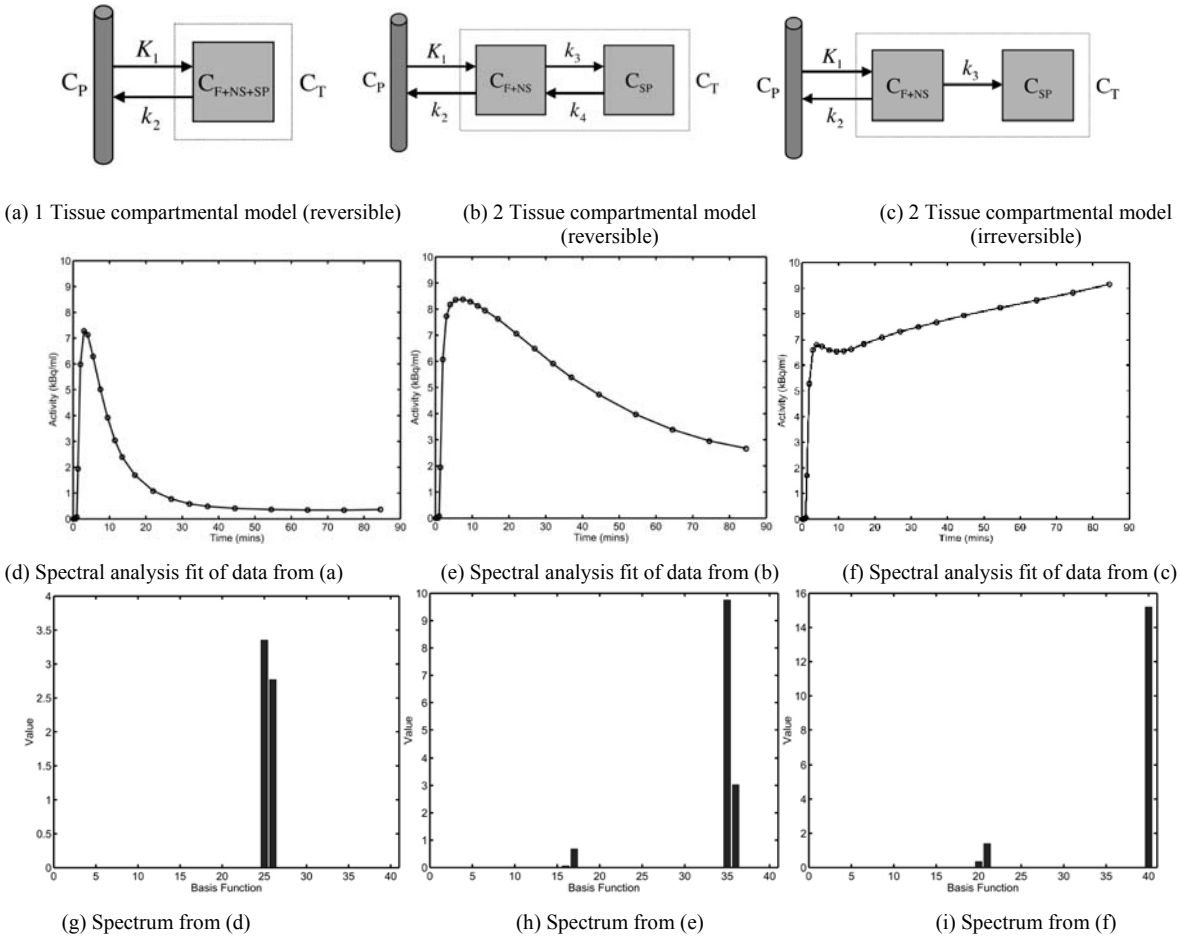

(a) 1 Tissue compartmental model (reversible) (b) 2 Tissue compartmental model (reversible) (c) 2 Tissue compartmental model (irreversible)

(d) Spectral analysis fit of data from (a) (e) Spectral analysis fit of data from (b) (f) Spectral analysis fit of data from (c)

(g) Spectrum from (d) (h) Spectrum from (e) (i) Spectrum from (f)

Figure 12-4: Spectral analysis applied to simulated data. (top row) Model used, (middle row) simulated data and spectral analysis fit, (bottom row) spectrum of coefficients (ϕ). (left column) Reversible 1 tissue-compartment model, (middle column) Reversible 2 tissue-compartment model, (right column) Irreversible 2 tissue-compartment model.

12.2.3 Basis Pursuit

Briefly, a third method called basis pursuit is considered. Basis pursuit denoising (Gunn et al. 2002a) offers another approach to solving the linear system of equations given in equation 12.24. The difference with this approach is that it does not constrain the coefficients (ϕ_i) to be positive. Instead a regularization term ($\mu\|\phi\|_1$) is included so that the underdetermined system of equations may be solved. Solutions are obtained by minimising the objective function,

$$\min_{\phi} \ \frac{1}{2}\|\mathbf{y}-\Psi\phi\|_2^2 + \mu\|\phi\|_1 \qquad (12.26)$$

using a quadratic program. Basis pursuit returns parameter estimates, information on the number of compartments and type of kinetics and thus is *transparent*.

12.3 Reference Tissue Input Models

Reference tissue input models were developed for the quantification of receptor binding studies which have a region devoid of specific binding that may be used as an input function. Particular reference tissue compartmental models have been introduced and discussed in Chapter 7. Let us consider a general reference tissue-compartmental system (see Figure 12-5).

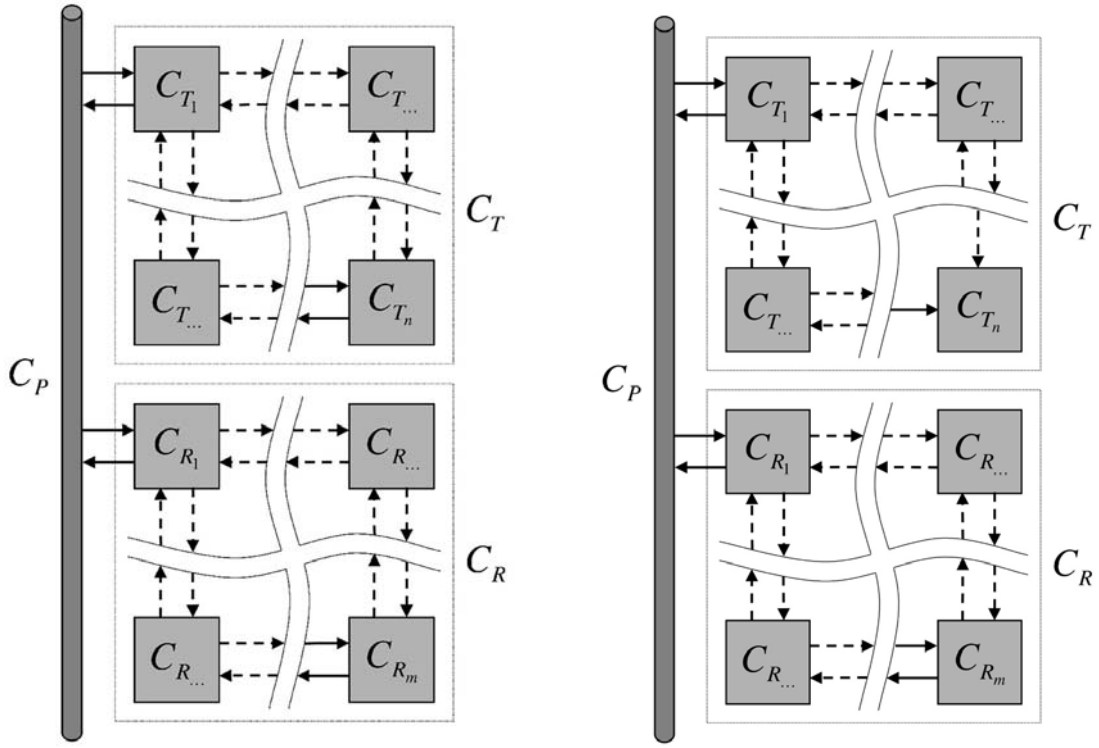

a) Reversible target tissue kinetics b) Irreversible target tissue kinetics

Figure 12-5: General reference tissue compartmental model (Reversible reference tissue kinetics)

It is possible to derive a general equation for systems using a reference tissue input function from linear systems theory (see (Gunn et al. 2001) for derivation). Here, the reference tissue is assumed to have reversible kinetics. The target tissue may be described in terms of the impulse response function for a reference tissue system,

$$IRF = \phi_0 \delta(t) + \sum_{i=1}^{m+n-1} \phi_i e^{-\theta_i t} \tag{12.27}$$

As an example, take the simplified reference tissue model, which is the simplest reference tissue model and has just a single compartment in both the reference and target regions $[\, m=1,\ n=1,\ \phi_0 = R_1,\ \phi_1 = R_1\left(k_2^{'} - k_2\right),\ \theta_1 = k_2\,]$

$$IRF = R_1 \delta(t) + R_1 (k_2^{'} - k_2) e^{-k_2 t} \tag{12.28}$$

The form of the general impulse response function is very similar to the plasma input form, except there is the addition of a delta function term. Hence, the general equation for a reference tissue input compartmental model is given by,

$$c_t = \phi_0 c_R + \sum_{i=1}^{m+n-1} \phi_i e^{-\theta_i t} \otimes c_R \tag{12.29}$$

where m is the total number of tissue-compartments in the reference tissue, and n is the total number of tissue-compartments in the target tissue, and $R_1 (= \phi_0)$ is the ratio of delivery of the tracer between the target and reference tissue. Here, parameters with primes pertain to the reference tissue.

Reversible Target Tissue Kinetics $[\theta_i > 0]$ For reference tissue models which exhibit reversible kinetics in both the target and reference tissues the volume of distribution ratio is given by the integral of the impulse response of the system,

$$\begin{aligned} \frac{V_d}{V_d'} &= \int_0^\infty IRF \quad dt \\ &= \phi_0 + \sum_{i=1}^{m+n-1} \frac{\phi_i}{\theta_i} \end{aligned} \tag{12.30}$$

This measure is useful for neuroreceptor studies as the binding potential may be obtained directly from it (assuming that the non-specific binding is the same in both tissues),

$$BP_{ND} = \frac{V_d}{V_d'} - 1 \tag{12.31}$$

Irreversible Target Tissue Kinetics $[\theta_{i \neq m+n-1} > 0, \ \theta_{m+n-1} = 0]$

For reference tissue models which exhibit irreversible kinetics in the target tissue and reversible kinetics in the reference tissue the normalised irreversible uptake rate constant from plasma is given by,

$$\begin{aligned} \frac{K_i}{V_d'} &= \lim_{t \to \infty} IRF \\ &= \phi_{m+n-1} \end{aligned} \tag{12.32}$$

In contrast to the plasma input model the coefficients (ϕ_i) are no longer guaranteed to be positive which means that a spectral analysis approach is not strictly valid (you can easily find a counter example by considering equation (12.28)). However, the graphical and basis pursuit methods are applicable.

12.3.1 Graphical methods

There are reference tissue versions of the Patlak and Logan graphical methods that are valid for an arbitrary number of compartments in the reference and target tissues. These may be derived in a similar manner to the graphical methods for a plasma input and this is left to the interested reader. Similarly, to the plasma input graphical methods the following equations are valid after a suitable time *t*.

Logan Plot (Reversible Kinetics) The Logan plot with a reference tissue input (Logan et al. 1996) is given by equation,

$$\frac{\int_0^t c_t \quad dt}{c_t} \cong \frac{V_d}{V_d'} \frac{\int_0^t c_r \quad dt}{c_t} \quad + \quad c \tag{12.33}$$

Patlak Plot (Irreversible Kinetics) The Patlak plot with a reference tissue input (Patlak & Blasberg 1985) is given by,

$$\frac{c_t}{c_r} \cong \frac{K_i}{V_d'} \frac{\int_0^t c_r \quad dt}{c_r} + c \tag{12.34}$$

12.3.2 Basis Pursuit

The general reference tissue model may be solved by basis pursuit (Gunn et al. 2002b) in a similar way to the plasma input case. Returning to the general equation (12.29) it can be seen that it constitutes a linear combination of the reference tissue time course and this function convolved with exponentials. Again, if we consider a discrete spectrum of values for θ then the general reference tissue equation can be expressed as an expansion on a basis (12.20) with,

$$\begin{aligned} \psi_0 &= c_r, \\ \psi_j &= e^{-\theta_j t} \otimes c_r \end{aligned} \tag{12.35}$$

This leads to the definition of the matrix of kinetic basis functions (or dictionary), $\mathbf{\Psi}$, as,

$$\begin{aligned} \Psi &= \begin{pmatrix} \psi_{01} & \psi_{11} & \cdots & \psi_{N1} \\ \vdots & \vdots & \vdots & \vdots \\ \psi_{0F} & \psi_{1F} & & \psi_{NF} \end{pmatrix}, \\ \psi_{0k} &= \frac{1}{t_j^e - t_j^s} \int_{t_j^s}^{t_j^e} c_r \, dt \\ \psi_{jk} &= \frac{1}{t_k^e - t_k^s} \int_{t_k^s}^{t_k^e} e^{-\theta_j t} \otimes c_r \, dt \end{aligned} \tag{12.36}$$

An example set of basis functions using a reference tissue input are shown in Figure 12-6.

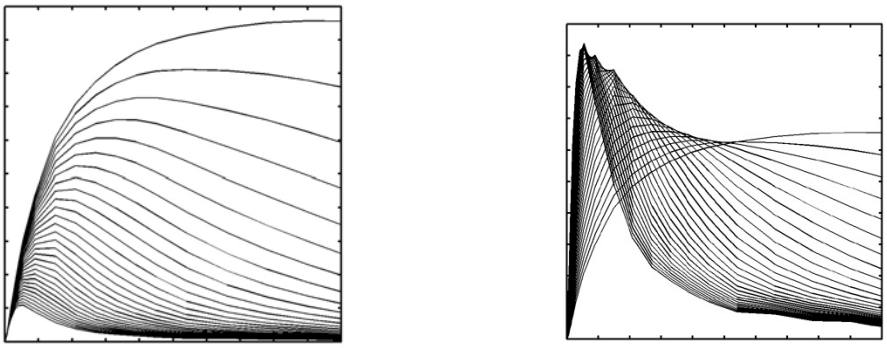

a) Reference tissue input basis b) Normalised reference tissue input basis

Figure 12-6: Set of Basis Functions (Ψ) for a reference tissue input.

To determine the fit to the data it is necessary, once again, to solve the underdetermined system of equations (12.24) and this can be solved using the identical objective function used for the plasma input case equation (12.26). The parameter values are then determined from the coefficients using either equation (12.30) or (12.32). The number of peaks in the spectrum will inform us of the total number of tissue-compartments in the target and reference tissue region.

12.4 Summary

The three *data-driven* methods (Table 12-1) can be derived from the general equation for a plasma input (12.3) or reference tissue input (12.29) compartmental model.

Table 12-1: Summary of the *Data Driven* methods.

Data driven method	Plasma input	Reference tissue input	Transparency
Graphical analysis	✓	✓	×
Spectral analysis	✓	×	✓
Basis Pursuit	✓	✓	✓

The data-driven methods can be implemented quickly on a computer and this is one reason why they are particularly useful for generating parametric images. These are obtained by applying the methods to each voxel time activity curve from the 4-dimensional data set. Figure 12-7 shows a parametric image of the opiate receptor ligand [11C]diprenorphine.

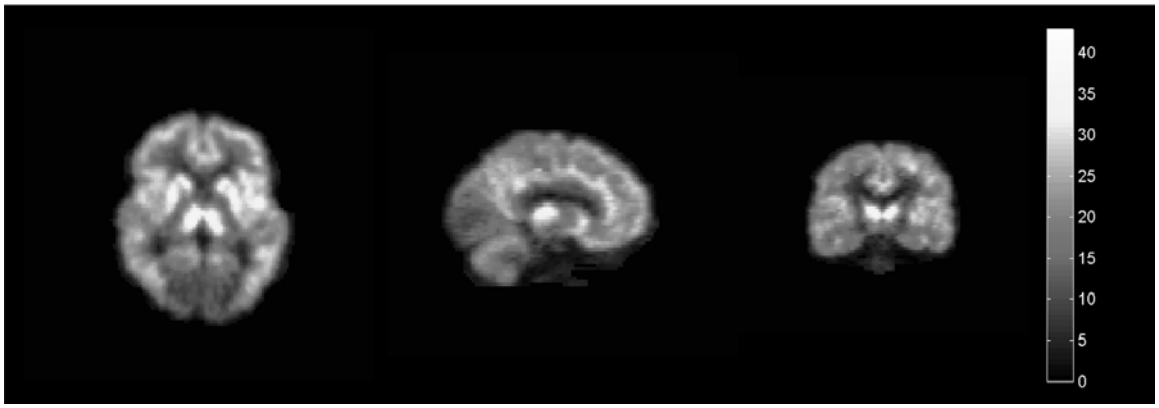

Figure 12-7: [^{11}C]Diprenorhpine: V_d image volume generated using basis pursuit and a plasma input function (transverse, sagittal and coronal sections displayed).

12.5 References

Cunningham, V. J. & Jones, T. 1993, "Spectral analysis of dynamic PET studies", *J Cereb.Blood Flow Metab*, vol. 13,no. 1, pp. 15-23.

Gunn, R. N., Gunn, S. R., & Cunningham, V. J. 2001, "Positron emission tomography compartmental models", *J Cereb.Blood Flow Metab*, vol. 21,no. 6, pp. 635-652.

Gunn, R. N., Gunn, S. R., Turkheimer, F. E., Aston, J. A., & Cunningham, V. J. 2002b, "Positron emission tomography compartmental models: a basis pursuit strategy for kinetic modeling", *J.Cereb.Blood.Flow.Metab.*, vol. 22,no. 12, pp. 1425-1439.

Gunn, R. N., Gunn, S. R., Turkheimer, F. E., Aston, J. A. D., & Cunningham, V. J. 2002a, "Tracer kinetic modeling via basis pursuit," in *Brain Imaging Using PET*.

Logan, J., Fowler, J. S., Volkow, N. D., Wang, G. J., Ding, Y. S., & Alexoff, D. L. 1996, "Distribution volume ratios without blood sampling from graphical analysis of PET data", *J Cereb.Blood Flow Metab*, vol. 16,no. 5, pp. 834-840.be the

Logan, J., Fowler, J. S., Volkow, N. D., Wolf, A. P., Dewey, S. L., Schlyer, D. J., MacGregor, R. R., Hitzemann, R., Bendriem, B., Gatley, S. J., & Christman, D. R. 1990, "Graphical Analysis of Reversible Radioligand Binding from Time-Activity Measurements Applied to [N-[C-11]-methyl-(-)-Cocaine PET Studies in Human Subjects", *J.Cereb.Blood Flow Metab.*, vol. 10, pp. 740-747.

Patlak, C. S. & Blasberg, R. G. 1985, "Graphical evaluation of blood-to-brain transfer constants from multiple- time uptake data. Generalizations", *J Cereb.Blood Flow Metab*, vol. 5,no. 4, pp. 584-590.

Patlak, C. S., Blasberg, R. G., & Fenstermacher, J. D. 1983, "Graphical evaluation of blood-to-brain transfer constants from multiple-time uptake data", *J Cereb.Blood Flow Metab*, vol. 3, pp. 1-7.

Schmidt, K. 1999, "Which linear compartmental systems can be analyzed by spectral analysis of PET output data summed over all compartments?", *J Cereb.Blood Flow Metab*, vol. 19,no. 5, pp. 560-569

Glossary [1]

B_{max} The maximum number of receptor binding sites in a given preparation.

BP Binding potential. There are three different in vivo binding potentials (BP_{ND}, BP_P, BP_F).

CBF Cerebral blood flow.

Compartment A distinct region or state in which substances are distributed uniformly. The amount of substance transported out of a compartment is proportional to the amount in the region or state.

Compartmental model A mathematical description of the transport/reaction pathways of tracers in terms of interconnected compartments.

Convolution A mathematical time integration operation that gives the result of an input function f(t) combining with a system's impulse response function g(t) to obtain its output. A traditional notation is $f(t) \otimes g(t)$. The operation is $\int f(\tau) \cdot g(t-\tau) d\tau$

Cost function Expression selected for optimization (minimization) when a model's best set of parameters have been found - generally a weighed sum of residuals squared.

Extraction fraction Fraction of substrate or tracer extracted from blood to tissue during the first passage through the organ.

FDG Fluor-Deoxy-D-Glucose

Fick principle Technique for determining consumption of a substance by an organ. It is calculated form the product of the arteriovenous concentration difference of the substance and blood flow.

Gauss-Newton method The most common algorithm used for nonlinear regression problems.

Gjedde-Patlak Plot A simple method for determining the rate uptake constant and volume of distribution of a tracer using a linearisation and linear regression.

Half life Time during which the amount of a substance decreases to half its original value.

Input function A time function providing excitation/changes to a system it acts upon; in this context the plasma concentration as a function of time.

Least squares A popular criteria used in the cost function: minimizing the sum of the squares of the residuals.

Ligand Any compound or drug (either agonist or antagonist) that binds to a receptor.

---

[1] Phelps, M. E., J. C. Mazziotta, et al. (1986). Positron Emission Tomography and Autoradiography (Principles and Applications for the Brain and Heart). New York, Raven.

Mathematical model The mathematical description of the behaviour of a system allowing calculation of predicted behaviour.

Maximum likelihood A technique for parameter estimation that chooses those parameter values that cause the observed data to be the most likely outcome.

MR = Metabolic rate The uptake rate of a sustance at equilibrium.

MRGLc Metabolic rate of glucose (μmole/min/g).

Parameter A numerical quantity whose value affects the response of a model. In tracer kinetic models, the parameters usually are the rate constants of transfer between the model's compartments. the meaning of these parameters is usually related to physiological or biochemical processes (e.g., blood flow, *PS* product, etc.).

Perfusion Blood flow per mass of tissue in ml/min/g or ml/min/ml.

PS Permeability surface product of the permeability of a substance or tracer across a capillary wall and the capillary surface area per unit weight of tissue. It determines the rate at which a substance or tracer is transported from the vascular to tissue space.

Rate constant (k) Parameter describing a particular part of a process, namely a specific contribution to a component's amount changing per unit time/amount present.

ROI Region of interest.

SA Specific activity. Radioactivity per unit mass (or volume).

Steady state Net flux of tracer between the compartments under study is zero. The total amount leaving is identical to the total amount entering the system.

Transient equilibrium With reference to neuroreceptor binding studies. The maximum turning point of the total tissue curve. At this point the rate of change of concentration in tissue is zero however the total loss from the system is not negligable (loss from non-specific binding).

Tracer A measurable substance used to mimic, follow, or trace a chemical compound or process without disturbing the process under study.

Weighted least squares A modified version of ordinary least squares estimation involving the determination of parameters by minimizing the weighted sum of squared deviations between the data and the model.

Index